

# VU Research Portal

## Microbubble-mediated Focused Ultrasound in Diffuse Midline Glioma H3 K27M

Haumann, Rianne

2022

### **document version**

Publisher's PDF, also known as Version of record

[Link to publication in VU Research Portal](#)

### **citation for published version (APA)**

Haumann, R. (2022). *Microbubble-mediated Focused Ultrasound in Diffuse Midline Glioma H3 K27M*. [PhD-Thesis - Research and graduation internal, Vrije Universiteit Amsterdam].

### **General rights**

Copyright and moral rights for the publications made accessible in the public portal are retained by the authors and/or other copyright owners and it is a condition of accessing publications that users recognise and abide by the legal requirements associated with these rights.

- Users may download and print one copy of any publication from the public portal for the purpose of private study or research.
- You may not further distribute the material or use it for any profit-making activity or commercial gain
- You may freely distribute the URL identifying the publication in the public portal ?

### **Take down policy**

If you believe that this document breaches copyright please contact us providing details, and we will remove access to the work immediately and investigate your claim.

### **E-mail address:**

[vuresearchportal.ub@vu.nl](mailto:vuresearchportal.ub@vu.nl)

# **Microbubble-mediated Focused Ultrasound in Diffuse Midline Glioma H3 K27M**

Rianne Haumann  
2022

Microbubble-mediated Focused Ultrasound in Diffuse Midline Glioma H3 K27M  
Rianne Haumann, The Netherlands, 2022

The work described in this thesis was financially supported by KWF-STW.

ISBN: 978-94-6419-624-5

Printed by: Gildeprint

Cover design by: R. Haumann

Layout by: R. Haumann

© 2022 R. Haumann, Amsterdam, The Netherlands

All rights reserved. No part of this thesis may be reproduced, stored or transmitted, in any form or by any means, without prior permission of the author or, when appropriate, of the publishers of the publication

VRIJE UNIVERSITEIT

**Microbubble-mediated Focused Ultrasound  
in Diffuse Midline Glioma H3 K27M**

ACADEMISCH PROEFSCHRIFT

ter verkrijging van de graad Doctor  
aan de Vrije Universiteit Amsterdam,  
op gezag van de rector magnificus  
prof.dr. J.J.G. Geurts,  
in het openbaar te verdedigen  
ten overstaan van de promotiecommissie  
van de Faculteit der Geneeskunde  
op dinsdag 6 december om 15.45 uur  
in een bijeenkomst van de universiteit,  
De Boelelaan 1105

door

Rianne Haumann

geboren te Doetinchem

promotor: prof.dr. G.J.L. Kaspers

copromotor: dr. E. Hulleman

promotiecommissie: prof.dr. E.W. Hoving  
dr. O. van Tellingen  
prof.dr. J.M. Kros  
dr. K. Kooiman  
prof.dr. A.W. Griffioen  
dr. W. Beaino

*Zonder strijd geen overwinning*

## Table of Contents

**CHAPTER 1** Introduction


**CHAPTER 2** Overview of Current Drug Delivery Methods Across the Blood-brain Barrier for the Treatment of Primary Brain Tumors  
*Published in CNS Drugs*

**CHAPTER 3** A High-throughput Image-guided Stereotactic Neuronavigation and Focused Ultrasound System for Blood-brain Barrier Opening in Rodents  
*Published in Journal of Visualized Experiments*

**CHAPTER 4** Imaged-guided Focused Ultrasound in Combination with Various Formulations of Doxorubicin for the Treatment of Diffuse Intrinsic Pontine Glioma  
*Published in Translational Medicine Communications*

**CHAPTER 5** The Neurovascular Unit in Diffuse Intrinsic Pontine Gliomas  
*Published in Free Neuropathology*

**CHAPTER 6** The Blood-brain Barrier in Xenograft Models of Diffuse Midline Glioma H3 K27M: A Pilot Study



**CHAPTER 7** General Discussion

**CHAPTER 8** Summary

**CHAPTER 9** Samenvatting

**CHAPTER 10** Appendices  
Curriculum Vitae  
PhD Portfolio  
List of Publications  
Dankwoord







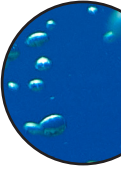
# Chapter 1

## Introduction



## CNS tumors

In the Netherlands, each year around 1400 patients, both adults and children, are diagnosed with cancer of the central nervous system (CNS) [1]. Cancer arises from a cell or a subset of cells that contains genetic mutations resulting in abnormal growth of these cells [2]. CNS tumors occur in the brain and spinal cord. Tumors can be divided into primary and secondary tumors; primary CNS tumors arise in the CNS while secondary CNS tumors arise from disseminated tumor cells from a cancer located elsewhere in the body. Furthermore, tumors can be benign or malignant. Benign tumors are well encapsulated, grow slowly and do not invade other tissues. Therefore, these tumors can often be resected and have a good prognosis. The most common benign CNS tumor is meningioma which arises in the meninges [3]. In contrast, malignant tumors invade tissue, have a faster growth rate, and are highly vascularized with distorted blood vessels. Malignant tumors usually arise in glial cells, astrocytes, ependymal cells, and oligodendrocytes resulting in gliomas, astrocytomas, ependymomas, and oligodendrogliomas, respectively (Figure 1). Of these tumors, glioma is the most prevalent type of malignant brain tumor [3]. A more comprehensive overview of the different types of brain tumors is given in Chapter 2.



## Classification of CNS tumors

The World Health Organization (WHO) classifies CNS tumors into different grades according to pathology and molecular analysis [4]. CNS tumors are classified as grade I, II, III, and IV. Grade I and II are both low grade tumors that grow slowly. Grade III and IV are high grade tumors that have a more infiltrative character with grade IV as the most malignant grade, with rapid growth, infiltration into other tissues and necrosis. The grade is indicative for the prognosis with low grade brain tumors having an average overall survival of 70 % while for high grade tumors the overall survival is only 8 % [5].

Only in the 2016 classification, the WHO started including molecular analysis into the CNS tumor classification [4, 6]. In the previous classification of 2007, tumors were classified according to pathology [6]. Since molecular analysis revealed more distinct subgroups, the classification was updated. Illustrative is the case of pediatric diffuse midline glioma (DMG), H3K27M-mutant grade IV that previously was not specifically graded as a separate entity. Molecular analysis of this pediatric brain tumor showed distinctive genetic markers. The subgrouping of these tumors revealed potential targetable proteins that with the previous classification was not specifically classified [4]. Of note, the WHO classification was updated in 2021 [7]. Here diffuse midline glioma, H3 K27M was now classified as diffuse midline glioma H3 K27-altered since multiple pathogenic pathways are affected in these tumors. Throughout this thesis DMG H3 K27-altered or DMG H3K27M-mutant is described as DMG H3 K27M or as the diffuse intrinsic pontine glioma (DIPG) the term of the 2007 WHO classification [4, 6, 7].

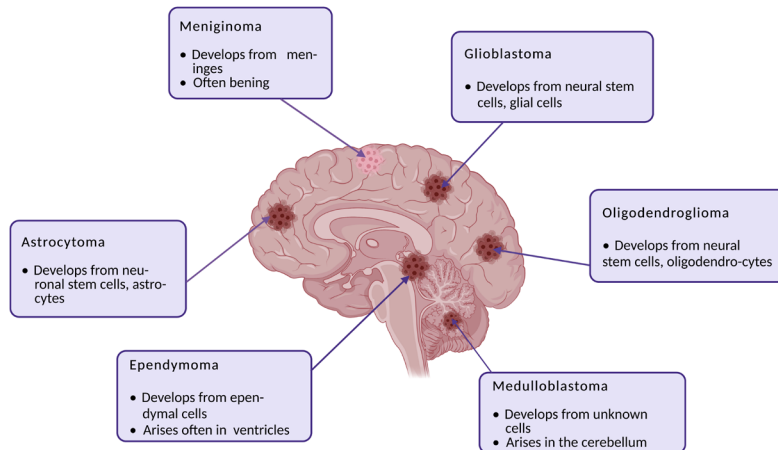


**Figure 1. | Origin of primary brain tumors.** Brain tumors arise in different types of tissues. Meningioma arises in the meninges and are often benign. Gliomas are the most prevalent malignant brain tumor. Gliomas can be subdivided in glioblastoma, oligodendroglioma, astrocytoma, and ependymoma which arise in neural stem cells and glial cells, oligodendrocytes, astrocytes, and ependymal cells, respectively. Some brain tumor origins remain partly unknown such as medulloblastoma. Adapted from Mulcahy, E. Q. X., et al. HGF/MET signaling in malignant brain tumors. *International Journal of Molecular Sciences* (2020), 21(20), 7546. Created with biorender.

## Pediatric CNS tumors

In children, cancer was an invariable deadly diagnosis many years ago; today the five-year survival has improved to over 80 % [8]. Nevertheless, the five-year survival of pediatric CNS tumors, in particular brain tumors, has not improved for several types of CNS tumors. The most common brain tumors in children aged 0 to 14 years are pilocytic astrocytoma, embryonal tumors, and high-grade gliomas (HGGs) [9]. Of these tumors, HGGs have one of the worst prognoses with a five-year survival rate of less than 5 % [3]. Pediatric CNS tumors account for approximately 40 % of cancer-related deaths [10]. Since these tumors do not respond well to existing treatments, new treatments need to be developed in order to improve survival for these patients. In this thesis we focus on pediatric high-grade glioma (HGG) and in particular DMG H3 K27M.

## Diffuse Midline Glioma

DMG H3 K27M is a group of pediatric brain tumors that arise in the midline structures of the brain such as brainstem and thalamus. While rare, the impact of this disease is immense with rapid progression and an overall survival of only 11 months [9, 11, 12]. One of the

reasons this disease has a dismal prognosis, is the location of the tumor. DMG H3 K27M resides in brain structures that are essential for the functioning of the human body such as breathing, consciousness and sleep. Resection of these tumors is difficult since this will impact vital functions.

DMG H3 K27M accounts for approximately 80 % of the brainstem gliomas classified as typical DMG H3 K27M [12, 13]. Typical DMG H3 K27M is characterized by specific clinical symptoms supported by magnetic resonance imaging (MRI). Children with a median age of 7 years often present with cerebellar signs, long-tract signs, and cranial nerve palsies. The extent and presence of these clinical symptoms are dependent on the location and growth pattern of the tumor [12, 14]. Diagnosis is confirmed by MRI where DMG H3 K27M resides in the ventral pons, includes 50-66 % of the axial diameter of the pons, and the basilar artery is engulfed by the tumor (Figure 2) [14-18]. Due to the rapid growth of the tumor, the time between the onset of symptoms and diagnosis is short, usually only one to three months [12, 14]. As the disease progresses, DMG H3 K27M often invades the cerebellum and supratentorial brain regions such as the thalamus, lateral ventricles, and cerebral cortex [16-18]. At end-stage disease patients present with ataxia, motor deficits, immobility, communication problems, and difficulty swallowing [19]. Patients receive palliative care until death.

### ***The Biology of Diffuse Midline Glioma H3 K27M***

Pathology revealed that DMG H3 K27M is a heterogenous tumor with different areas resembling both WHO I and WHO IV tumors [17, 18, 20]. Only recently, DMG tissue became available for molecular analysis which showed a distinct mutation, K27M, in histone 3 [21]. Histones play a key role in regulation of transcription, DNA repair, DNA replication and chromosomal stability. Histone H3 is subdivided into multiple isoforms with specific functions. Isoforms H3.1 and H3.2 are synthesized during the S phase of the cell cycle in which they regulate the packaging of newly replicated DNA. Isoform H3.3 is synthesized throughout the cell cycle and replaces histones that are lost during processes that disrupt nucleosomes [22]. The mutation K27M, lysine-to-methionine at position 27, is the most predominant mutation (78 %) in DMG H3 K27M that is observed in both H3.3 and H3.1 isoforms [18, 23]. K27M mutations occur at the lysine methylation/acetylation site where trimethylation of lysine 27 results in interaction with polycomb repressive complex (PRC2). PRC2 represses transcription of target genes, a process key in stem cell regulation and development [18]. A mutation of K27M will result in an altered post-translational modification. Under physiological circumstances, post-translational modifications result in the formation of functional complexes that regulate cellular processes such as transcription, DNA repair, and DNA replication [18]. Upon genetic modification, normal cellular processes are affected which could potentially lead to cancer.

The distinct isoforms have different clinical perspectives. The H3.3 K27M mutation often accompanied with loss of p53 has the worst prognosis with an overall survival of only 9 months while H3.1 K27M has a median survival of 15 months [20, 23]. Isoform H3.1 is often observed in younger children (4-5 years) and respond better to radiotherapy, have fewer relapses, and have less metastasis than H3.3 tumors [20].

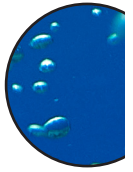




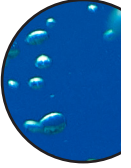
**Figure 2. | MRI.** Left panel: MRI of a healthy three-year-old. Case courtesy of Dr Derek Smith, Radiopaedia.org, rID: 53992. Right panel: MRI of a DIPG patient where the pontine area is enlarged (yellow). Copied with permission from National Cancer Institute courtesy of Dr. Rishi Lulla MD.

### ***Diffuse Midline Glioma H3 K27M animal models***

Since the brainstem is a vital structure, historically pontine DMG H3 K27M biopsies were deemed unsafe and unnecessary due to the distinct clinical symptoms and identification of the tumor with MRI [15, 24]. However, new clinical research showed that biopsy of the brainstem has a very low morbidity if performed by a trained surgeon and therefore biopsies are now performed more regularly in DMG H3 K27M patients [15, 24]. This resulted in an availability of tissue for preclinical research. In addition, autopsy protocols were established that aided in the availability of tissue for preclinical research. Autopsies need to be performed quickly after death to ensure viability of tumor cells [25]. These cells can then be cultured directly for *in vitro* research or can be used for *in vivo* animal models. *In vivo* animal models can be established after expansion of the DMG H3 K27M cells in culture or DMG H3 K27M cells can be injected directly into the mouse brain after autopsy in order to establish a mouse model. These methods result in human or murine tumors, respectively [26, 27]. It is surprising that direct injection of human cells results in murine tumors, with no evidence of human DNA. The human DMG H3 K27M tumors cells are able to convert murine cells into murine tumor cells. Several research groups established multiple xenograft models of DMG H3 K27M tumors [26, 28]. These animal models are useful for preclinical research of potential new drugs and drug delivery methods.

### ***Treatment of Diffuse Midline Glioma***

The main course of treatment of DMG H3 K27M tumors is radiation therapy where patients receive 54-60 Gray (Gy) in total over a period of 6 weeks. At the moment, radiation therapy



is the only effective – but not curative - treatment that can temporary relieve neurological symptoms in 70-80 % of the patients [12, 14]. Radiation therapy has increased overall survival from 9 to 11 months, however, adjuvant therapies, such as chemotherapy, radiosensitizers, and targeted medicines, have not resulted in significant improvement of overall survival [12, 14].

*In vitro* drug screens against different DMG H3 K27M cell lines showed sensitivity to conventional chemotherapy drugs such as melphalan, doxorubicin, mitoxantrone, and BCNU [29]. Furthermore, other drugs have been tested against DMG H3 K27M such as histone deacetylase (HDAC) inhibitors and BMS-754807 that also showed efficacy against DMG H3 K27M [30, 31]. HDAC inhibitors inhibit gene transcription, however chronic exposure led to resistance [30]. IGF-IR/insulin receptor inhibitor, BMS-754807, also showed efficacy against DMG H3 K27M cells [31]. However, *in vivo* these drugs have not been successful in increasing survival. One of the hypotheses for this lack of effect *in vivo* and the lack of survival benefit in patients is the presence of a blood-brain barrier (BBB). The BBB is a protective barrier that prevents drugs from entering the brain parenchyma and actively exports drugs out of the brain [29, 32, 33]. The BBB is heterogenous throughout the brain with the cortex more permeable and the pontine region less permeable for drugs as observed in healthy non-human primates [34, 35]. The heterogeneity of the BBB might also be affected by the tumor; however, little is known about the influence of DMG H3 K27M on BBB integrity.

## Microbubble-mediated focused ultrasound

In order to overcome the BBB, drug delivery techniques have been used for the treatment of DMG H3 K27M. An extensive review on the BBB and different drug delivery techniques is described in Chapter 2. Several drug delivery techniques have been used for the treatment of DMG H3 K27M. So far, these drug delivery techniques have not yet led to a significant increase in survival. Since the brainstem is a delicate structure, a non-invasive technique is preferred. Microbubble-mediated focused ultrasound is such a minimally invasive method that can be used to open the BBB temporarily.

Ultrasound is a well-known diagnostic technique in medicine and is routinely used in gynecology, cardiology and internal medicine. Ultrasound can also be used for therapeutic applications such as BBB opening, ablation and neuromodulation [36-41]. In this thesis we focus on the use of ultrasound for BBB opening. BBB opening is achieved with microbubble-mediated focused ultrasound. Here, microbubbles, lipid particles filled with inert gas, are injected into the veins. In the presence of acoustic sound waves emitted from the ultrasound transducer directed at the tumor area, microbubbles oscillate (expansion and compression of the microbubbles). Oscillation of the microbubbles in the vicinity of endothelial cells result in the disruption of the tight junctions enabling paracellular transport of drugs [42]. Acoustic pressure influences the oscillation of the microbubbles which ranges from stable oscillation, i.e., stable cavitation, at low acoustic pressure to bubble collapse, i.e., inertial cavitation, at high acoustic pressure [42-44]. Inertial cavitation achieved at high acoustic pressure is often associated with brain hemorrhage [43, 44]. The use of microbubbles is essential for lowering acoustic pressure and for more control of the biological effects. In the past, focused ultrasound without microbubbles resulted in unpredictable tissue effects ran-



ging from no damage to BBB opening to hemorrhage [41]. Microbubble-mediated focused ultrasound can controllably open the BBB in a reversible matter [45]. After BBB opening, the BBB closes gradually over time where it closes first for larger molecules while small molecules have a greater window of passing the BBB after focused ultrasound [46].

*In vivo*, stable and reproducible BBB opening has been achieved in rabbits [47, 48]. Henceforth, focused ultrasound has been successfully used in preclinical adult glioma models to deliver temozolomide, bevacizumab, and doxorubicin [49-53]. Median survival of two different glioma xenograft models significantly increased using temozolomide in combination with microbubble-mediated focused ultrasound [51, 52]. Also, bevacizumab combined with focused ultrasound increased median survival by 136 % compared to non-treated animals in a U87 glioma mouse model [53]. Doxorubicin, also effective against DIPG cells, significantly improved survival by 12 % to 68 % in glioma (SMA 560 and GL261) mouse models, respectively [49]. Overall survival of different adult glioma xenograft models shows promise of this technique for clinical trials.

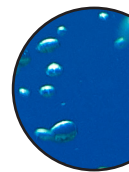
Clinical translation of focused ultrasound requires adjustments of the system. In animal studies, focused ultrasound is achieved with one transducer element. In humans, the skull hampers the acoustic energy transfer because the skull attenuates acoustic energy (loss of energy). Due to the attenuation a higher acoustic pressure is required to achieve BBB opening [54]. However, a high acoustic pressure results in an increase of temperature leading to unwanted side effects such as burns and irreversible tissue damage. Furthermore, the variations in skull shape and thickness influence the beam propagation [54]. The irregular shape of the skull results in different attenuations and thus the energy transmitted is not homogenous. These problems can be overcome with a phased array transducer where multiple small transducers emit acoustic waves that focus on one spot in the brain [54]. Additionally, a cooling system is integrated in the focused ultrasound system to cool down the skull. The adjusted system was applied to non-human primates and resulted in a reproducible, safe, and predictable BBB opening [54].

The non-invasive character of microbubble-mediated focused ultrasound in combination with some (feasible) adjustments to the system makes this a suitable system for the preclinical treatment of DMG H3 K27M and possible clinical translation. The use of this system in combination with FDA or EMA approved drugs makes fast clinical translation possible.

## Thesis outline

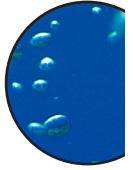
The main aim of this thesis was to investigate microbubble-mediated focused ultrasound as a new drug delivery method for the treatment of DMG H3 K27M. The second aim was to characterize the BBB in DMG H3 K27M in both human samples and xenograft mouse models. In **Chapter 2** we review the properties of the BBB and vasculature in both adult and pediatric brain tumors. Furthermore, we describe the various drug delivery techniques that have been used for the treatment of brain cancer. One of the drug delivery techniques is microbubble-mediated focused ultrasound that has been successfully used in adult xenograft mouse models. Here we investigated microbubble-mediated focused ultrasound for the treatment of a DMG H3 K27M mouse model. In **Chapter 3** we describe our protocol

for preclinical microbubble-mediated focused ultrasound for small rodents. The in-house built focused ultrasound system was optimized for high-throughput *in vivo* experiments. In **Chapter 4** we used the high-throughput focused ultrasound system to study the efficacy of various formulations of doxorubicin on survival of mice in a DMG H3 K27M xenograft mouse model. Since therapies have not been successful, we characterized the BBB and vasculature that are important mechanisms that influence drug delivery. We immunohistochemically stained human DMG H3 K27M and age-matched control samples, **Chapter 5**. This study led to a follow-up pilot study that characterized the BBB in various DMG H3 K27M mouse models shown in **Chapter 6**. Finally, we conclude with a **Discussion** followed by a **Summary** on our work presented in this thesis.



## References

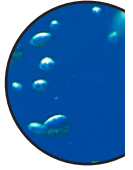
1. Incidentie, Stichting STOPhersentumoren. [cited 2022 16th of January]; Available from: <https://hersentumor.stophersentumoren.nl/hersentumoren/hersentumor-cijfers-aantal-patienten-diagnoses>.
2. Hanahan, D. and R.A. Weinberg, *Hallmarks of cancer: the next generation*. *cell*, 2011. **144**(5): p. 646-674.
3. Ostrom, Q.T., et al., *CBTRUS statistical report: primary brain and central nervous system tumors diagnosed in the United States in 2007–2011*. *Neuro-oncology*, 2014. **16**(suppl\_4): p. iv1-iv63.
4. Louis, D.N., et al., *The 2016 World Health Organization Classification of Tumors of the Central Nervous System: a summary*. *Acta Neuropathol*, 2016. **131**(6): p. 803-820.
5. Overleving, Stichting STOPhersentumoren. [cited 2022 16th of January]; Available from: <https://hersentumor.stophersentumoren.nl/hersentumoren/hersentumor-cijfers-sterfte-en-overleving-hersentumoren>
6. Louis, D.N., et al., *The 2007 WHO classification of tumours of the central nervous system*. *Acta neuropathologica*, 2007. **114**(2): p. 97-109.
7. Louis, D.N., et al., *The 2021 WHO classification of tumors of the central nervous system: a summary*. *Neuro-oncology*, 2021. **23**(8): p. 1231-1251.
8. *Overleving*. Intergraal Kankercentrum Nederland. Available from: <https://iknl.nl/kankersoorten/kanker-bij-kinderen/registratie/overleving>.
9. Wells, E.M. and R.J. Packer, *Pediatric brain tumors*. Continuum (Minneap Minn), 2015. **21**(2 Neuro-oncology): p. 373-96.
10. Yang, F.-Y., et al., *Pharmacokinetic changes induced by focused ultrasound in glioma-bearing rats as measured by dynamic contrast-enhanced MRI*. *PLoS one*, 2014. **9**(3): p. e92910.
11. Veldhuijzen van Zanten, S.E.M., et al., *External validation of the diffuse intrinsic pontine glioma survival prediction model: a collaborative report from the International DIPG Registry and the SIOPE DIPG Registry*. *J Neurooncol*, 2017. **134**(1): p. 231-240.
12. Veldhuijzen van Zanten, S.E., et al., *A twenty-year review of diagnosing and treating children with diffuse intrinsic pontine glioma in The Netherlands*. *Expert review of anti-cancer therapy*, 2015. **15**(2): p. 157-164.
13. Recinos, P.F., D.M. Sciubba, and G.I. Jallo, *Brainstem tumors: where are we today?* *Pediatric neurosurgery*, 2007. **43**(3): p. 192-201.
14. Vanan, M.I. and D.D. Eisenstat, *DIPG in Children - What Can We Learn from the Past?* *Front Oncol*, 2015. **5**: p. 237.

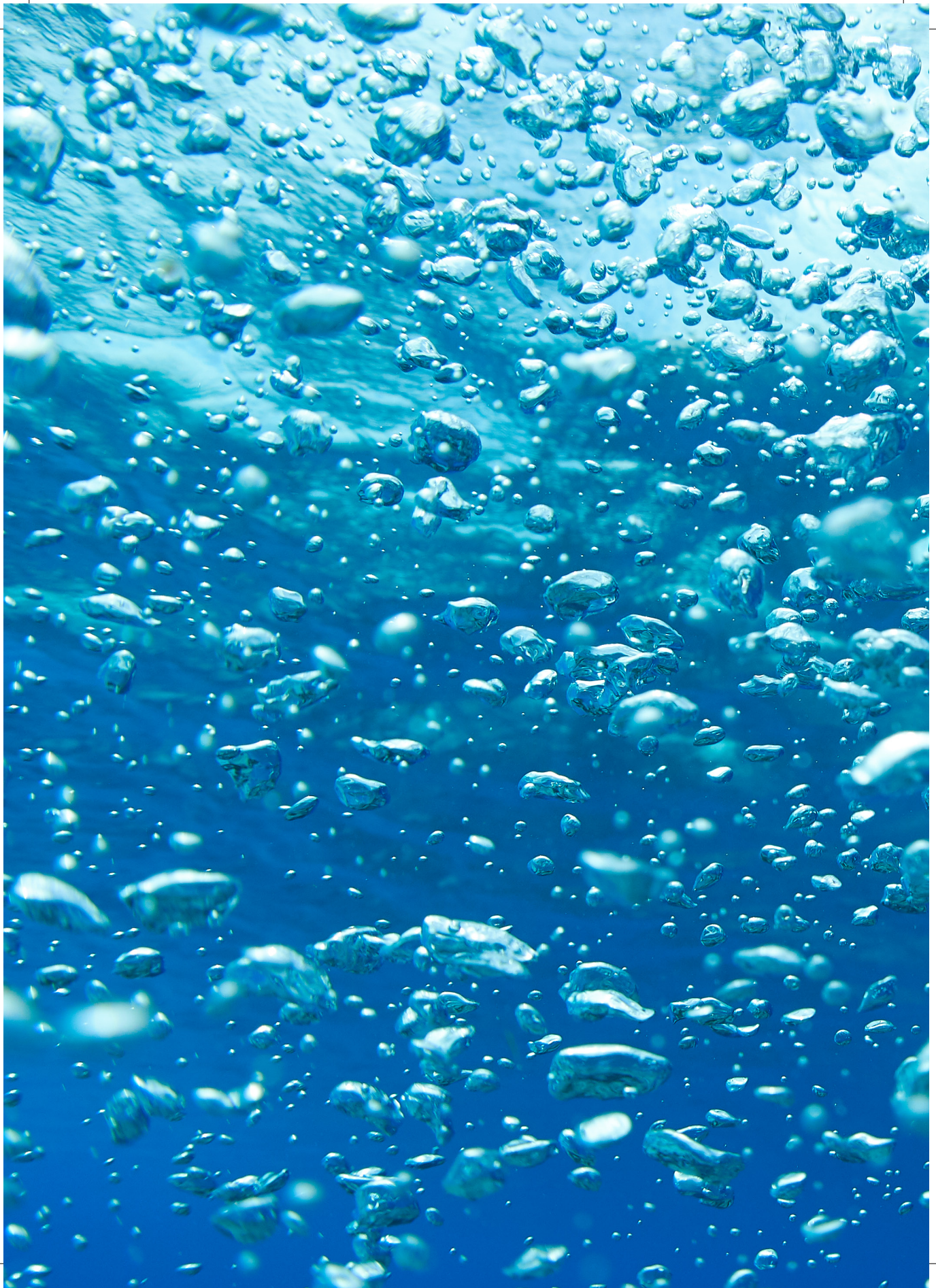


15. Puget, S., et al., *Biopsy in a series of 130 pediatric diffuse intrinsic Pontine gliomas*. Child's Nervous System, 2015. **31**(10): p. 1773-1780.
16. Yoshimura, J., et al., *Clinicopathological study of diffuse type brainstem gliomas: analysis of 40 autopsy cases*. Neurologia medico-chirurgica, 2003. **43**(8): p. 375-382.
17. Bugiani, M., et al., *Deceptive morphologic and epigenetic heterogeneity in diffuse intrinsic pontine glioma*. Oncotarget, 2017. **8**(36): p. 60447.
18. Jones, C. and S.J. Baker, *Unique genetic and epigenetic mechanisms driving paediatric diffuse high-grade glioma*. Nature Reviews Cancer, 2014. **14**(10): p. 651-661.
19. van Zanten, S.E.V., et al., *Palliative and end-of-life care for children with diffuse intrinsic pontine glioma: results from a London cohort study and international survey*. Neuro-oncology, 2016. **18**(4): p. 582.
20. Castel, D., et al., *Histone H3F3A and HIST1H3B K27M mutations define two subgroups of diffuse intrinsic pontine gliomas with different prognosis and phenotypes*. Acta neuropathologica, 2015. **130**(6): p. 815-827.
21. Paugh, B.S., et al., *Integrated molecular genetic profiling of pediatric high-grade gliomas reveals key differences with the adult disease*. Journal of clinical oncology, 2010. **28**(18): p. 3061.
22. Elsaesser, S.J., A.D. Goldberg, and C.D. Allis, *New functions for an old variant: no substitute for histone H3*. 3. Current opinion in genetics & development, 2010. **20**(2): p. 110-117.
23. Khuong-Quang, D.-A., et al., *K27M mutation in histone H3. 3 defines clinically and biologically distinct subgroups of pediatric diffuse intrinsic pontine gliomas*. Acta neuropathologica, 2012. **124**(3): p. 439-447.
24. Cage, T.A., et al., *Feasibility, safety, and indications for surgical biopsy of intrinsic brainstem tumors in children*. Child's Nervous System, 2013. **29**(8): p. 1313-1319.
25. Caretti, V., et al., *Implementation of a multi-institutional diffuse intrinsic pontine glioma autopsy protocol and characterization of a primary cell culture*. Neuropathol Appl Neurobiol, 2013. **39**(4): p. 426-436.
26. Caretti, V., et al., *Human pontine glioma cells can induce murine tumors*. Acta neuropathologica, 2014. **127**(6): p. 897-909.
27. Hashizume, R., et al., *Characterization of a diffuse intrinsic pontine glioma cell line: implications for future investigations and treatment*. Journal of neuro-oncology, 2012. **110**(3): p. 305-313.
28. Jansen, M.H., et al., *Bevacizumab targeting diffuse intrinsic pontine glioma: results of <sup>89</sup>Zr-bevacizumab PET imaging in brain tumor models*. Molecular cancer therapeutics, 2016. **15**(9): p. 2166-2174.

29. Veringa, S.J., et al., *In vitro drug response and efflux transporters associated with drug resistance in pediatric high grade glioma and diffuse intrinsic pontine glioma*. PLoS One, 2013. **8**(4): p. e61512.
30. Grasso, C.S., et al., *Functionally defined therapeutic targets in diffuse intrinsic pontine glioma*. Nature medicine, 2015. **21**(6): p. 555-559.
31. Halvorson, K.G., et al., *A high-throughput in vitro drug screen in a genetically engineered mouse model of diffuse intrinsic pontine glioma identifies BMS-754807 as a promising therapeutic agent*. PloS one, 2015. **10**(3): p. e0118926.
32. Grasso, C.S., et al., *Functionally defined therapeutic targets in diffuse intrinsic pontine glioma*. Nat Med, 2015. **21**(6): p. 555-559.
33. Haumann, R., et al., *Overview of Current Drug Delivery Methods Across the Blood-Brain Barrier for the Treatment of Primary Brain Tumors*. CNS Drugs, 2020. **34**(11): p. 1121-1131.
34. Warren, K.E., *Beyond the blood: brain barrier: the importance of central nervous system (CNS) pharmacokinetics for the treatment of CNS tumors, including diffuse intrinsic pontine glioma*. Frontiers in oncology, 2018. **8**: p. 239.
35. McCully, C.M., et al., *Model for concomitant microdialysis sampling of the pons and cerebral cortex in rhesus macaques (Macaca mulatta)*. Comparative medicine, 2013. **63**(4): p. 355-360.
36. Newman, P.G. and G.S. Rozycki, *The history of ultrasound*. Surgical clinics of north America, 1998. **78**(2): p. 179-195.
37. Meng, Y., et al., *Safety and efficacy of focused ultrasound induced blood-brain barrier opening, an integrative review of animal and human studies*. J Control Release, 2019. **309**: p. 25-36.
38. Burgess, A. and K. Hynynen, *Noninvasive and targeted drug delivery to the brain using focused ultrasound*. ACS chemical neuroscience, 2013. **4**(4): p. 519-526.
39. Darrow, D.P., *Focused Ultrasound for Neuromodulation*. Neurotherapeutics, 2019. **16**(1): p. 88-99.
40. Zhou, Y.F., *High intensity focused ultrasound in clinical tumor ablation*. World J Clin Oncol, 2011. **2**(1): p. 8-27.
41. Vykhodtseva, N., K. Hynynen, and C. Damianou, *Histologic effects of high intensity pulsed ultrasound exposure with subharmonic emission in rabbit brain in vivo*. Ultrasound in medicine & biology, 1995. **21**(7): p. 969-979.
42. Dasgupta, A., et al., *Ultrasound-mediated drug delivery to the brain: principles, progress and prospects*. Drug Discov Today Technol, 2016. **20**: p. 41-48.

43. Bader, K.B. and C.K. Holland, *Gauging the likelihood of stable cavitation from ultrasound contrast agents*. *Physics in Medicine & Biology*, 2012. **58**(1): p. 127.
44. Neppiras, E., *Acoustic cavitation series: part one: Acoustic cavitation: an introduction*. *Ultrasonics*, 1984. **22**(1): p. 25-28.
45. E Konofagou, E., et al., *Ultrasound-induced blood-brain barrier opening*. *Current pharmaceutical biotechnology*, 2012. **13**(7): p. 1332-1345.
46. Marty, B., et al., *Dynamic study of blood–brain barrier closure after its disruption using ultrasound: a quantitative analysis*. *Journal of Cerebral Blood Flow & Metabolism*, 2012. **32**(10): p. 1948-1958.
47. Hynynen, K., et al., *Noninvasive MR imaging–guided focal opening of the blood-brain barrier in rabbits*. *Radiology*, 2001. **220**(3): p. 640-646.
48. McDannold, N.J., N.I. Vykhodtseva, and K. Hynynen, *Microbubble contrast agent with focused ultrasound to create brain lesions at low power levels: MR imaging and histologic study in rabbits*. *Radiology*, 2006. **241**(1): p. 95-106.
49. Kovacs, Z., et al., *Prolonged survival upon ultrasound-enhanced doxorubicin delivery in two syngenic glioblastoma mouse models*. *Journal of controlled release*, 2014. **187**: p. 74-82.
50. Treat, L.H., et al., *Improved anti-tumor effect of liposomal doxorubicin after targeted blood-brain barrier disruption by MRI-guided focused ultrasound in rat glioma*. *Ultrasound Med Biol*, 2012. **38**(10): p. 1716-25.
51. Liu, H.-L., et al., *Pharmacodynamic and therapeutic investigation of focused ultrasound-induced blood-brain barrier opening for enhanced temozolomide delivery in glioma treatment*. *PloS one*, 2014. **9**(12): p. e114311.
52. Wei, K.-C., et al., *Focused ultrasound-induced blood–brain barrier opening to enhance temozolomide delivery for glioblastoma treatment: a preclinical study*. *PloS one*, 2013. **8**(3): p. e58995.
53. Liu, H.-L., et al., *Focused ultrasound enhances central nervous system delivery of bevacizumab for malignant glioma treatment*. *Radiology*, 2016. **281**(1): p. 99-108.
54. McDannold, N., et al., *Temporary disruption of the blood–brain barrier by use of ultrasound and microbubbles: safety and efficacy evaluation in rhesus macaques*. *Cancer research*, 2012. **72**(14): p. 3652-3663.







## Chapter 2

### **Overview of Current Drug Delivery Methods Across the Blood-brain Barrier for the Treatment of Primary Brain Tumors**

This chapter was originally published as Haumann, R., Videira, J. C., Kaspers, G. J., van Vuurden, D. G., Hulleman, E. Overview of Current Drug Delivery Methods Across the Blood Brain Barrier for the Treatment of Primary Brain Tumors. *CNS Drugs* 34,1121–1131 (2020).

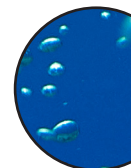


## Abstract

Existing drug delivery methods have not led to a significant increase in survival for patients with malignant primary brain tumors. While the combination of conventional therapies consisting of surgery, radiotherapy, and chemotherapy has improved survival for some types of brain tumors (*e.g.*, WNT medulloblastoma), other types of brain tumors (*e.g.*, glioblastoma and diffuse midline glioma) still have a poor prognosis. The reason for the differences in response can be largely attributed to the blood-brain barrier (BBB), a specialized structure at the microvasculature level that regulates the transport of molecules across the blood vessels into the brain parenchyma. This structure hampers the delivery of most chemotherapeutic agents for the treatment of primary brain tumors. Several drug delivery methods such as nanoparticles, convection enhanced delivery, focused ultrasound, intranasal delivery, and intra-arterial delivery have been developed to overcome the BBB in primary brain tumors. However, prognosis of most primary brain tumors still remains poor. The heterogeneity of the BBB in primary brain tumors and the distinct vasculature of tumors make it difficult to design a drug delivery method that targets the entire tumor. Drug delivery methods that combine strategies such as focused ultrasound and nanoparticles might be a more successful approach. However, more research is needed to optimize and develop new drug delivery techniques to improve survival of patients with primary brain tumors.

## Introduction

Most primary brain tumors, such as high-grade glioma, have an exceedingly poor prognosis due to their tumor location and fast development in both adult and pediatric patients [1-4]. The presence of the blood-brain barrier (BBB) is an important obstacle for drug delivery in most brain cancers [2, 5-8]. The BBB is a complex interplay between endothelial cells, astrocytes, pericytes, basal lamina, and extracellular matrix (ECM). These components, together with smooth muscle cells and neurons, form the neurovascular unit (NVU), which in turn regulates cerebral blood flow and BBB function [9-11]. The consequence of this tightly regulated barrier is that toxins and drugs, including chemotherapy, do not readily cross the BBB, posing a problem for drug delivery into the brain.



In order for a therapeutic intervention to be effective, chemotherapy must be capable of traversing the BBB and penetrating the brain parenchyma [5, 6, 12]. Systemic delivery of drugs (via the blood stream) is possible for molecules with a molecular weight of < 500 Dalton (Da) and a high lipophilicity [13, 14]. However, as only 5% of drugs meet these requirements, adequate drug delivery methods are needed to efficiently deliver the remaining 95% of drugs into the brain [12, 15, 16]. Current research on central nervous system (CNS) drug development predominantly focuses on either optimizing systemic drug delivery to the brain, or on circumventing the BBB (Figure 1) [5, 6, 17-19]. Systemic delivery can be achieved with nanomedicine [20, 21]; drugs that are not likely to cross the BBB can be adapted or packed into liposomes to make them more lipophilic [22, 23]. Nanomedicine can also be used for targeted therapy where nanoparticles can be equipped with specific proteins to target the tumor [23]. In contrast, the BBB can also be disrupted or circumvented by microbubble-mediated focused ultrasound (FUS), convection enhanced delivery (CED), intranasal delivery, and intra-arterial delivery [24-27]. Microbubble-mediated FUS uses microbubbles to locally and temporarily open the BBB, enabling drugs to accumulate in the brain parenchyma, while CED is a more invasive method for bypassing the BBB using surgically implanted catheters to administer drugs locally into the tumor [24, 25]. Intranasal delivery uses the direct anatomical relationship of the olfactory neuro-epithelium to the brain to circumvent the BBB, whereas intra-arterial delivery locally administers the drug in the artery [26, 27]. As promising as all these methods are, they have not led to a significant improvement of drug delivery for most malignant primary brain tumors. The phenotypic heterogeneity of the BBB across primary brain tumors makes it difficult to determine the best drug delivery method. Therefore, knowledge about BBB pathology is essential to determine the optimal drug delivery method. In the following paragraphs we will elaborate more on BBB pathology and the different methods for drug delivery in primary brain tumors.

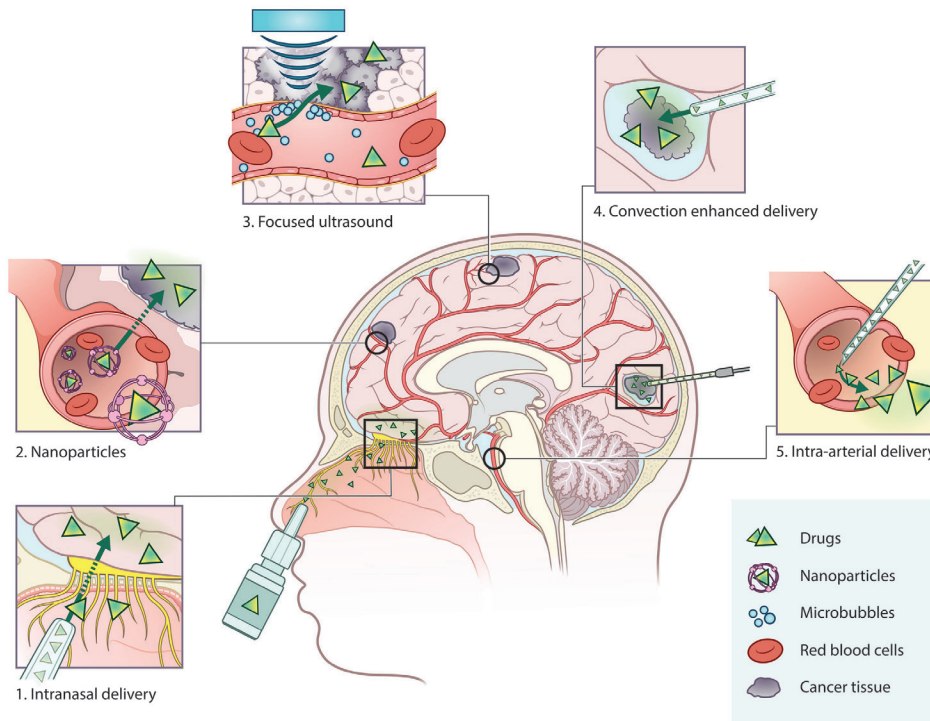


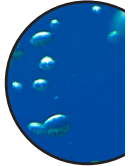
**Figure 1. | Overview of current drug delivery methods for the treatment of primary brain tumors.** Panel 1 intranasal drug delivery: drug is formulated in spray particles that enter the brain through the nasal cavity via the neuroepithelium. Here, the drug can enter without interference of the blood-brain barrier (BBB). Panel 2 nanoparticles: nanoparticles encapsulate drugs to increase plasma half-life and allow entry to the brain parenchyma by the enhanced permeability and retention (EPR) effect, endocytosis, and receptor-mediated transcytosis. Panel 3 microbubble-mediated focused ultrasound: microbubbles are intravenously administered and upon the application of focused ultrasound, microbubbles start to oscillate. The oscillation disrupts the BBB, temporarily opening it to allow drugs to enter the brain parenchyma. Panel 4 Convection enhanced delivery (CED): surgical placement of catheters in the brain to administer the drug directly in the tumor site. Panel 5: intra-arterial drug delivery: catheterization of the blood vessel and injection of drugs directly in the vicinity of the tumor, sometimes in combination with hyperosmolar drugs that open the BBB.

## BBB Physiology

The tightly regulated BBB is impermeable for most conventional chemotherapeutics [28]. Transport across the BBB is restricted by specialized endothelial cells [29, 30], which have specific characteristic properties that create an impermeable barrier. The first is the presence of tight junctions, which prevent paracellular passage of molecules. The main tight junction proteins are occludins, tricellulins, claudins, and junctional adhesion molecules [29]. Second, CNS endothelial cells express efflux transporters that regulate the movement of substrates across the BBB [31]. Various drugs are substrates for efflux transporters, thus hampering drug accumulation in the brain parenchyma. These efflux transporters belong to

the class of ATP-binding cassette (ABC) transporters, with the most important transporters being multidrug resistance receptors (MDRs, ABCB), multidrug resistance proteins (MRPs, ABCC), and the breast cancer resistance protein (BCRP/ABCG2) [32]. In the brain, MDR1 (ABCB1, P-glycoprotein [P-gp]) - the most extensively researched ABC-transporter - plays a role in the efflux of numerous drugs [33]. Third, transcytosis by pinocytotic and endocytotic vesicles is limited due to the low density of these vesicles in CNS endothelial cells [34]. Finally, CNS endothelial cells are able to limit the entry of immune cells into the brain due to their low expression of leukocyte adhesion molecules, consequently hampering immunotherapy [29].

Proper function of the BBB also requires other cells such as astrocytes, pericytes, basal lamina, neurons and the ECM. Astrocytes are vital for BBB formation and maintenance [29], being closely linked to the endothelial cells by astrocytic endfeet, which cover more than 99% of the capillaries [35]. The endfeet produce a variety of proteins that regulate the composition of the ECM, immune cell infiltration, BBB permeability, and BBB integrity [29, 33, 36]. Astrocytic endfeet are important for maintaining junctional complexes regulating BBB permeability [36]. Pericytes are multi-functional cells that are key regulators of BBB permeability and vascular function, regulating vessel formation and vessel maturation [29, 30, 36]. The basal lamina, formed by endothelial cells, astrocytes, and pericytes, consists of an ECM that is both responsible and influential to proper BBB function [36]. Microglia are resident immune cells that act as a first line of defense in the CNS by screening the brain parenchyma for blood-borne substances and potential inflammatory stimuli [37]. Due to their low turnover rate, these cells exist as permanent populations within the brain [38]. Microglia, in combination with macrophages, also play a role in the regulation of vascular growth by secreting various signals [39]. Together these structures create an impermeable barrier.



## **BBB/Blood-Tumor Barrier (BTB) Pathology**

The presence of a brain tumor disrupts the regulation of the BBB, resulting in an altered BBB phenotype that is referred to as the blood-tumor barrier (BTB) [36, 40]. Characterization of the BBB/BTB phenotypes of different tumors is important to understand the extent of effectiveness of drug delivery for the treatment of primary brain tumors. In the following paragraphs, the BBB/BTB of several primary brain tumors is discussed.

### ***Adult Glioblastoma***

The most common malignant primary brain tumor in adults is glioblastoma (GBM), with patients having a median survival of one year. It is believed that the presence of the BBB/BTB is a major influence on the effectiveness of drug delivery [41, 42]. GBM is a highly heterogeneous malignancy characterized by aggressive and invasive growth, and is one of the most hypoxic and angiogenic brain tumors [43, 44]. The microenvironment of GBM consists of specialized niches, each of which display different BBB properties [37, 43]. In the core of the tumor, higher oxygen demands lead to severe hypoxia and necrosis, and subsequent BBB/BTB defects, especially in late-stage disease. Glioma cells that have migrated further

into the brain parenchyma reside behind an intact BBB, demonstrating the heterogeneity of GBM [37, 44]. This heterogeneity can be visualized by magnetic resonance imaging (MRI), where the core of the tumor is enhanced by contrast agent on MRI, indicating a disrupted BBB/BTB, while (often large) areas are not enhanced on MRI, showing a mostly intact BBB of the diffusely growing tumor [44].

GBM vessel areas that are contrast-enhanced on MRI are characterized by aberrant and disorganized angiogenesis, resulting in permeable vessels with defective pericyte coverage and an abnormal basement membrane- all suggestive of BBB breakdown [43, 45, 46]. The disrupted BBB is typified by a disturbed organization of permeable endothelial cell junctions due to the downregulation of claudin-5, claudin-3, and occludin [37, 47, 48]. *In vitro*, it was shown that GBM cells disrupt the BBB by secreting soluble factors that break down tight junctions [49]. The BBB is then further degraded via displacement of non-neoplastic astrocytes by tumor cells, that in turn allow tumor-derived chemokines and cytokines to cross the BBB [50]. Furthermore, the loss of aquaporin 4 (AQP4) results in the polarization of astrocytic endfeet, reducing the astrocytic endfeet coverage of the endothelial cells, resulting in BBB disruption [51, 52]. A study showed that relocation of AQP4 in GBM coincides with a redistributed or diminished expression of argin, which is associated with the loss of several tight junction proteins [53, 54].

The presence of ABC transporters and organic anion transporting polypeptides (OATP) transporters influences the resistance of tumor cells to chemotherapeutics [55]. These transporters have been identified in both GBM tumor vasculature and tumor cells [55, 56]. Remarkably, MDR1, MRP4, and MRP5 are expressed in glioma cells and astrocytes, while these receptors are usually not expressed by glial cells and astrocytes [55, 56]. In addition, BCRP expression is also increased in GBM cells [56, 57]. OATPA2 and OATP2B1 have been detected on the luminal membrane of endothelial cells in both the BBB and BTB, but not in glioma cells themselves [55].

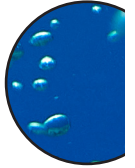
### ***Pediatric Brain Tumors***

In children, primary brain tumors are the leading cause of cancer-related morbidity and mortality [3, 4]. The most common malignant pediatric primary brain tumors are medulloblastoma, ependymoma, diffuse intrinsic pontine glioma (DIPG), and atypical teratoid/rhabdoid tumor (AT/RT) [3, 4, 58]. Even though advances in surgery, adjuvant therapy, and research have resulted in the increase of survival rates of some of these brain tumor types, such as medulloblastoma, other tumor types still have a dismal prognosis [4, 58, 59]. Like for adult brain tumors, the poor prognosis can in part be attributed to the BBB phenotype of malignant pediatric brain cancers.

### ***Medulloblastoma***

Medulloblastoma is the most common malignant embryonal brain tumor [3, 58, 60]. These tumors can be classified based on histology (distinguishing classic-, desmoplastic-, and

large-cell medulloblastoma), or molecular signature (WNT, Sonic hedgehog [SHH], Group 3 and Group 4) [60, 61]. Despite the general survival of medulloblastoma patients having increased significantly in the past decades, a subset of patients still have poor outcomes, partly due to compromised vasculature and the presence of an intact BBB [3, 7, 58]. Medulloblastomas have a low capillary permeability and blood flow compared with normal cerebellum, although the capillary density is heterogeneous throughout the tumor [62, 63]. Some types of medulloblastoma show an absence of astrocytes while other types show disruption of astrocytes from endothelial cells in the tumor parenchyma [63]. In addition, over 40% of medulloblastomas demonstrate the expression of MDR1 efflux transporters in the tumor, indicating an effective BTB [64]. Group 3 medulloblastoma specifically overexpress BCRP, MRP7 (ABCC10), MRP5 (ABCC5), and MRP1 [65]. As an exception, WNT medulloblastomas, which have the best prognosis of the different subgroups, lack a functional BBB [3, 58, 60]. This BBB dysfunction is likely due to aberrant, antagonistic medulloblastoma-endothelial cell WNT signaling, which renders the non-CNS vasculature porous, resulting in a hemorrhagic vasculature, aberrant fenestration, and higher vascular density compared with the other subtypes [7]. Overall, the BBB/BTB and the vasculature are affected in medulloblastoma, influencing the outcome of therapy.



### ***Ependymoma***

Ependymomas are slow-growing tumors that are treated with surgery and local fractionated radiotherapy, while the potential benefit of chemotherapy is still under debate [3, 4, 58]. Ependymomas overexpress vascular endothelial growth factor (VEGF), a main marker of angiogenesis [66]. Ependymomas exert an aberrant vasculature, the extent of which is dependent on tumor grade [67, 68]. The mean vessel area is larger for myxopapillary ependymoma grade I, low-grade ependymoma grade II, and anaplastic ependymoma grade III compared with normal cerebral and cerebellar tissue [67]. In addition, grade III has a higher blood vessel density compared with grade II, but the diameter of blood vessels for grade II was found to be larger than that for grade III [67, 68]. Subependymoma grade I has fewer vessels than normal cerebral tissue [67]. In contrast, Wagemakers *et al.* found that microvessel density in neovasculature does not differ by age, gender, tumor location, or tumor grade. The microvessel density of ependymoma was increased and comparable to GBM [66]. Little is known about the expression of BBB proteins and transporters in ependymomas. MDR1, BCRP, and ABCB1 were not significantly altered in grade II and III ependymomas [69, 70]. Hence, the different ependymoma grades have characteristic vasculature profiles, however little is known about the BBB.

### ***Diffuse Intrinsic Pontine Glioma***

DIPG is a high-grade glioma of the brainstem with a median survival of 11 months [59]. The poor prognosis is mainly due to the tumor location making complete resection of the tumor impossible [71]. At diagnosis, many patients have an absence of contrast enhancement on MRI [72]. Little is known about the BBB/BTB pathology in DIPG. One study indicated highly active SHH signaling which decreased BBB permeability in DIPG [73, 74]. Furthermore, efflux transporters MDR1, BCRP, and MRP1 are present in endothelial cells, and MRP1 is expressed in tumor cells [75]. Not only the tumor, but also its location can affect the BBB phenotype.

In healthy non-human primates, BBB heterogeneity was observed with differential penetration of temozolomide between the pontine region, the cortex, and the CSF [72, 76]. Since the brain region already has an influence on the BBB permeability, tumor in the pontine region might have a different effect compared with other supratentorial tumors. However, there is no direct evidence that the BBB is intact in DIPG.

### ***Atypical Teratoid/Rhabdoid Tumor***

AT/RT tumors are highly aggressive embryonal tumors most commonly found in infants and young children [3, 77]. The overall median survival is 17 months [78]. Improvement of treatment protocols has resulted in only a small increase of survival, as only a subset of patients respond to treatment [77, 79, 80]. MRI images of AT/RT patients show contrast enhancement, indicating BBB disruption [79, 81]. However, little is known about the BBB/BBB and the vasculature in AT/RT. Only one paper has been published on the vasculature and BBB alterations in AT/RT, showing a significant decrease in vessel density and an increase in vessel diameter of the tumor vasculature [79]. Endothelial cells in existing blood vessels maintained expression of claudin-5 but showed displacement of claudin-5 localization compared with healthy tissue [79]. In neovasculature, expression of claudin-5 was lost. In contrast, glucose transporter 1 (GLUT1) was lost in both existing endothelial cells as well as in neovasculature [79]. In order to improve median survival, more research is needed to determine to what extent the BBB/BBB is compromised, and how this can be used for efficient drug delivery.

## **Drug Delivery Methods to Overcome the BBB**

Several drug delivery methods have been used to overcome the BBB. Nanoparticles can be used to modify the drug permeability of an existing drug. Other methods such as FUS, CED, intranasal and intra-arterial delivery can be used to temporarily disrupt or bypass the BBB to deliver drugs into the brain parenchyma.

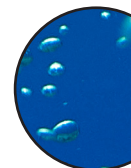
### ***Nanoparticles***

Nanoparticles are particles created from different packaging materials such as lipids, polymers, and metals that can be utilized as a proxy to efficiently deliver drugs. These particles can be designed in various compositions that, for example, increase their half-life or ability to target a specific receptor [23, 36]. Nanoparticles have been successfully used in the treatment of several types of cancer [21].

Nanoparticles cross the BBB in a variety of ways, including endocytosis, receptor-mediated transcytosis, or the enhanced permeability and retention (EPR) effect [82-84]. The EPR effect exploits the leaky vasculature of solid tumors where the nanoparticle can extravasate locally into the tumor [83]. After the nanoparticle is extravasated, the encapsulated drugs are slowly released into the tissue. Since nanoparticles are not able to cross normal vascula-

ture in most organs, this reduces both peripheral and systemic toxicities [6, 21, 84].

Nanoparticles are able to cross the leaky BBB, which could be a potential method for drug delivery for brain tumors. However, in clinical trials nanoparticles have not been able to reach therapeutic concentrations in the tumor [20, 36]. For example, GBM is characterized by both intact and disrupted BBB niches. Due to the heterogenous BBB/BTB in GBM, drugs are not homogenously distributed in the tumor leaving parts of the tumor untreated. In addition, GBM is characterized by high interstitial pressure and hypoxia which negatively influences the passage of nanoparticles in these areas [84]. Therefore, the use of nanoparticles as a delivery method for the treatment of brain cancer has not yet been successful [36]. However, nanoparticles exhibiting beneficial properties, such as sustained release of a drug over a prolonged period of time, could potentially be useful in combination with other drug delivery methods for treatment of brain tumors [85, 86].



### ***Focused Ultrasound***

Microbubble-mediated focused ultrasound (FUS), or sonoporation, is a minimally/non-invasive method for targeted drug delivery into the brain tumor [25, 87, 88]. Upon acoustic pressure from a transducer, microbubbles are pressed against the endothelial cell wall and start to vibrate. The vibration induces stress on the endothelial cell wall resulting in the temporary and local disruption of the BBB [89]. The combination of ultrasound with microbubbles is considered to be safe, since no neuronal damage, apoptosis, ischemia or long-term vascular damage has been observed upon treatment [87]. The combination of FUS with conventional chemotherapeutics, antibodies, nanoparticles, and gene-based therapies allows for a range of possibilities [36, 85, 90].

The therapeutic window of microbubble-mediated FUS is dependent on the closure dynamics of the BBB after disruption. The BBB slowly closes within several hours, whereas larger molecules such as nanoparticles have a shorter therapeutic window compared with smaller molecules [91]. In addition, drug half-life and penetration depth after sonoporation is also drug dependent. Therefore, the pharmacokinetic profile of the drug is an important parameter for treatment success [92]. The heterogeneous nature of the BBB phenotype poses less of a problem for FUS since the focused ultrasound can be applied over the entire tumor area. Furthermore, the vasculature is important for the delivery of microbubbles and drugs since the blood vessels are key to deliver microbubbles and drugs to the tumor. Brain tumors with a low vessel density might be less suited for focused ultrasound. Moreover, efflux transporters hamper drug accumulation in the brain. However, it was recently discovered that FUS suppresses MDR1, which could aid in the increase of drug accumulation in the tumor tissue [93]. Many brain tumors such as GBM, medulloblastoma, and DIPG express ABC transporters. The use of FUS could potentially increase the accumulation of drugs in these tumors.

For diffuse infiltrating tumors such as GBM and DIPG, FUS is a promising technique since it is a non-invasive drug delivery method and that can target the tumor. Recently, the first clinical MRI-guided FUS study was concluded for GBM patients [94]. A 1.5- to sevenfold increased concentration of temozolomide in sonicated versus unsonicated tumor tissue was observed



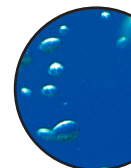
in two patients whose tissue could be analyzed. The treatment was well tolerated in all patients [94]. Implanted ultrasound devices have been studied in several clinical studies: CarThera (SonoCloud) is an implantable ultrasound device that has been used in phase I clinical studies in combination with systemic administration of carboplatin [95, 96]. Treatment via FUS prolonged progression-free survival in 11 GBM patients presenting BBB disruption compared with 8 patients with intact BBB [95, 96]. The downside of implanted ultrasound devices is the requirement of invasive surgery, they do not specifically target the tumor site, and are mostly suitable for superficial brain tumors. As such, these devices will be limited for treating DIPG as they do not reach the pontine region. Furthermore, combining FUS with immunotherapy might be a powerful combination for the treatment of brain cancer. Immune cells are not able to cross the BBB since CNS endothelial cells have a low expression of leukocyte adhesion molecules [29]. Immune cells can extravasate after the BBB is disrupted with FUS. *In vivo* studies are now investigating the possibilities of immunotherapy in combination with FUS [36]. The non-invasive nature of FUS in combination with numerous drugs makes FUS a versatile and promising technique for drug and/or immune therapy delivery for various brain tumors.

### ***Convection Enhanced Delivery***

CED has been proposed as a promising strategy for drug delivery to the CNS. This method involves placing one or more intracranial catheters connected to an external infusion pump, which allows for the direct delivery of therapeutic agents into target tissues via an established pressure gradient [24, 97, 98]. The local infusion ensures a higher therapeutic concentration in the brain parenchyma with less systemic toxicity [24, 97]. The pressure-driven bulk flow of the desired drug solution allows for more uniform infusion over larger volumes [98-101]. The infusion volume is not dependent on molecule size and weight [98, 101]. The drug can travel for a few centimeters, increasing the volume treated, and makes it suitable for tumors with a low vascular density [101]. However, this technique also has some caveats. Highly vascular tumors are potentially less suited since the infused drugs can be excreted/absorbed into the vasculature [102]. The catheters should not be placed inside or around necrotic tissues since the drug can pool together in this necrotic area, thereby not exposing the entire tumor to the drug [101].

CED is in clinical trials for multiple brain cancers, with most trials focusing on GBM and DIPG [100, 103, 104]. However, clinical trials have had major setbacks and so far only one phase III trial has been completed [101, 104, 105]. In this multicenter phase III study, which included 276 patients with recurrent GBM, no difference in median survival was observed between treatment with CED using cintredekin besudotox (IL13-PE38QQR) and GLIADEL wafers, a carmustine implant [105]. For DIPG, only phase I studies have been conducted but without significant improvement in survival. While CED in combination with IL13-PE38QQR reported that tumor coverage was not optimal, 124I-8H9 administered with CED did show good tumor coverage with a single dose [103, 106]. The study was not powered for survival and a follow-up phase II study will soon be initiated [103]. Besides the fact that the optimal CED drug with the highest therapeutic index has yet to be found, the limited success of CED can be attributed to a number of factors. First, CED causes a heterogeneous pressure gradient in the tumor, resulting in a non-uniform drug distribution and inhomogeneous drug

concentrations in the treated area [99]. Second, catheter-induced tissue damage and reflux can be seen contiguous to the catheter, with 'intrinsic' backflow of solute and air bubbles [99]. Third, the mixed tissue environment can cause rapid efflux of many drugs lowering the concentration of drugs in the brain [107]. Additionally, other factors may affect efficient delivery, such as high and varying tumor interstitial fluid pressure, which are reviewed elsewhere [100, 99]. Provided that these problems can be resolved, CED represents a suitable technique to overcome the BBB.



### ***Intranasal Delivery***

Intranasal delivery is an alternative method to overcome the BBB. The nasal cavity provides access to the brain parenchyma without interference of the BBB. The drugs are delivered to the brain via paracellular, transcellular, and neuronal transport from the neuroepithelium of the nasal cavity to the CNS. However, not all drugs are suitable for intranasal drug delivery, since specific physicochemical properties and formulations determine the bioavailability of the drug in the brain. Generally, lipophilic drugs with low molecular weight show a more ready bioavailability after nasal administration than charged hydrophilic drugs. Drug formulations can be modified to increase drug bioavailability with, for example, liposomes, cyclodextrans, and nanoparticles. In addition, the advantage of drug delivery through the nose is that the drugs are not metabolized by first-pass metabolism. However, a disadvantage is the small volume that can be administered via intranasal delivery [26, 108, 109].

Only limited results have been published on clinical trials using intranasal drug delivery. Perillyl alcohol has been used as an intranasal drug for the treatment of malignant glioma [110, 111]. The four-times daily administration of perillyl alcohol resulted in a 6-month progression-free survival in ~ 45% of a limited number of cases [110, 111]. Potential problems with intranasal drug delivery are the non-specificity of drugs, which can result in toxicity. Toxicity can be minimized by targeting tumor cells. For example, GRN163 has been investigated *in vivo* which specifically targets telomerase. The treatment resulted in specific targeting of the tumor and minimal toxicity [112]. Other ways to decrease toxicity to surrounding brain tissue is the combination of intranasal drug delivery with microbubble-mediated FUS. The combination of these methods has shown an increased and specific drug uptake in the targeted tumor region [113, 114]. Only a few studies have investigated the use of intranasal drug delivery for the treatment of primary brain tumors; therefore, it is difficult to conclude if intranasal drug delivery is a suitable technique to overcome the BBB.

### ***Intra-Arterial Drug Delivery***

Intra-arterial drug delivery administers drugs directly into an artery in the proximity of the tumor [27, 115]. After the targeted area is cannulated, the drug is released into the blood vessel. In addition to the drug, a hyperosmolar drug such as mannitol can be administered to open the BBB locally [115, 116]. This technique has been successful in the treatment of retinoblastoma and liver cancer [27]. However, several clinical trials and cases did not report significant improvement in survival. Intra-arterial drug delivery in a small set of medulloblas-

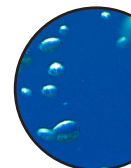
toma patients treated with celyvir (autologous mesenchymal stem cells infected with adenovirus ICOVIR5), a 7-day treatment course of oral procarbazine, intravenous vincristine in combination with four cycles of intra-arterial carmustine, or conventional chemotherapeutics in combination with mannitol, did not lead to remission of the disease in most patients [117-119]. In ependymoma, a small cohort of patients were treated with intra-arterial drug delivery with carmustine, bevacizumab, and cetuximab, and responded to the treatment [120, 121]. However, toxicity concerns arose for the treatment with carmustine, epipodophyllotoxin, and cisplatin [120]. Several clinical studies investigated the use of intra-arterial drug delivery for GBM patients. The reported survival ranged from 20 weeks to 10 months following treatment with nimustine, bevacizumab, or carboplatin in combination with other conventional chemotherapy [122-125]. Toxicity and low drug efficacy seem to hamper the use of intra-arterial drug delivery in primary brain tumors [27, 115, 120, 126].

## Conclusions

Is there a way to overcome the BBB to give modern therapy a chance? So far, we have discussed several drug delivery techniques that have been developed to overcome the BBB. However, most techniques have not led to a significant increase in survival in patients with primary brain tumors. One of the main reasons that drug delivery techniques have not been successful is the limited knowledge of the BBB/BBB and vasculature in both adult and pediatric brain tumors. We have reviewed several BBB pathologies, of which almost all have incomplete information regarding the BBB pathology of specific tumors. Pediatric medulloblastoma has illustrated the importance of knowledge about the characterization of the BBB to improve survival. Medulloblastoma WNT subtype has a dysfunctional and high vascular density compared with the other subtypes, making this tumor subtype treatable with conventional therapies. Understanding BBB/BBB properties and challenges can provide more insight into the optimization of drug delivery techniques. For example, highly vascularized tumors might benefit more from FUS, as this technique requires the systemic administration of microbubbles and drugs. Furthermore, FUS can suppress efflux transporters, which could potentially benefit the accumulation and retainment of drugs in the brain parenchyma. In contrast, CED is especially suited for tumors that have a low vascular density and an intact BBB to prevent 'leakage' of infused drugs from the tumor site. A multimodal approach might even be necessary to treat brain tumors by combining strategies such as FUS with nanoparticles or immunotherapy. We therefore urge the collaboration of physicians, researchers, and biotechnical companies to characterize BBB/BBB from patient samples to help personalize the chemotherapy delivery method.

## References

1. Howlader N, N.A., Krapcho M, Miller D, Brest A, Yu M, Ruhl J, Tatalovich Z, Mariotto A, Lewis DR, Chen HS, Feuer EJ, Cronin KA *SEER Cancer Statistics Review 1975-2016*. Available from: [https://seer.cancer.gov/csr/1975\\_2016/](https://seer.cancer.gov/csr/1975_2016/).
2. Allemani, C., et al., *Global surveillance of trends in cancer survival 2000–14 (CONCORD-3): analysis of individual records for 37 513 025 patients diagnosed with one of 18 cancers from 322 population-based registries in 71 countries*. *The Lancet*, 2018. **391**(10125): p. 1023-1075.
3. Wells, E.M. and R.J. Packer, *Pediatric brain tumors*. CONTINUUM: Lifelong Learning in Neurology, 2015. **21**(2): p. 373-396.
4. Karajannis, M., J.C. Allen, and E.W. Newcomb, *Treatment of pediatric brain tumors*. *Journal of cellular physiology*, 2008. **217**(3): p. 584-589.
5. Patel, M.M. and B.M. Patel, *Crossing the blood–brain barrier: recent advances in drug delivery to the brain*. *CNS drugs*, 2017. **31**(2): p. 109-133.
6. Dong, X., *Current Strategies for Brain Drug Delivery*. *Theranostics*, 2018. **8**(6): p. 1481-1493.
7. Phoenix, T.N., et al., *Medulloblastoma genotype dictates blood brain barrier phenotype*. *Cancer Cell*, 2016. **29**(4): p. 508-522.
8. Hobbs, S.K., et al., *Regulation of transport pathways in tumor vessels: role of tumor type and microenvironment*. *Proceedings of the National Academy of Sciences*, 1998. **95**(8): p. 4607-4612.
9. Hawkins, B.T. and T.P. Davis, *The blood-brain barrier/neurovascular unit in health and disease*. *Pharmacological reviews*, 2005. **57**(2): p. 173-185.
10. Ladecola, C., *Neurovascular regulation in the normal brain and in Alzheimer’s disease*. *Nature Reviews Neuroscience*, 2004. **5**(5): p. 347-360.
11. Abbott, N.J., L. Rönnebeck, and E. Hansson, *Astrocyte–endothelial interactions at the blood–brain barrier*. *Nature reviews neuroscience*, 2006. **7**(1): p. 41-53.
12. Partridge, W., *The blood-brain barrier: bottleneck in brain development*. *J. Am. Soc. Exp. Neuro Ther*, 2005. **2**: p. 3-14.
13. Abbott, N.J., et al., *Structure and function of the blood–brain barrier*. *Neurobiology of disease*, 2010. **37**(1): p. 13-25.
14. Liu, X., et al., *Development of a computational approach to predict blood-brain barrier permeability*. *Drug metabolism and disposition*, 2004. **32**(1): p. 132-139.
15. Lipinski, C.A., *Lead- and drug-like compounds: the rule-of-five revolution*. *Drug Discov*

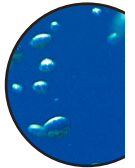


Today Technol, 2004. **1**(4): p. 337-341.

16. Ghose, A.K., V.N. Viswanadhan, and J.J. Wendoloski, *A knowledge-based approach in designing combinatorial or medicinal chemistry libraries for drug discovery. 1. A qualitative and quantitative characterization of known drug databases*. Journal of combinatorial chemistry, 1999. **1**(1): p. 55-68.
17. Azad, T.D., et al., *Therapeutic strategies to improve drug delivery across the blood-brain barrier*. Neurosurgical focus, 2015. **38**(3): p. E9.
18. Zhan, C. and W. Lu, *The blood-brain/tumor barriers: challenges and chances for malignant gliomas targeted drug delivery*. Current pharmaceutical biotechnology, 2012. **13**(12): p. 2380-2387.
19. Pardridge, W.M., *Blood-brain barrier delivery*. Drug Discov Today, 2007. **12**(1-2): p. 54-61.
20. Bobo, D., et al., *Nanoparticle-based medicines: a review of FDA-approved materials and clinical trials to date*. Pharmaceutical research, 2016. **33**(10): p. 2373-2387.
21. Lockman, P.R., et al., *Nanoparticle Technology for Drug Delivery Across the Blood-Brain Barrier*. Drug Development and Industrial Pharmacy, 2002. **28**(1): p. 1-13.
22. Matsumura, Y. and H. Maeda, *A new concept for macromolecular therapeutics in cancer chemotherapy: mechanism of tumorotropic accumulation of proteins and the antitumor agent smancs*. Cancer research, 1986. **46**(12 Part 1): p. 6387-6392.
23. Gaillard, P.J., et al., *Pharmacokinetics, brain delivery, and efficacy in brain tumor-bearing mice of glutathione pegylated liposomal doxorubicin (2B3-101)*. PloS one, 2014. **9**(1): p. e82331.
24. Bobo, R.H., et al., *Convection-enhanced delivery of macromolecules in the brain*. Proceedings of the National Academy of Sciences, 1994. **91**(6): p. 2076-2080.
25. Hynynen, K., et al., *Noninvasive MR imaging-guided focal opening of the blood-brain barrier in rabbits*. Radiology, 2001. **220**(3): p. 640-646.
26. Pires, A., et al., *Intranasal drug delivery: how, why and what for?* Journal of pharmacy & pharmaceutical sciences, 2009. **12**(3): p. 288-311.
27. Joshi, S., et al., *Intraarterial drug delivery for glioblastoma multiforme*. Journal of neuro-oncology, 2015. **124**(3): p. 333-343.
28. Banerjee, S. and M.A. Bhat, *Neuron-glia interactions in blood-brain barrier formation*. Annu. Rev. Neurosci., 2007. **30**: p. 235-258.
29. Langen, U.H., S. Ayloo, and C. Gu, *Development and cell biology of the blood-brain barrier*. Annual review of cell and developmental biology, 2019. **35**: p. 591-613.
30. Daneman, R. and B. Engelhardt, *Brain barriers in health and disease*. Neurobiology of

Disease, 2017. **107**: p. 1-3.

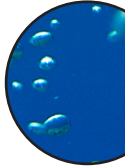
31. Löscher, W. and H. Potschka, *Drug resistance in brain diseases and the role of drug efflux transporters*. Nature Reviews Neuroscience, 2005. **6**(8): p. 591-602.
32. Löscher, W. and H. Potschka, *Blood-brain barrier active efflux transporters: ATP-binding cassette gene family*. NeuroRx, 2005. **2**(1): p. 86-98.
33. Bart, J., et al., *The blood-brain barrier and oncology: new insights into function and modulation*. Cancer treatment reviews, 2000. **26**(6): p. 449-462.
34. Reese, T. and M.J. Karnovsky, *Fine structural localization of a blood-brain barrier to exogenous peroxidase*. The Journal of cell biology, 1967. **34**(1): p. 207-217.
35. Mathiisen, T.M., et al., *The perivascular astroglial sheath provides a complete covering of the brain microvessels: an electron microscopic 3D reconstruction*. Glia, 2010. **58**(9): p. 1094-1103.
36. Arvanitis, C.D., G.B. Ferraro, and R.K. Jain, *The blood–brain barrier and blood–tumour barrier in brain tumours and metastases*. Nature Reviews Cancer, 2019: p. 1-16.
37. Liebner, S., et al., *Functional morphology of the blood–brain barrier in health and disease*. Acta neuropathologica, 2018: p. 1-26.
38. Charles, N.A., et al., *The brain tumor microenvironment*. Glia, 2011. **59**(8): p. 1169-1180.
39. Engelhardt, B. and S. Liebner, *Novel insights into the development and maintenance of the blood–brain barrier*. Cell and tissue research, 2014. **355**(3): p. 687-699.
40. Wei, X., et al., *Brain tumor-targeted drug delivery strategies*. Acta pharmaceutica sinica B, 2014. **4**(3): p. 193-201.
41. Ostrom, Q.T., et al., *CBTRUS statistical report: primary brain and other central nervous system tumors diagnosed in the United States in 2010–2014*. Neuro-oncology, 2017. **19**: p. 1-88.
42. Liu, X.-m., et al., *Clinical significance of vasculogenic mimicry in human gliomas*. Journal of neuro-oncology, 2011. **105**(2): p. 173-179.
43. Hambardzumyan, D. and G. Bergers, *Glioblastoma: defining tumor niches*. Trends in cancer, 2015. **1**(4): p. 252-265.
44. Van Tellingen, O., et al., *Overcoming the blood–brain tumor barrier for effective glioblastoma treatment*. Drug Resistance Updates, 2015. **19**: p. 1-12.
45. Ferrara, N. and A.P. Adamis, *Ten years of anti-vascular endothelial growth factor therapy*. Nature reviews Drug discovery, 2016. **15**(6): p. 385-403.
46. Quail, D.F. and J.A. Joyce, *The microenvironmental landscape of brain tumors*. Cancer cell, 2017. **31**(3): p. 326-341.



47. Liebner, S., et al., *Claudin-1 and claudin-5 expression and tight junction morphology are altered in blood vessels of human glioblastoma multiforme*. *Acta neuropathologica*, 2000. **100**(3): p. 323-331.
48. Wolburg, H., et al., *Localization of claudin-3 in tight junctions of the blood-brain barrier is selectively lost during experimental autoimmune encephalomyelitis and human glioblastoma multiforme*. *Acta neuropathologica*, 2003. **105**(6): p. 586-592.
49. Schneider, S.W., et al., *Glioblastoma cells release factors that disrupt blood-brain barrier features*. *Acta neuropathologica*, 2004. **107**(3): p. 272-276.
50. Bergers, G. and S. Song, *The role of pericytes in blood-vessel formation and maintenance*. *Neuro-oncology*, 2005. **7**(4): p. 452-464.
51. Nicchia, G., et al., *The role of aquaporin-4 in the blood–brain barrier development and integrity: studies in animal and cell culture models*. *Neuroscience*, 2004. **129**(4): p. 935-944.
52. Mader, S. and L. Brimberg, *Aquaporin-4 water channel in the brain and its implication for health and disease*. *Cells*, 2019. **8**(2): p. 90.
53. Warth, A., S. Kröger, and H. Wolburg, *Redistribution of aquaporin-4 in human glioblastoma correlates with loss of agrin immunoreactivity from brain capillary basal laminae*. *Acta neuropathologica*, 2004. **107**(4): p. 311-318.
54. Rascher, G., et al., *Extracellular matrix and the blood-brain barrier in glioblastoma multiforme: spatial segregation of tenascin and agrin*. *Acta neuropathologica*, 2002. **104**(1): p. 85-91.
55. Bronger, H., et al., *ABCC drug efflux pumps and organic anion uptake transporters in human gliomas and the blood-tumor barrier*. *Cancer research*, 2005. **65**(24): p. 11419-11428.
56. Wijaya, J., Y. Fukuda, and J.D. Schuetz, *Obstacles to brain tumor therapy: key ABC transporters*. *International journal of molecular sciences*, 2017. **18**(12): p. 2544.
57. Bhatia, P., et al., *Breast cancer resistance protein (BCRP/ABCG2) localises to the nucleus in glioblastoma multiforme cells*. *Xenobiotica*, 2012. **42**(8): p. 748-755.
58. Pollack, I.F., S. Agnihotri, and A. Broniscer, *Childhood brain tumors: current management, biological insights, and future directions: JNSPG 75th Anniversary Invited Review Article*. *Journal of Neurosurgery: Pediatrics*, 2019. **23**(3): p. 261-273.
59. Hoffman, L.M., et al., *Clinical, radiologic, pathologic, and molecular characteristics of long-term survivors of diffuse intrinsic Pontine Glioma (DIPG): a collaborative report from the international and European Society for Pediatric Oncology DIPG registries*. *Journal of Clinical Oncology*, 2018. **36**(19): p. 1963–1972.
60. Northcott, P.A., et al., *Medulloblastoma comprises four distinct molecular variants*.

Journal of clinical oncology, 2011. **29**(11): p. 1408-1414.

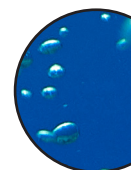
61. Taylor, M.D., et al., *Molecular subgroups of medulloblastoma: the current consensus*. Acta neuropathologica, 2012. **123**(4): p. 465-472.
62. Warnke, P.C., et al., *Capillary physiology of human medulloblastoma: impact on chemotherapy*. Cancer: Interdisciplinary International Journal of the American Cancer Society, 2006. **107**(9): p. 2223-2227.
63. Hong, C.S., et al., *Characterization of the blood brain barrier in pediatric central nervous system neoplasms*. Journal of interdisciplinary histopathology, 2016. **4**(2): p. 29-33.
64. Othman, R.T., et al., *Overcoming multiple drug resistance mechanisms in medulloblastoma*. Acta neuropathologica communications, 2014. **2**(57).
65. Morfouace, M., et al., *ABCG2 transporter expression impacts group 3 medulloblastoma response to chemotherapy*. Cancer research, 2015. **75**(18): p. 3879-3889.
66. Wagemakers, M., et al., *Tumor vessel biology in pediatric intracranial ependymoma*. Journal of Neurosurgery: Pediatrics, 2010. **5**(4): p. 335-341.
67. Gilhuis, H.J., et al., *Three-dimensional (3D) reconstruction and quantitative analysis of the microvasculature in medulloblastoma and ependymoma subtypes*. Angiogenesis, 2006. **9**(4): p. 201-208.
68. Duda-Szymanska, J. and W.a. Papierz, *Morphological analysis of vascular density in ependymomas*. Folia neuropathologica, 2007. **45**(3): p. 115-119.
69. Chou, P.M., et al., *Ependymomas in children express the multidrug resistance gene: immunohistochemical and molecular biologic study*. Pediatric Pathology & Laboratory Medicine, 1996. **16**(4): p. 551-561.
70. Ginguené, C., et al., *P-glycoprotein (ABCB1) and Breast Cancer Resistance Protein (ABCG2) Localize in the Microvessels Forming the Blood-Tumor Barrier in Ependymomas*. Brain Pathology, 2010. **20**(5): p. 926-935.
71. Jansen, M.H., et al., *Bevacizumab targeting diffuse intrinsic pontine glioma: results of <sup>89</sup>Zr-bevacizumab PET imaging in brain tumor models*. Molecular cancer therapeutics, 2016. **15**(9): p. 2166-2174.
72. Warren, K.E., *Beyond the blood: brain barrier: the importance of central nervous system (CNS) pharmacokinetics for the treatment of CNS tumors, including diffuse intrinsic pontine glioma*. Frontiers in oncology, 2018. **8**: p. 239.
73. Sajesh, B., et al., *DIPG-18. Sonic hedgehog (SHH) signalling promotes blood brain barrier (BBB) integrity in diffuse intrinsic pontine glioma (DIPG)*. Neuro-Oncology, 2019. **21**(Suppl 2): p. ii72.
74. Chapouly, C., et al., *Role of Hedgehog Signaling in Vasculature Development, Differen-*





- tiation, and Maintenance*. International journal of molecular sciences, 2019. **20**(12): p. 3076.
75. Veringa, S.J., et al., *In vitro drug response and efflux transporters associated with drug resistance in pediatric high grade glioma and diffuse intrinsic pontine glioma*. PloS one, 2013. **8**(4).
76. McCully, C.M., et al., *Model for concomitant microdialysis sampling of the pons and cerebral cortex in rhesus macaques (Macaca mulatta)*. Comparative medicine, 2013. **63**(4): p. 355-360.
77. Chi, S.N., et al., *Intensive multimodality treatment for children with newly diagnosed CNS atypical teratoid rhabdoid tumor*. Journal of Clinical Oncology, 2009. **27**(3): p. 385-389.
78. Ginn, K.F. and A. Gajjar, *Atypical teratoid rhabdoid tumor: current therapy and future directions*. Frontiers in oncology, 2012. **2**: p. 114.
79. Meel, M.H., et al., *MEK/MELK inhibition and blood–brain barrier deficiencies in atypical teratoid/rhabdoid tumors*. Neuro-oncology, 2020. **22**(1): p. 58-69.
80. Hilden, J.M., et al., *Central nervous system atypical teratoid/rhabdoid tumor: results of therapy in children enrolled in a registry*. Journal of clinical oncology, 2004. **22**(14): p. 2877-2884.
81. Arslanoglu, A., et al., *Imaging findings of CNS atypical teratoid/rhabdoid tumors*. American journal of neuroradiology, 2004. **25**(3): p. 476-480.
82. Vieira, D.B. and L.F. Gamarra, *Getting into the brain: liposome-based strategies for effective drug delivery across the blood–brain barrier*. International journal of nanomedicine, 2016. **11**: p. 5381–5414.
83. Allen, T.M. and P.R. Cullis, *Drug delivery systems: entering the mainstream*. Science, 2004. **303**(5665): p. 1818-1822.
84. Zhao, M., et al., *Nanocarrier-based drug combination therapy for glioblastoma*. Theranostics, 2020. **10**(3): p. 1355.
85. Etame, A.B., et al., *Enhanced delivery of gold nanoparticles with therapeutic potential into the brain using MRI-guided focused ultrasound*. Nanomedicine: Nanotechnology, Biology and Medicine, 2012. **8**(7): p. 1133-1142.
86. Sawyer, A.J., et al., *Convection-enhanced delivery of camptothecin-loaded polymer nanoparticles for treatment of intracranial tumors*. Drug delivery and translational research, 2011. **1**(1): p. 34-42.
87. McDannold, N., et al., *Temporary disruption of the blood–brain barrier by use of ultrasound and microbubbles: safety and efficacy evaluation in rhesus macaques*. Cancer research, 2012. **72**(14): p. 3652-3663.

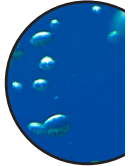
88. Burgess, A. and K. Hynynen, *Noninvasive and targeted drug delivery to the brain using focused ultrasound*. ACS chemical neuroscience, 2013. **4**(4): p. 519-526.
89. Dasgupta, A., et al., *Ultrasound-mediated drug delivery to the brain: principles, progress and prospects*. Drug Discov Today Technol, 2016. **20**: p. 41-48.
90. Etame, A.B., et al., *Focused ultrasound disruption of the blood-brain barrier: a new frontier for therapeutic delivery in molecular neurooncology*. Neurosurgical focus, 2012. **32**(1): p. E3.
91. O'Reilly, M.A., O. Hough, and K. Hynynen, *Blood-Brain Barrier Closure Time After Controlled Ultrasound-Induced Opening Is Independent of Opening Volume*. J Ultrasound Med, 2017. **36**(3): p. 475-483.
92. Arvanitis, C.D., et al., *Mechanisms of enhanced drug delivery in brain metastases with focused ultrasound-induced blood-tumor barrier disruption*. Proceedings of the National Academy of Sciences, 2018. **115**(37): p. E8717-E8726.
93. Aryal, M., et al., *Effects on P-glycoprotein expression after blood-brain barrier disruption using focused ultrasound and microbubbles*. PLoS One, 2017. **12**(1).
94. Mainprize, T., et al., *Blood-Brain Barrier Opening in Primary Brain Tumors with Non-invasive MR-Guided Focused Ultrasound: A Clinical Safety and Feasibility Study*. Scientific reports, 2019. **9**(1): p. 321.
95. Carpentier, A., et al., *Clinical trial of blood-brain barrier disruption by pulsed ultrasound*. Science translational medicine, 2016. **8**(343): p. 343re2-343re2.
96. Idbaih, A., et al., *Safety and feasibility of repeated and transient blood-brain barrier disruption by pulsed ultrasound in patients with recurrent glioblastoma*. Clinical Cancer Research, 2019. **25**(13): p. 3793-3801.
97. De Vries, N.A., et al., *Blood-brain barrier and chemotherapeutic treatment of brain tumors*. Expert review of neurotherapeutics, 2006. **6**(8): p. 1199-1209.
98. Lonser, R.R., et al., *Convection-enhanced delivery to the central nervous system*. Journal of neurosurgery, 2015. **122**(3): p. 697-706.
99. Bidros, D.S. and M.A. Vogelbaum, *Novel drug delivery strategies in neuro-oncology*. Neurotherapeutics, 2009. **6**(3): p. 539-546.
100. Jahangiri, A., et al., *Convection-enhanced delivery in glioblastoma: a review of preclinical and clinical studies*. Journal of neurosurgery, 2017. **126**(1): p. 191-200.
101. Mehta, A., A. Sonabend, and J. Bruce, *Convection-enhanced delivery*. Neurotherapeutics, 2017. **14**(2): p. 358-371.
102. Brady, M.L., et al., *Pathways of infusate loss during convection-enhanced delivery into the putamen nucleus*. Stereotactic and functional neurosurgery, 2013. **91**(2): p. 69-78.



103. Souweidane, M.M., et al., *A phase I study of convection enhanced delivery (CED) of 124I-8H9 radio-labeled monoclonal antibody in children with diffuse intrinsic pontine glioma (DIPG)*. 2017, American Society of Clinical Oncology.
104. Clinical trials. Available from: <https://www.clinicaltrials.gov>.
105. Kunwar, S., et al., *Phase III randomized trial of CED of IL13-PE38QQR vs Gliadel wafers for recurrent glioblastoma*. *Neuro-oncology*, 2010. **12**(8): p. 871-881.
106. Heiss, J.D., et al., *Phase I trial of convection-enhanced delivery of IL13-Pseudomonas toxin in children with diffuse intrinsic pontine glioma*. *Journal of Neurosurgery: Pediatrics*, 2018. **23**(3): p. 333-342.
107. Muldoon, L.L., et al., *Chemotherapy delivery issues in central nervous system malignancy: a reality check*. *Journal of clinical oncology*, 2007. **25**(16): p. 2295-2305.
108. Van Woensel, M., et al., *Formulations for intranasal delivery of pharmacological agents to combat brain disease: a new opportunity to tackle GBM?* *Cancers*, 2013. **5**(3): p. 1020-1048.
109. League-Pascual, J.C., et al., *Plasma and cerebrospinal fluid pharmacokinetics of select chemotherapeutic agents following intranasal delivery in a non-human primate model*. *Journal of neuro-oncology*, 2017. **132**(3): p. 401-407.
110. Da Fonseca, C.O., et al., *Ras pathway activation in gliomas: a strategic target for intranasal administration of perillyl alcohol*. *Archivum immunologiae et therapiae experimentalis*, 2008. **56**(4): p. 267-276.
111. Da Fonseca, C.O., et al., *Preliminary results from a phase I/II study of perillyl alcohol intranasal administration in adults with recurrent malignant gliomas*. *Surgical neurology*, 2008. **70**(3): p. 259-266.
112. Hashizume, R., et al., *New therapeutic approach for brain tumors: Intranasal delivery of telomerase inhibitor GRN163*. *Neuro-oncology*, 2008. **10**(2): p. 112-120.
113. Ye, D., et al., *Focused ultrasound combined with microbubble-mediated intranasal delivery of gold nanoclusters to the brain*. *Journal of controlled release*, 2018. **286**: p. 145-153.
114. Chen, H., et al., *A new brain drug delivery strategy: focused ultrasound-enhanced intranasal drug delivery*. *PLoS One*, 2014. **9**(10): p. e108880.
115. Warren, K.E., *Novel therapeutic delivery approaches in development for pediatric gliomas*. *CNS oncology*, 2013. **2**(5): p. 427-435.
116. Basso, U., S. Lonardi, and A.A. Brandes, *Is intra-arterial chemotherapy useful in high-grade gliomas?* *Expert review of anticancer therapy*, 2002. **2**(5): p. 507-519.
117. Carceller, F., et al., *Superselective intracerebral catheterization for administration of*

*oncolytic virotherapy in a case of diffuse intrinsic pontine glioma*. Journal of pediatric hematology/oncology, 2014. **36**(7): p. e430-e432.

118. Jahnke, K., et al., *Intraarterial chemotherapy and osmotic blood-brain barrier disruption for patients with embryonal and germ cell tumors of the central nervous system*. Cancer: Interdisciplinary International Journal of the American Cancer Society, 2008. **112**(3): p. 581-588.
119. Watne, K., B. Hager, and H. Hirschberg, *Intra-arterial BCNU in the treatment of recurrent medulloblastoma*. Journal of neuro-oncology, 1990. **8**(2): p. 139-143.
120. David, J.S., et al., *Intracarotid Chemotherapy with a Combination of 1, 3-Bis (2-chloroethyl)-1-nitrosourea (BCNU), cis-Diaminedichloroplatinum (Cisplatin), and 4'-O-Demethyl-1-O-(4, 6-O-2-thenylidene-β-D-glucopyranosyl) epipodophyllotoxin (VM-26) in the Treatment of Primary and Metastatic Brain Tumors*. Neurosurgery, 1984. **15**(6): p. 828-833.
121. Rajappa, P., et al., *Super-selective basilar artery infusion of bevacizumab and cetuximab for multiply recurrent pediatric ependymoma*. Interventional Neuroradiology, 2011. **17**(4): p. 459-465.
122. Happold, C., et al., *ACNU-based chemotherapy for recurrent glioma in the temozolomide era*. Journal of neuro-oncology, 2009. **92**(1): p. 45-48.
123. Vega, F., et al., *Treatment of malignant gliomas with surgery, intraarterial chemotherapy with ACNU and radiation therapy*. Journal of neuro-oncology, 1992. **13**(2): p. 131-135.
124. Newton, H.B., et al., *Intra-arterial carboplatin and intravenous etoposide for the treatment of recurrent and progressive non-GBM gliomas*. Journal of neuro-oncology, 2002. **56**(1): p. 79-86.
125. Burkhardt, J.-K., et al., *Intra-arterial delivery of bevacizumab after blood-brain barrier disruption for the treatment of recurrent glioblastoma: progression-free survival and overall survival*. World neurosurgery, 2012. **77**(1): p. 130-134.
126. Muldoon, L.L., et al., *Intra-arterial administration improves temozolomide delivery and efficacy in a model of intracerebral metastasis, but has unexpected brain toxicity*. Journal of neuro-oncology, 2016. **126**(3): p. 447-454.







## Chapter 3

### **A High-throughput Image-guided Stereotactic Neuronavigation and Focused Ultrasound System for Blood-brain Barrier opening in Rodents**

This chapter was originally published as Haumann, R., 't Hart, E., Derieppe, M.P.P., Besse, H.C., Kaspers, G. J., Hoving, E., van Vuurden, D. G., Hulleman, E., Ries, M. "A High-Throughput Image-Guided Stereotactic Neuronavigation and Focused Ultrasound System for Blood-Brain Barrier Opening in Rodents." *Journal of Visualized Experiments: Jove* 161 (2020).

## Abstract

The blood-brain barrier (BBB) has been a major hurdle for the treatment of various brain diseases. Endothelial cells, connected by tight junctions, form a physiological barrier preventing large molecules (> 500 Da) from entering the brain tissue. Microbubble-mediated focused ultrasound (FUS) can be used to induce transient local BBB opening, allowing larger drugs to enter the brain parenchyma.

In addition to large-scale clinical devices for clinical translation, preclinical research for therapy response assessment of drug candidates requires dedicated small animal ultrasound setups for targeted BBB opening. Preferably, these systems allow high-throughput workflows with both high-spatial precision as well as integrated cavitation monitoring, while still being cost effective in both initial investment and running costs.

Here, we present a bioluminescence and X-ray guided stereotactic small animal FUS system that is based on commercially available components and fulfills the aforementioned requirements. A particular emphasis has been placed on a high degree of automation facilitating the challenges typically encountered in high-volume preclinical drug evaluation studies. Examples of these challenges are the need for standardization in order to ensure data reproducibility, reduce intra-group variability, reduce sample size and thus comply with ethical requirements and decrease unnecessary workload. The proposed BBB system has been validated in the scope of BBB opening facilitated drug delivery trials on patient-derived xenograft models of glioblastoma multiforme and diffuse midline glioma.

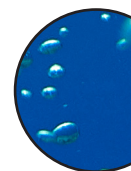
## Introduction

The blood-brain barrier (BBB) is a major obstacle for drug delivery into the brain parenchyma. Most therapeutic drugs that have been developed do not cross the BBB due to their physicochemical parameters (e.g., lipophilicity, molecular weight, hydrogen bond acceptors and donors) or are not retained due to their affinity for efflux transporters in the brain [1, 2]. The small group of drugs that can cross the BBB are typically small lipophilic molecules, which are only effective in a limited number of brain diseases [1, 2]. As a consequence, for the majority of brain diseases, pharmacological treatment options are limited and new drug delivery strategies are needed [3, 4].

Therapeutic ultrasound is an emerging technique that can be used for different neurological applications such as BBB disruption (BBBD), neuromodulation, and ablation [4-7]. In order to achieve a BBB opening with an extracorporeal ultrasound emitter through the cranium, focused ultrasound (FUS) is combined with microbubbles. Microbubble-mediated FUS results in increased bioavailability of drugs in the brain parenchyma [5, 8, 9]. In the presence of sound waves, microbubbles start to oscillate initiating transcytosis and disruption of the tight junctions between the endothelial cells of the BBB, enabling paracellular transport of larger molecules [10]. Previous studies confirmed the correlation between the intensity of the acoustic emission and the biological impact on the BBB opening [11-14]. FUS in combination with microbubbles has already been used in clinical trials for the treatment of glioblastoma using temozolomide or liposomal doxorubicin as the chemotherapeutic agent, or for therapy of Alzheimer's disease and amyotrophic lateral sclerosis [5, 9, 15].

Since ultrasound mediated BBB opening results in entirely new possibilities for pharmacotherapy, preclinical research for clinical translation is needed to assess the therapy response of selected drug candidates. This typically requires a high-throughput workflow with both high-spatial precision and preferably an integrated cavitation detection for monitoring of targeted BBB opening with a high reproducibility. If possible, these systems need to be cost effective in both initial investment and running costs in order to be scalable according to the study size. Most preclinical FUS systems are combined with MRI for image-guidance and treatment planning [15-18]. Although MRI gives detailed information about the tumor anatomy and volume, it is an expensive technique, which is generally performed by trained/skilled operators. In addition, high-resolution MRI may not always be available for researchers in preclinical facilities and requires long scanning times per animal, making it less suitable for a high-throughput pharmacological studies. Noteworthy is that, for preclinical research in the field of neuro-oncology, in particular infiltrative tumor models, the possibility to visualize and target the tumor is essential for treatment success [19]. Currently, this requirement is only fulfilled by MRI or by tumors transduced with a photoprotein, enabling visualization with bioluminescence imaging (BLI) in combination with administration of the photoprotein substrate.

MRI-guided FUS systems often use a water bath to ensure ultrasound wave propagation for transcranial applications, whereby the head of the animal is partly submerged in the water, the so called "bottom-up" systems [15-17]. While these designs work generally well in smaller animal studies, they are a compromise between animal preparation times, portability and realistically maintainable hygienic standards during usage. As an alternative to MRI, other guidance methods for stereotactic navigation encompass the use of a rodent





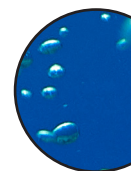
anatomical atlas [20-22], laser pointer assisted visual siting [23], pinhole-assisted mechanical scanning device [24], or BLI [25]. Most of these designs are “top-down” systems in which the transducer is placed on top of the animal’s head, with the animal in a natural position. The “top-down” workflow consists either of a water bath [21, 24, 25] or a water-filled cone [20, 23]. The benefit of using a transducer inside a closed cone is the more compact footprint, shorter setup time and straight-forward decontamination possibilities simplifying the entire workflow.

The interaction of the acoustic field with the microbubbles is pressure dependent and ranges from low-amplitude oscillations (referred to as stable cavitation) to transient bubble collapse (referred to as inertial cavitation) [26, 27]. There is an established consensus that ultrasound-BBBD requires an acoustic pressure well above the stable cavitation threshold to achieve successful BBBD, but below the inertial cavitation threshold, which is generally associated with vascular/neuronal damage [28]. The most common form of monitoring and control is the analysis of the (back-)scattered acoustic signal using passive cavitation detection (PCD), as suggested by McDannold et al. [12]. PCD relies on the analysis of the Fourier spectra of microbubble emission signals, in which the strength and appearance of stable cavitation hallmarks (harmonics, subharmonics, and ultraharmonics) and inertial cavitation markers (broadband response) can be measured in real-time.

A “one size fits all” PCD-analysis for precise pressure control is complicated due to the polydispersity of the microbubble formulation (the oscillation amplitude depends strongly on the bubble diameter), the differences in bubble shell properties between brands, and the acoustic oscillation, which depends strongly on frequency and pressure [29-31]. As a consequence, many different PCD detection protocols have been suggested, which have been adapted to particular combinations of all these parameters and have been used in various application scenarios (ranging from *in vitro* experimentation over small animal protocols to PCD for clinical usage) for robust cavitation detection and even for retroactive feedback control of the pressure [11, 14, 29-34]. The PCD protocol employed in the scope of this study is derived directly from McDannold et al. [12] and monitors the harmonic emission for the presence of stable cavitation and broadband noise for inertial cavitation detection.

We have developed an image-guided neuronavigation FUS system for transient opening of the BBB to increase drug delivery into the brain parenchyma. The system is based on commercially available components and can be easily adapted to several different imaging modalities, depending on the available imaging techniques in the animal facility. Since we require a high-throughput workflow, we have opted to use X-ray and BLI for image-guidance and treatment planning. Tumor cells transduced with a photoprotein (*e.g.*, luciferase) are suitable for BLI imaging [19]. After administration of the photoprotein substrate, tumor cells can be monitored *in vivo* and tumor growth and location can be determined [19, 35]. BLI is a low-cost imaging modality, it enables to follow the tumor growth over time, it has fast scanning times and it correlates well with tumor growth measured with MRI [35, 36]. We have opted to replace the water bath with a water-filled cone attached to the transducer to enable flexibility to freely move the platform on which the rodent is mounted [8, 23]. The design is based on a detachable platform equipped with integration of (I) small-animal stereotactic platform, (II) fiducial markers with both X-ray and optical-image compatibility, (III) rapid-detachable anesthesia mask, and (IV) integrated temperature regulated animal heating system. After the initial induction of anesthesia, the animal is mounted in a precise posi-

tion on the platform where it remains during the entire procedure. Consequently, the entire platform passes all stations of the workflow of the entire intervention, while maintaining an accurate and reproducible positioning and sustained anesthesia. The control software allows the automatic detection of the fiducial markers and automatically registers all types of images and image modalities (i.e., micro-CT, X-ray, BLI and fluorescence imaging) into the frame of reference of the stereotactic platform. With help of an automatic calibration procedure, the focal length of the ultrasound transducer is precisely known within, which enables the automatic fusion of interventional planning, acoustic delivery and follow-up imaging analysis. As shown in **Figure 1** and **Figure 2**, this setup provides a high degree of flexibility to design dedicated experimental workflows and allows interleaved handling of the animal at different stations, which in-turn facilitates high-throughput experiments. We have used this technique for successful drug delivery in mouse xenografts of high-grade glioma such as diffuse midline glioma.



## Protocol

All *in vivo* experiments were approved by the Dutch ethical committee (license permit number AVD114002017841) and the Animal Welfare Body of the Vrije Universiteit Amsterdam, the Netherlands. The investigators were trained in the basics of the FUS system in order to minimize the discomfort of the animals.

### 1. Focused Ultrasound System

NOTE: The described setup is an inhouse built BBB disruption system based on commercially available components and includes a 3D-printed custom-made cone and detachable stereotactic platform. The system is designed modular, which facilitates modifications according to available equipment and specific use. The protocol describes the procedure for the sonoporation of a larger area in the pontine region of the mouse brain. By adjusting the target location, different parts of the brain could be targeted. In this study a 1 MHz mono-element transducer with a focal length of 75 mm, an aperture of 60 mm and a focal area of 1.5 x 1.5 x 5 mm (FWHM of peak pressure) was used. The focal plane of the transducer is positioned through the cranium of the animal in the horizontal plane intersecting with the ear bars.

#### 1.1. Select an appropriate transducer for BBB opening in rodents.

NOTE: Based on the properties of the microbubbles and the employed frequency, the acoustic settings, in particular the mechanical index (MI), are subject to change[13][37].

#### 1.2. Place the transducer in the 3D-printed cone.

1.3. Employ an acoustically transparent mylar membrane at the bottom-end of the cone to achieve acoustic coupling of the beam propagation path, and fill the cone with degassed water.

1.4. Mount the transducer above the animal on a motorized linear stage as shown in **Figure 1** allowing automatic vertical positioning of the transducer.

1.5. Design a detachable stereotactic platform based on the requirements of the study, which includes temperature regulated heating, bite and ear bars, anesthesia and multi-modality fiducial markers, as shown in **Figure 1** and **Figure 2**. The mounting of the stereotactic platform consists of a 2D linear stage system, which allows precise automatic positioning (< 0.1 mm) of the animal under the beam.

1.6. Connect the transducer to the acoustic emission chain shown in **Figure 1** consisting of a transducer, a function generator and a power amplifier.

1.7. Devise an image-processing pipeline to detect the multi-modality fiducial markers that allows precise sonoporation targeting of the brain area of interest and collection of the cavitation data detected by the needle hydrophone.

1.8. Calibrate the system and determine the focus point of the transducer in correspondence to vertical positioning of the animal on the stereotactic platform.

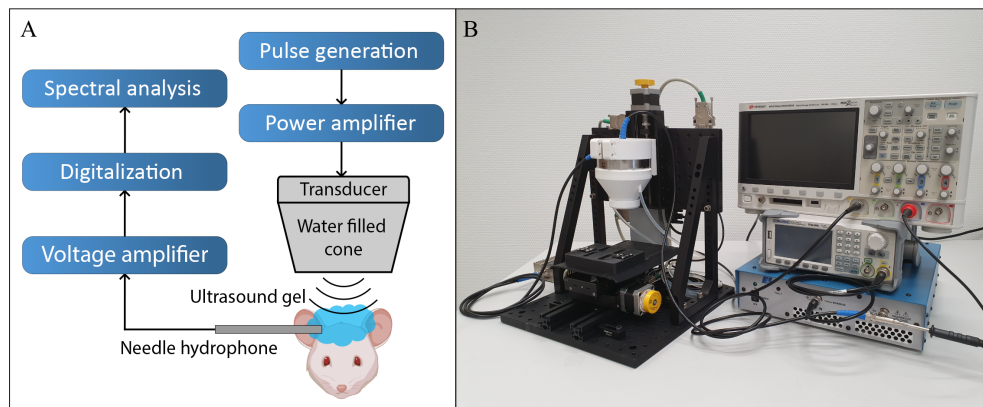


**Figure 1. | Focused ultrasound setup.** A: Schematic representation of the focused ultrasound set up. and B: Picture of the focused ultrasound set up. The system consists of a top-down mounted transducer on a 1D linear stage over a second 2D stage for automatic 3D positioning. The transducer is built in a water filled beam-cone, closed at the bottom with an acoustically transparent mylar membrane, which conducts the sound to the cranium of the animal. The transducer is connected to a power amplifier, which is in-turn connected to an arbitrary waveform generator (AWG) for signal generation. For cavitation detection a detachable hydrophone in combination with a low-noise voltage amplifier is used. The hydrophone is placed in the direct vicinity of the occipital bone. The external hydrophone has a 2 mm active surface and is acoustically coupled with ultrasound gel. Both the high-voltage signal of the excitation pulse as well as the recorded cavitation signal are digitalized by a standard 200 MHz oscilloscope and relayed to a control computer (not shown) for on-the-fly processing and real-time control.

## 2. Animal Preparation

NOTE: The following protocol is specified for mice but can be adapted for rats. For these experiments female athymic nude *Foxn1*<sup>-/-</sup> mice (6-8 week old) were used.

2.1. Allow the animal to acclimatize for at least one week in the animal facility and weigh the animal regularly.

2.2. Administer buprenorphine (0.05 mg/kg) via subcutaneous (s.c.) injection 30 min prior to FUS treatment to start analgesic treatment.

2.3. Anesthetize the animal with 3% isoflurane, 2 L/min O<sub>2</sub> and verify that the animal is deeply anesthetized. Keep the animals anesthetized during the whole procedure and monitor the breathing frequency and heart rate to adjust the concentration of isoflurane as required.

2.4. Apply eye ointment to prevent dry eyes and avoid possible injury.

2.5. Remove hair on the top of the head with a razor and depilatory cream and wash afterwards with water to remove any residues to avoid irritation to the skin.

2.6. For experiments with BLI tumor models, inject 150 µL of D-luciferin (30 mg/mL) intraperitoneal (i.p.) with a 29 G insulin syringe for BLI image-guidance.

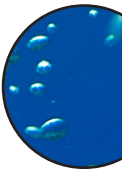
2.7. Insert a 26-30 G tail vein catheter and flush the catheter and vein with a small volume of heparin solution (5 UI/mL). Fill the catheter with heparin solution to avoid blood clotting.

NOTE: Good catheterization is seen when there is a reflux of blood into the catheter. Avoid air bubbles in the catheter to prevent emboli. To avoid excessive injection pressure, make sure the length of the catheter is as short as possible.

2.8. Place the animal on the temperature regulated stereotactic platform to avoid hypothermia.

NOTE: Hypothermia reduces blood circulation, which can affect the injection/circulation of microbubbles and the pharmacokinetics of the drugs[39].

2.9. Immobilize and fix the head of the animal on the stereotactic platform using ear bars and a bite bar. Fixate the body with a strap and tape the tail of the animal to the platform.



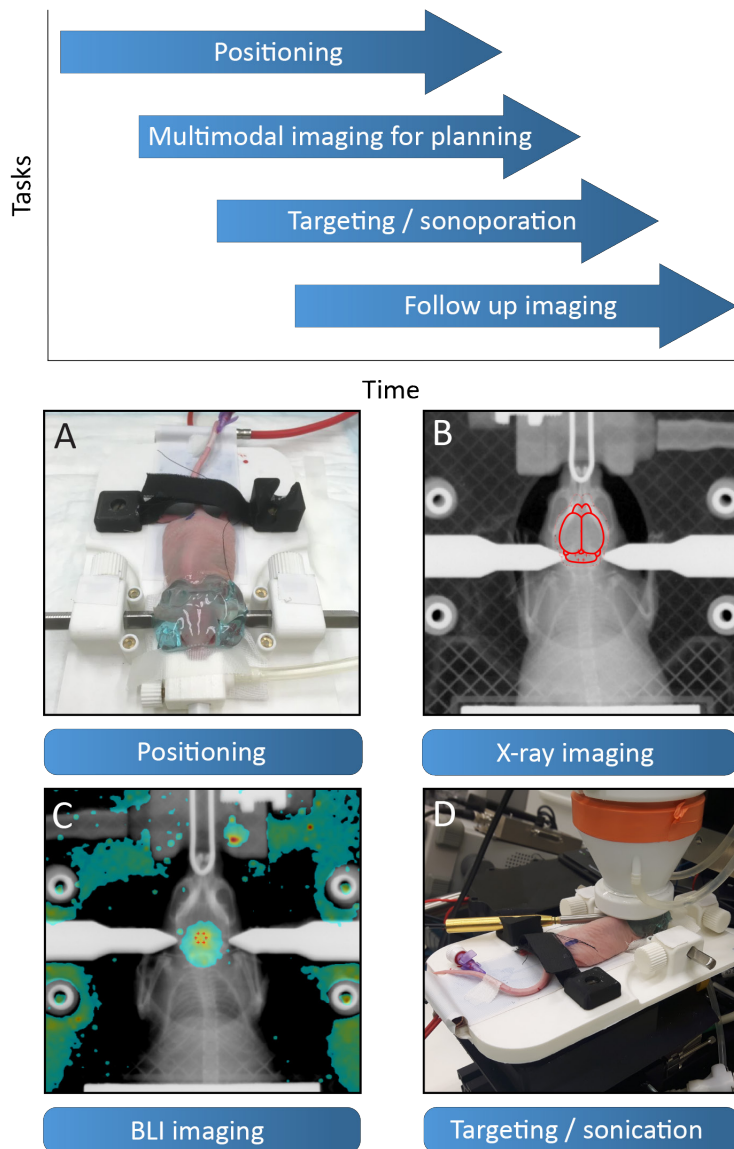


**Figure 2. | Focused ultrasound workflow.** The proposed workflow of the focused ultrasound system starts with A: The initial positioning of animal on a detachable stereotactic platform, note the application of the acoustic coupling gel (applied post BLI/X-ray). Simultaneously multimodal imaging can be conducted for targeting. B: At first X-ray imaging is a possibility, whereas a region of interest can be targeted with the help of an outline of the brain (which in turn is referenced to the mouse brain atlas [38], adapted to the size and posture of the skull). C: Alternatively, a BLI image of a luciferase transfected diffuse midline glioma tumor overlaid on an X-ray maximum intensity projection can be applied for targeting. D: Subsequently, the stereotactic platform is mounted with the animal in therapy position with both hydrophone and transducer attached. The transducer automatically drives in therapy position and sonicates the chosen trajectory post bolus injection. The system is optimized for high-throughput experiments, whereby multiple platforms allow interleaved work, as shown on top.

### 3. In Vivo Image-guided Focused Ultrasound

NOTE: For this protocol a 1 MHz mono-element transducer with a tone-burst pulse with a 10 ms duration, a MI of 0.4 and a pulse repetition frequency of 1.6 Hz with 40 cycles for 240 s was used. The protocol is optimized for microbubbles stabilized by phospholipids containing sulphur hexafluoride ( $\text{SF}_6$ ) as an innocuous gas, whereby the mean bubble diameter is 2.5  $\mu\text{m}$  and more than 90% of the bubbles are smaller than 8  $\mu\text{m}$ .

3.1. Place the stereotactic platform with the mounted animal in the imaging modality (e.g., BLI or X-ray) and take image(s) of the animal.

3.2. Use the multi-modality fiducial markers in combination with the image-processing pipeline to mark the position of the animal according to the focus point of the transducer.

3.3. Determine the target area by placing a brain outline over the acquired X-ray image or using BLI images to determine the center of the tumor (**Figure 2**). The position of specific parts of the brain are specified in the Paxinos Brain Atlas[38] using the skull markings bregma and lambda as reference points. For example the pons is located  $x=-1.0$ ,  $y=-0.8$  and  $z=-4.5$  from lambda.

3.4. Shield the animal's nostrils and mouth with adhesive tape to prevent ultrasound gel interfering with breathing.

3.5. Apply ultrasound gel on top of the animal's head.

3.6. Retract the skin of the animals' neck, lubricate the needle hydrophone with ultrasound gel and place the needle hydrophone in the direct vicinity of the occipital bone.

3.7. Guide the transducer to the correct position using the image-processing pipeline and the focus point.

3.8. Apply the preconfigured settings to all attached devices and target the brain region of interest.

NOTE: Depending on the research question, tumor or brain regions can be sonoporated as a single focal point or as volumetric shape, as shown in **Figure 2**.

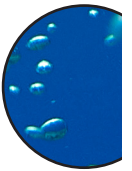
3.9. Activate microbubbles as described by the manufacturer. Inject one bolus of 120  $\mu\text{L}$  (5.4  $\mu\text{g}$ ) of microbubbles.

3.10. Flush the tail vein catheter with saline to check the opening of the catheter.

3.11. Inject the microbubbles and start the insonation.

3.12. Record microbubble cavitation with the needle hydrophone.

3.13. Administer an intravascular contrast agent or drug after sonoporation. The dose, timing and planning are dependent on the purpose of the study and the drug.



NOTE: Evans blue is a common color agent to assess BBB opening [40].

3.14. Monitor the animal until the predetermined time point or before the humane endpoint.

#### 4. Analysis of Microbubble Cavitation

NOTE: Here the applied procedure is described, which is suitable for *in vivo* experimentation for SF<sub>6</sub>-phospholipid microbubbles with an average diameter of 2.5 μm (80% of the bubbles below 8 μm) excited with a burst-tone pulse of 10 ms duration at a frequency of 1 MHz, as originally suggested by McDannold et al.[12].

4.1. Fourier-transform the recorded PCD signal from the time-domain into the frequency domain.

4.2. Integrate the resulting spectral power for stable cavitation detection around the 2<sup>nd</sup> and 3<sup>rd</sup> harmonic (± 50 kHz), as shown in **Figure 3** (green box at 2 and 3 MHz).

4.3. Integrate the spectral power for inertial cavitation detection, between principal frequency, the 2<sup>nd</sup>, 3<sup>rd</sup> harmonic, the 1<sup>st</sup> and 2<sup>nd</sup> ultraharmonic and the first sub-harmonic (± 150 kHz), as shown in **Figure 3** (red boxes).

4.4. Integrate the spectral power around the principle frequency (1 MHz ± 50 kHz) for the normalization of both previously obtained PCD signals.

NOTE: The PCD signal, for SF<sub>6</sub>-phospholipid microbubbles *in vivo* experiments at 1 MHz, does not display ultraharmonics or subharmonics before inertial cavitation sets in, as shown in **Figure 3**.

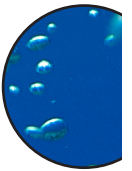
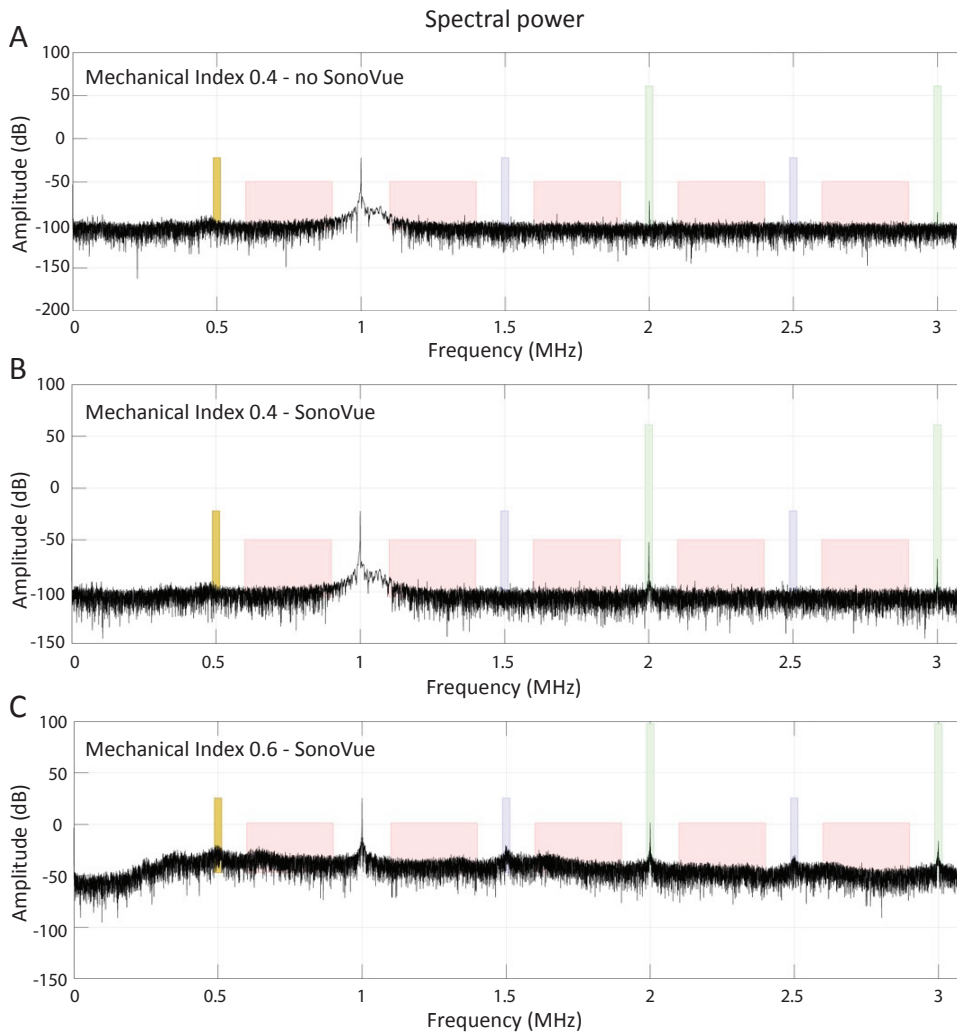


**Figure 3. | Cavitation monitoring.** A: Frequency spectrum of an in vivo experiment in the absence of microbubble administration at a MI of 0.4 at 1 MHz B: Shown is the corresponding spectrum at peak-bolus after injection of microbubbles. Note the increase of the higher harmonics, which is indicative for stable cavitation of the microbubbles. C: Corresponding spectrum observed at a higher MI of 0.6 in combination with microbubble injection, within the transition band to the onset of inertial cavitation, leading to an increase in noise floor up to 25 dB and the appearance of ultraharmonics and subharmonics



## Results

The described FUS system (**Figure 1** and **Figure 2**) and the associated workflow have been used in over a 100 animals and produced reproducible data on both healthy and tumor bearing mice. Based on the recorded cavitation and the spectral density at the harmonics at the peak moment of the microbubble bolus injection, the spectral power of each frequency can be calculated using the Fourier analysis as explained in step 4 of the Protocol. Based on the acoustic protocol (1 MHz, 10 ms pulse duration) with a MI of 0.4 in combination with microbubbles, the normalized integrated power spectrum at the 2<sup>nd</sup> and 3<sup>rd</sup> harmonics normalized the integrated power spectrum of the excitation frequency observed in **Figure 3**. This provided a very sensitive and reliable means of stable cavitation detection, in comparison to no detection of subharmonics when no microbubbles were injected or the observation of inertial cavitation when a MI of 0.6 was applied. In case of inertial cavitation, an increased broad-band noise floor of up to 25 dB was detected as well as the appearance of ultra-harmonics and subharmonics. Although an acoustic pressure of an MI of 0.4 and 0.6 resulted in no macroscopic damage, microscopic damage was evidenced histologically at a MI of 0.6, as shown in **Figure 4**. A further increase of the pressure amplitude up to a MI of 0.8 resulted in a macroscopic brain hemorrhage of larger vessels and wide-spread tissue lysis with the extravasation of erythrocytes. The histological findings corresponded to the acoustic data from the passive cavitation sensor, as shown in **Figure 3**, confirming the damaging properties of inertial cavitation of the brain tissue. As a consequence, a MI of 0.4 was chosen as the safe pressure amplitude that provided very reproducible BBB-opening, while providing a safe margin to the inertial cavitation regime, as observed before [11].

Intravenous Evans blue was injected to validate the opening of the BBB in the pontine region. The strong albumin-binding of Evans blue leads to a large molecule of more than 66 kDa [41]. At the level of the pons and partly the cerebellum, extravasation of Evans blue-conjugated albumin was observed in the mouse treated with FUS and microbubbles in contrast to the mouse without microbubbles (**Figure 5**). This emphasizes the precise targeting of the region of interest based on image-guided stereotactic navigation with the in-house build FUS system and the described protocol.

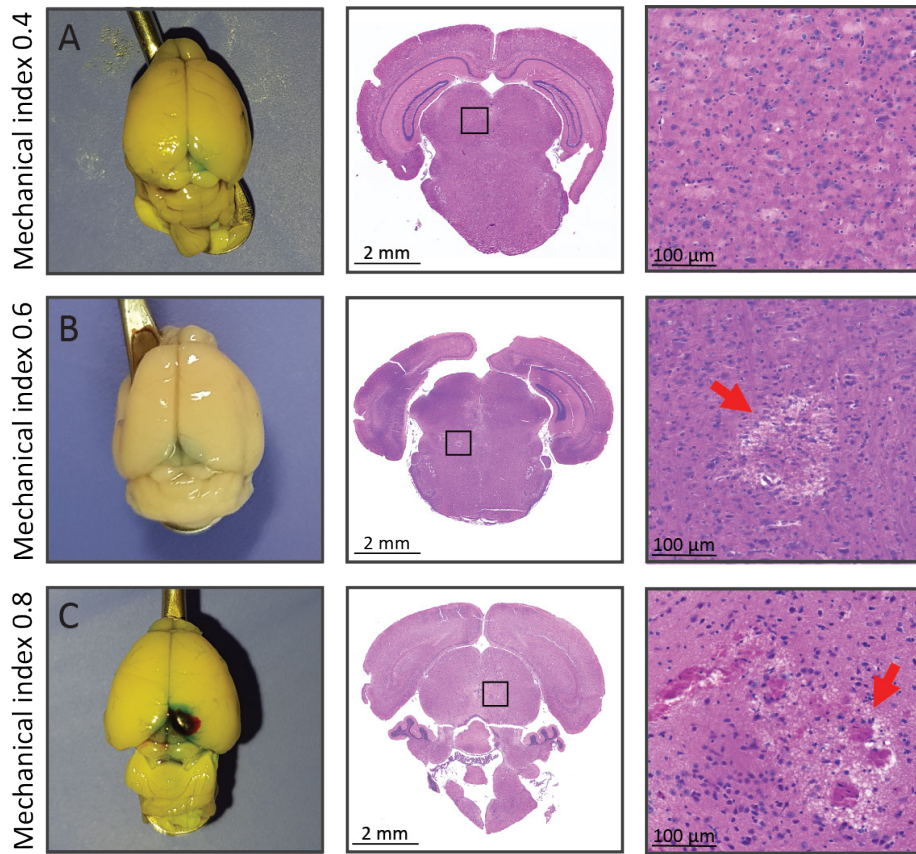


**Figure 4. | BBB opening and associated histology.** A: Stable cavitation using an MI of 0.4 evidenced an intact brain parenchyma in both white light macroscopy and HE stained microscopy. B: After a MI of 0.6 first signs of local irreversible tissue damage of the brain parenchyma is becoming apparent in the HE stained histological data. C: For even higher mechanical pressure of MI 0.8 macroscopic hemorrhaging is apparent as well as wide-spread tissue lysis of the brain parenchyma and the extravasation of erythrocytes due to micro-hemorrhaging. The blue hue in the white light macroscopy is indicative for the extravasation of the co-injected intra-vascular contrast agent Evans blue indicating BBB opening (see **Figure 5** for a sagittal view).

## Evans blue extravasation

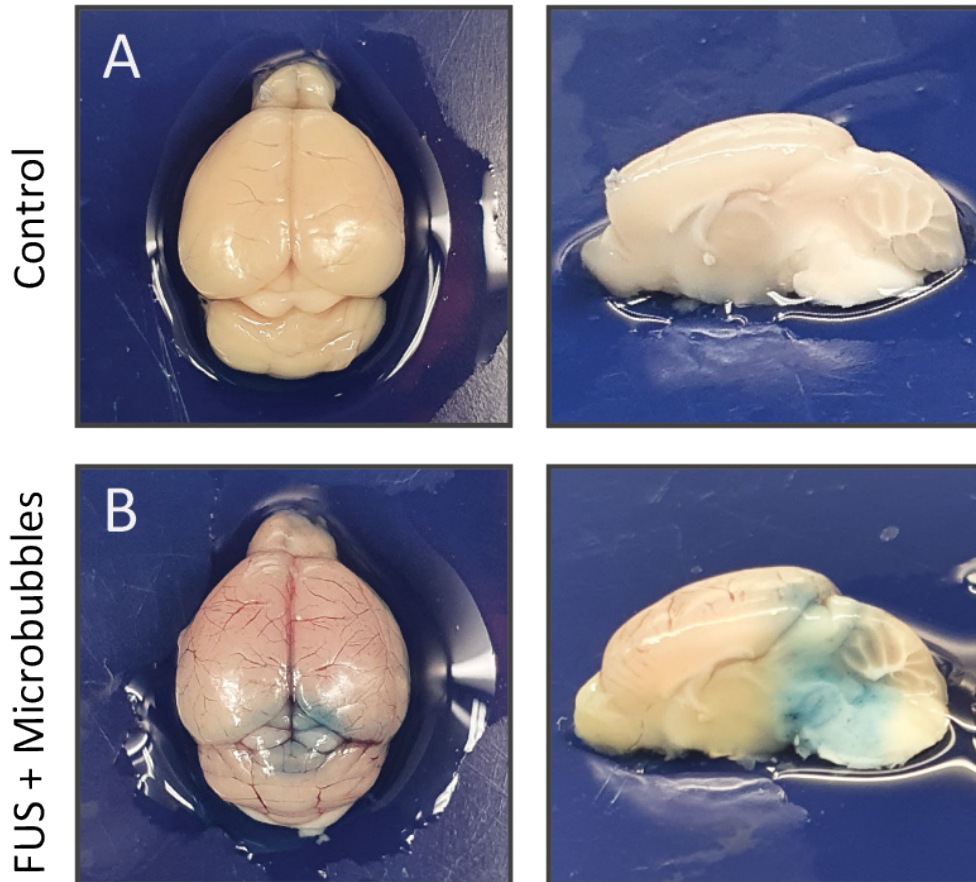


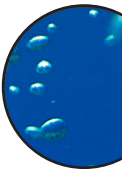
**Figure 5. | Validation of BBB opening.** Demonstration of successful BBB opening in the stable cavitation regime (B) compared to control (A), no microbubbles injected. In this case Evans blue has been used as an intravascular contrast agent. The strong albumin-binding of Evans blue leads to a large molecule of more than 66 kDa. As a consequence, evidence of the Evans blue extravasation is indicative for paracellular transport across the BBB due to a (partial) opening of the tight junctions.

## Discussion

In this study, we developed a cost-effective image guided based FUS system for transient BBB disruption for increased drug delivery into the brain parenchyma. The system was largely built with commercially available components and in conjunction with X-ray and BLI. The modularity of the proposed design allows the use of several imaging modalities for planning and assessment in high-throughput workflows. The system can be combined with more comprehensive high-resolution 3D imaging modalities, for example high-resolution MRI or micro-CT, while for the bulk of the study 2D imaging modalities such as 2D X-ray and/or BLI are used. 2D X-ray and/or BLI are both considerably more cost effective as well as ideal for high-volume studies due to their respective short acquisition times. The transducer described here is well suited to produce BBBD in larger areas (on the scale of a mouse brain) in deeper parts of the brain (f number of 1.25). We have used the system for diffusely growing tumors in the pontine region [42, 43]. For these regions a larger volume needs to be sonoporated that encompasses the entire tumor region in the pons. The modular system can easily be adjusted for other types of brain tumors in more supratentorial parts of the brain. In order to decide on the transducer type one should hold into account the f-number, focal length and frequency.

The overall design proposes thereby two refinements compared to previously suggested designs: (I) Frequently a water bath is used for ultrasound wave transmission of therapeutic systems. For transcranial applications in small animals this type of design results in larger and inverted setups, whereby the animal is partially submerged [11, 21, 24]. While these designs work generally very well in the scope of smaller animal studies, they are a compromise with respect to setup times, portability and realistically maintainable hygienic standards during usage. In particular the latter is of considerable importance in the scope studies encompassing immunocompromised animals and thus strict hygienic standards. As a consequence, in order to design a system with a more compact footprint, shorter setup time, easy decontamination possibilities and a natural position of the animal during the entire workflow, a “top-down” design was chosen. (II) The second design choice that differs from several previously described designs was to omit the direct integration of the acoustic delivery system into a medical imaging system such as an MRI or a micro-CT [15-18, 44]. While fully integrated systems are ideal for longitudinal pharmacokinetic studies or explorative research on a limited number of animals, such setups are generally less suitable for high-volume pharmacological studies due to considerably increased complexity, high running-costs and need for trained/skilled operators. Furthermore, such systems are generally limited to only one imaging modality. As a consequence, the proposed design here relies on a modular detachable stereotactic platform, which is compatible with several imaging modalities (micro-CT, small animal MRI, a variety of BLI/fluorescence cameras, these with or without integrated X-ray imaging) and provides also multi-modality fiducial markers for automatic fusion of all image data in a common frame of reference for both interventional planning and the follow-up post BBB opening.

With respect to practical considerations, the most critical point of failure in the procedure is the stability of the microbubbles due to their limited lifetime and their fragile nature. We would like to emphasize that the following discussion concerns microbubbles stabilized by phospholipids and containing sulphur hexafluoride ( $\text{SF}_6$ ) as an innocuous gas [45, 46], while



other microbubble formulations will generally display different properties.

Timing before microbubble injection: The advertised lifespan of commercially available microbubbles after re-hydration is between as 3 and 4 hours. While this is suitable for diagnostic ultrasound applications, it should be noted that during this entire period the microbubbles continuously lose gas and consequently the mean bubble diameter is subject to a continuous downward-drift from the initial average size of 2.5  $\mu\text{m}$ . For therapeutic applications such as ultrasound-mediated BBBB this implies much stricter timing-imperatives, since the oscillation amplitude of stable cavitation (at a given frequency and pressure) and the onset-threshold of inertial cavitation are as a direct consequence also subject to a continuous drift. In our experience, we have observed that microbubbles are best used within 30 minutes after rehydration in order to obtain reproducible results, similar to previous reportings [47].

Timing after microbubble injection: In larger primates, commercially available  $\text{SF}_6$ -phospholipid microbubbles display a blood-plasma elimination half-life of about 6 minutes and more than 80% of the administered gas is exhaled via the lungs after only 11 minutes [47]. In small mammals such as mice and rats the blood-plasma elimination half-life of this type of microbubbles *in vivo* is with 90-120 seconds considerably shorter due to the higher heart rate<sup>20</sup>. As a consequence, the rapid dynamic of the microbubble concentration directly after bolus injection and the fast subsequent plasma elimination combined with the continuous gas volume loss of the bubbles imposes strict timing requirements on the sonication / injection protocol in order to obtain reproducible results within the short duration of 3-4 minutes post-injection. Longer procedures or more extensive volumes of BBBB require preferably a continuous administration of microbubbles. However, such an approach is complicated by the buoyancy of the bubbles in both syringe and feeding-system and also introduces a considerably increased dead volume by the required infusion tubing. In our experience the simpler solution of splitting the total injection volume into 2 to 3 smaller sub-doses provided a robust and reproducible results.

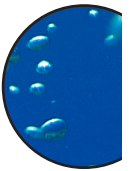
In addition, microbubbles are very pressure sensitive and high hydrostatic pressures during injection are therefore not recommended. As a consequence, large needles (>19 G) are recommended for the transfer of microbubbles into a plastic tube or to draw up microbubbles with a syringe [48]. For i.v. injection in mice 26-30 G needles are recommended; since larger needles are more difficult to insert into the tail vein. The 26 G needle is recommended since the hydrostatic pressure is lower with this needle. However, in case of difficult venous access the 30 G needle is recommended.

The cranium of the mouse is an important attenuator of the pressure amplitude that significantly lowers the pressure amplitude at the focus. Attenuation is determined by the frequency of the transducer and the density of the medium the ultrasound wave propagates. Higher ultrasound frequencies and high tissue densities, like bone results in high attenuation. The pressure amplitude is partially absorbed by bone and some pressure amplitude is lost by reflection and scattering [49]. In our experiments we have determined in mouse cadavers that the attenuation at 1 MHz is  $14.5 \pm 1.3$  dB/cm with an average skull thickness of 0.9 mm as shown before [20, 49]. Cavitation monitoring is highly recommended since microbubbles reflect distinct acoustic emissions during stable cavitation and inertial cavitation. Wideband emission is a distinct acoustic emission for inertial cavitation[12]. Real-time

monitoring makes it possible to detect inertial cavitation and lower the pressure amplitude accordingly to avoid tissue damage.

Previous reports described the influence of the type of anesthesia on the achieved BBB permeability [11]. For isoflurane-based anesthesia, a vasodilation occurs shortly after anesthesia initiation, which is associated with a slight reduction of the cerebral blood flow. Furthermore, anesthesia over extended durations, in particular in absence of a temperature stabilization, leads to a reduced heart rate. Since both factors can potentially lead to a larger variance of the cerebral concentration of both microbubbles or co-administered drugs, a strict anesthesia protocol is advisable to achieve reproducible results [50]. Anesthesia with 1.5% v/v isoflurane in 2 L/min oxygen for 35 to 45 minutes was not problematic, as advised by Constantinides et al. [50]. In contrast to McDannold et al. [51] who showed that this gas mixture in combination with the specific type of their microbubbles was problematic [51], we have not observed noteworthy problems with this type of microbubbles. Alternatively, the animals can be anesthetized with a mix of ketamine/xylazine, which has no known vasoactive effects [52].

In summary, the imaging-guided BBB-opening technique described here has been used for high-volume preclinical drug evaluation studies, that demonstrated the efficiency of the suggested workflow. The system could thereby be operated by non-technical personal after an only short training due to the high degree of automation. This in combination with the simplicity of the setup resulted in a high degree of standardization, which in turn ensures experimental reproducibility, reduced intra-group variability and thus allows to reduce the required sample size.

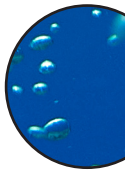


## References

1. Lipinski, C.A., *Lead- and drug-like compounds: the rule-of-five revolution*. Drug Discov Today Technol, 2004. **1**(4): p. 337-341.
2. Pardridge, W.M., *Blood-brain barrier delivery*. Drug Discov Today, 2007. **12**(1-2): p. 54-61.
3. Alli, S., et al., *Brainstem blood brain barrier disruption using focused ultrasound: A demonstration of feasibility and enhanced doxorubicin delivery*. Journal of Controlled Release, 2018. **281**: p. 29-41.
4. Burgess, A. and K. Hynynen, *Noninvasive and targeted drug delivery to the brain using focused ultrasound*. ACS chemical neuroscience, 2013. **4**(4): p. 519-526.
5. Meng, Y., et al., *Safety and efficacy of focused ultrasound induced blood-brain barrier opening, an integrative review of animal and human studies*. J Control Release, 2019. **309**: p. 25-36.
6. Darrow, D.P., *Focused Ultrasound for Neuromodulation*. Neurotherapeutics, 2019. **16**(1): p. 88-99.
7. Zhou, Y.F., *High intensity focused ultrasound in clinical tumor ablation*. World J Clin Oncol, 2011. **2**(1): p. 8-27.
8. O'Reilly, M.A., O. Hough, and K. Hynynen, *Blood-Brain Barrier Closure Time After Controlled Ultrasound-Induced Opening Is Independent of Opening Volume*. J Ultrasound Med, 2017. **36**(3): p. 475-483.
9. Mainprize, T., et al., *Blood-Brain Barrier Opening in Primary Brain Tumors with Non-invasive MR-Guided Focused Ultrasound: A Clinical Safety and Feasibility Study*. Scientific reports, 2019. **9**(1): p. 321.
10. Dasgupta, A., et al., *Ultrasound-mediated drug delivery to the brain: principles, progress and prospects*. Drug Discov Today Technol, 2016. **20**: p. 41-48.
11. O'Reilly, M.A., et al., *MRI-guided disruption of the blood-brain barrier using transcranial focused ultrasound in a rat model*. J Vis Exp, 2012(61).
12. McDannold, N., N. Vykhodtseva, and K. Hynynen, *Targeted disruption of the blood-brain barrier with focused ultrasound: association with cavitation activity*. Physics in Medicine & Biology, 2006. **51**(4): p. 793.
13. McDannold, N., N. Vykhodtseva, and K. Hynynen, *Blood-brain barrier disruption induced by focused ultrasound and circulating preformed microbubbles appears to be characterized by the mechanical index*. Ultrasound Med Biol, 2008. **34**(5): p. 834-840.
14. Sun, T., et al., *Closed-loop control of targeted ultrasound drug delivery across the blood-brain/tumor barriers in a rat glioma model*. Proceedings of the National Aca-

demy of Sciences, 2017. **114**(48): p. E10281-E10290.

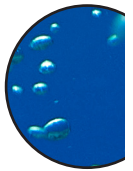
15. Lipsman, N., et al., *Blood-brain barrier opening in Alzheimer's disease using MR-guided focused ultrasound*. Nat Commun, 2018. **9**(1): p. 2336.
16. Chopra, R., et al., *An MRI-compatible system for focused ultrasound experiments in small animal models*. Medical physics, 2009. **36**(5): p. 1867-1874.
17. Kinoshita, M., et al., *Targeted delivery of antibodies through the blood-brain barrier by MRI-guided focused ultrasound*. Biochemical and biophysical research communications, 2006. **340**(4): p. 1085-1090.
18. Larrat, B., et al., *MR-guided transcranial brain HIFU in small animal models*. Physics in medicine & biology, 2009. **55**(2): p. 365.
19. Contag, C.H., et al., *Use of reporter genes for optical measurements of neoplastic disease in vivo*. Neoplasia (New York, NY), 2000. **2**(1-2): p. 41-52.
20. Choi, J.J., et al., *Noninvasive, transcranial and localized opening of the blood-brain barrier using focused ultrasound in mice*. Ultrasound in medicine & biology, 2007. **33**(1): p. 95-104.
21. Bing, C., et al., *Trans-cranial opening of the blood-brain barrier in targeted regions using stereotaxic brain atlas and focused ultrasound energy*. Journal of therapeutic ultrasound, 2014. **2**(1): p. 13.
22. Marquet, F., et al., *Real-time, transcranial monitoring of safe blood-brain barrier opening in non-human primates*. PloS one, 2014. **9**(2).
23. Anastasiadis, P., et al., *Design, characterization and evaluation of a laser-guided focused ultrasound system for preclinical investigations*. Biomed Eng Online, 2019. **18**(1): p. 36.
24. Liu, H.-L., et al., *Opening of the blood-brain barrier by low-frequency (28-kHz) ultrasound: a novel pinhole-assisted mechanical scanning device*. Ultrasound in medicine & biology, 2010. **36**(2): p. 325-335.
25. Zhu, L., et al., *Focused ultrasound-enabled brain tumor liquid biopsy*. Scientific reports, 2018. **8**(1): p. 1-9.
26. Bader, K.B. and C.K. Holland, *Gauging the likelihood of stable cavitation from ultrasound contrast agents*. Physics in Medicine & Biology, 2012. **58**(1): p. 127.
27. Neppiras, E., *Acoustic cavitation series: part one: Acoustic cavitation: an introduction*. Ultrasonics, 1984. **22**(1): p. 25-28.
28. Aryal, M., et al., *Ultrasound-mediated blood-brain barrier disruption for targeted drug delivery in the central nervous system*. Advanced drug delivery reviews, 2014. **72**: p. 94-109.

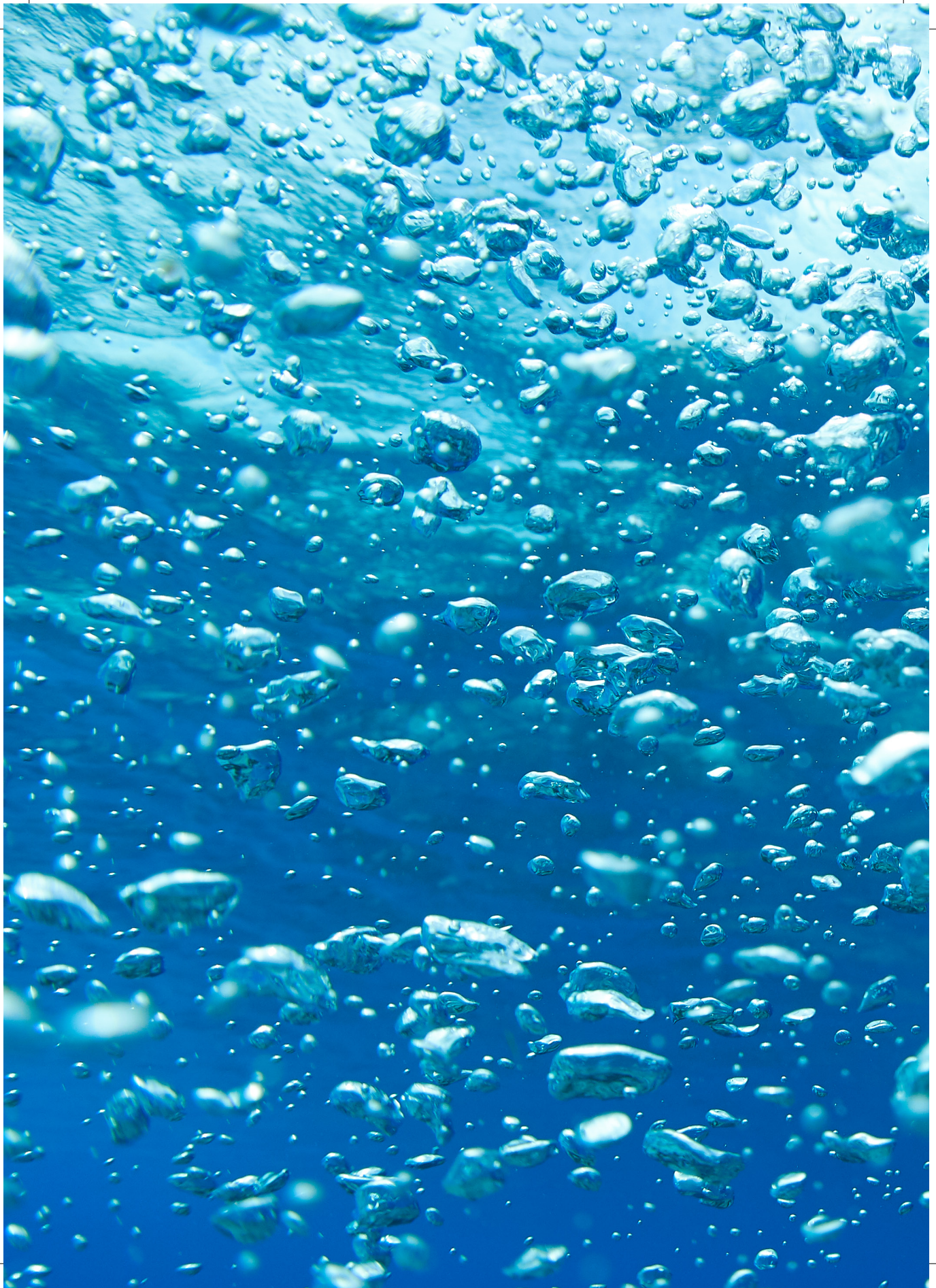




29. Tung, Y.-S., et al., *Identifying the inertial cavitation threshold and skull effects in a vessel phantom using focused ultrasound and microbubbles*. *Ultrasound in medicine & biology*, 2010. **36**(5): p. 840-852.
30. Arvanitis, C.D., et al., *Controlled ultrasound-induced blood-brain barrier disruption using passive acoustic emissions monitoring*. *PLoS one*, 2012. **7**(9).
31. Tsai, C.-H., et al., *Real-time monitoring of focused ultrasound blood-brain barrier opening via subharmonic acoustic emission detection: implementation of confocal dual-frequency piezoelectric transducers*. *Physics in Medicine & Biology*, 2016. **61**(7): p. 2926.
32. Chen, W.-S., et al., *Inertial cavitation dose and hemolysis produced in vitro with or without Optison®*. *Ultrasound in medicine & biology*, 2003. **29**(5): p. 725-737.
33. Qiu, Y., et al., *The correlation between acoustic cavitation and sonoporation involved in ultrasound-mediated DNA transfection with polyethylenimine (PEI) in vitro*. *Journal of Controlled Release*, 2010. **145**(1): p. 40-48.
34. Sun, T., et al., *Ambient pressure dependence of the ultra-harmonic response from contrast microbubbles*. *The Journal of the Acoustical Society of America*, 2012. **131**(6): p. 4358-4364.
35. Rehemtulla, A., et al., *Rapid and quantitative assessment of cancer treatment response using in vivo bioluminescence imaging*. *Neoplasia*, 2000. **2**(6): p. 491-495.
36. Puaux, A.-L., et al., *A comparison of imaging techniques to monitor tumor growth and cancer progression in living animals*. *International journal of molecular imaging*, 2011.
37. Wu, S.-K., et al., *Characterization of different microbubbles in assisting focused ultrasound-induced blood-brain barrier opening*. *Scientific reports*, 2017. **7**: p. 46689.
38. Paxinos, G. and K.B. Franklin, *Paxinos and Franklin's the mouse brain in stereotaxic coordinates*. 2019: Academic press.
39. van den Broek, M.P., et al., *Effects of hypothermia on pharmacokinetics and pharmacodynamics*. *Clinical pharmacokinetics*, 2010. **49**(5): p. 277-294.
40. Saunders, N.R., et al., *Markers for blood-brain barrier integrity: how appropriate is Evans blue in the twenty-first century and what are the alternatives?* *Frontiers in neuroscience*, 2015. **9**: p. 385.
41. Yao, L., et al., *Evans blue dye: a revisit of its applications in biomedicine*. *Contrast media & molecular imaging*, 2018.
42. Caretti, V., et al., *Monitoring of tumor growth and post-irradiation recurrence in a diffuse intrinsic pontine glioma mouse model*. *Brain Pathology*, 2011. **21**(4): p. 441-451.
43. Yoshimura, J., et al., *Clinicopathological study of diffuse type brainstem gliomas: analy-*

- sis of 40 autopsy cases. *Neurologia medico-chirurgica*, 2003. **43**(8): p. 375-382.
44. Yang, F.-Y., et al., *Micro-SPECT/CT-based pharmacokinetic analysis of <sup>99m</sup>Tc-diethylenetriaminepentaacetic acid in rats with blood-brain barrier disruption induced by focused ultrasound*. *Journal of Nuclear Medicine*, 2011. **52**(3): p. 478-484.
  45. Sirsi, S. and M. Borden, *Microbubble compositions, properties and biomedical applications*. *Bubble Science, Engineering & Technology*, 2009. **1**(1-2): p. 3-17.
  46. Greis, C., *Technology overview: SonoVue (Bracco, Milan)*. *European radiology*, 2004. **14**: p. P11-5.
  47. Schneider, M., *Characteristics of sonovue™*. *Echocardiography*, 1999. **16**: p. 743-746.
  48. Talu, E., et al., *Needle size and injection rate impact microbubble contrast agent population*. *Ultrasound in medicine & biology*, 2008. **34**(7): p. 1182-1185.
  49. Pinton, G., et al., *Attenuation, scattering, and absorption of ultrasound in the skull bone*. *Medical physics*, 2012. **39**(1): p. 299-307.
  50. Constantinides, C., R. Mean, and B.J. Janssen, *Effects of isoflurane anesthesia on the cardiovascular function of the C57BL/6 mouse*. *ILAR journal/National Research Council, Institute of Laboratory Animal Resources*, 2011. **52**: p. e21.
  51. McDannold, N., Y. Zhang, and N. Vykhodtseva, *The effects of oxygen on ultrasound-induced blood-brain barrier disruption in mice*. *Ultrasound in medicine & biology*, 2017. **43**(2): p. 469-475.
  52. McDannold, N., Y. Zhang, and N. Vykhodtseva, *Blood-brain barrier disruption and vascular damage induced by ultrasound bursts combined with microbubbles can be influenced by choice of anesthesia protocol*. *Ultrasound Med Biol*, 2011. **37**(8): p. 1259-70.







## Chapter 4

### **Imaged-guided Focused Ultrasound in Combination with Various Formulations of Doxorubicin for the Treatment of Diffuse Intrinsic Pontine Glioma**

This chapter was originally published as Haumann, R., Bianoc, J.I., Waranecki, P.M., Gaillard, P.J., Storm, G., Ries, M., van Vuurden, D.G., Kaspers, G.J.L., Hulleman, E." Imaged-guided focused ultrasound in combination with various formulations of doxorubicin for the treatment of diffuse intrinsic pontine glioma." *Translational Medicine Communication* 7:8 (2022).

## Abstract

Diffuse intrinsic pontine glioma (DIPG) is a notoriously difficult tumor to treat, with an overall survival of DIPG patients being only 11 months. One of the major obstacles for the effective treatment of DIPG is the blood-brain barrier (BBB). In order to circumvent the BBB, drug delivery methods are needed that target the pontine area. One such approach is microbubble-mediated focused ultrasound (FUS) - a non-invasive method that can temporarily and locally open the BBB. Previously, it was shown that FUS is safe with minimal side effects and rapid recovery times in preclinical animal models with different DIPG tumors. However, recent studies have shown that combining FUS with a single treatment of the chemotherapeutic drug doxorubicin did not improve survival in a DIPG xenograft model. As the duration of doxorubicin exposure might play a role in tumor response, we hypothesized that the use of a long-circulation (PEGylated) liposomal formulation of doxorubicin could lead to improved overall survival through a longer exposure time to the tumor.

DIPG xenograft models were established with orthotopic injections of HSJD-DIPG-07 tumor cells into the pontine area of female athymic nude-foxn1<sup>nu</sup> mice. Tumor engraftment was confirmed with bioluminescence imaging (BLI) 40 days post-inoculation. Mice were randomized into groups receiving either liposomal formulations of doxorubicin (2B3-101 or Caelyx<sup>®</sup>) or free doxorubicin in combination with or without FUS treatment. Treatment groups received 5 mg/kg 2B3-101 or Caelyx<sup>®</sup> 1 h before FUS treatment or 5 mg/kg free doxorubicin immediately after FUS.

Histological analysis, however, revealed liposome extravasation in healthy controls but not in HSJD-DIPG-07 xenograft 24 h after treatment. Furthermore, BLI monitoring did not show reduced signal after treatment, which was further illustrated with a survival analysis, showing no significant difference between treated and control animals ( $p = 0.3$ ).

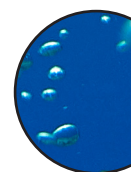
We did not observe a treatment effect after a single dose of free doxorubicin or the liposomal formulations 2B3-101 or Caelyx<sup>®</sup> in combination with FUS in DIPG-bearing mice.

## Background

Diffuse intrinsic pontine glioma (DIPG) is an aggressive, inoperable pediatric brain tumor with very limited and ineffective treatment options outside radiation therapy. Neoadjuvant or adjuvant systemic therapy in combination with radiotherapy only prolongs survival for several months[1-3]. With an overall survival of only 11 months, new drug delivery methods are needed to increase the selective tumor exposure to chemotherapeutic drugs. Several attributes exacerbate the poor prognosis of DIPG, including location and maintained integrity of the blood-brain barrier (BBB)[4, 5]. The BBB is a major obstacle for the efficacy of chemotherapeutics in the treatment of brain tumors as it prevents most large molecules to readily enter the brain parenchyma, resulting in the low efficacy of most chemotherapeutics[6]. As only 2 % of small molecules (< 500 Da) are able to passively cross the BBB, effective drug delivery methods that increase the exposure of drugs in the brain parenchyma are urgently needed[6]. There are several methods to circumvent or temporarily open the BBB, including the use of nanoparticles, convection enhanced delivery (CED), intranasal, and intra-arterial drug delivery[7, 8]. Although encouraging results have been seen, to date these methods have not led to a significant increase in the treatment of several brain tumors, including gliomas.

DIPGs in particular maintain an intact BBB and thus limited penetration and effectiveness of therapeutics, in comparison to glioblastoma which has a heterogenous BBB with regions of necrosis harboring areas with both a disrupted and intact BBB[4, 5, 9]. Since DIPG resides in the pons, a fragile and inoperable structure of the brain, a non-invasive method of delivery is preferred.

Focused ultrasound (FUS) is a non-invasive method that can temporarily and locally open the BBB in a reversible fashion[10, 11]. FUS has been used both preclinically and clinically in growing numbers of clinical trials for the treatment of adult gliomas[12-16]. Previous research has shown that FUS can be safely used in a xenograft model of DIPG to effectively open the BBB and increase the passage of chemotherapeutics such as doxorubicin to the targeted area[14, 16]. Although the use of doxorubicin in these experiments did not lead to significant improvement of survival in vivo, doxorubicin was shown to be effective against several patient-derived DIPG cell lines in preclinical studies[16, 17], and lack of efficacy in vivo could have been caused by multiple dose toxicities[14]. To reduce toxicity of systemic administration, liposomal formulations of doxorubicin can be employed[18, 19]. Caelyx® and 2B3-101 are liposomes loaded with doxorubicin which are 80-100 nm large vesicles that have a long plasma-half-life due to polyethylene glycol (PEG) coating. 2B3-101 liposomes have been shown to have a better brain distribution compared to non-targeted PEG liposomal doxorubicin[20, 21] because they are conjugated with the brain-targeting ligand glutathione (GSH). Both liposomal formulations release the drug over a prolonged period of time reducing toxicity[20, 22]. We hypothesize that the use of FUS in combination with liposomal formulations of doxorubicin – that are less toxic and expose the tumor over a prolonged period through sustained release – may have a significant effect in prolonging survival in a pre-clinical DIPG mouse model. Furthermore, we aimed to investigate the difference between Caelyx® and the 2B3-101 in combination with FUS. Here we describe the use of FUS in combination with free doxorubicin and liposomal formulations of doxorubicin in a HSJD-DIPG-07 xenograft model. We show that treatment with both free and liposomal doxorubicin is safe and well tolerated. However, single treatment did not significantly improve survival in the



treatment groups, possibly due to the lack of sustained tumor exposure, even after the application of FUS. The results of this study will contribute to increased knowledge for the use of FUS for the treatment of DIPG and to advice physicians on clinical trials.

## **Materials and methods**

### ***Cell culture***

DIPG cell line HSJD-DIPG-07 harboring H3F3A K27M and ACVR1 mutations was kindly provided by Dr. Ángel Montero Carcaboso (Hospital San Joan de Déu Barcelona, Spain). This cell line was transduced with the green fluorescent marker ZsGreen and luciferase as described in Meel et al.[23]. Cells were cultured in tumor stem medium (TSM; 50% DMEM-F12/50% Neurobasal-A, Gibco, UK) base supplemented with penicillin-streptomycin (100 U/ml, PAA Laboratories GmbH, Austria), 1X B27 supplement (without vitamin A, Thermo Fisher, Waltham, MA, USA), 20 ng/ml human basic fibroblast growth factor (bFGF, Peprotech, London, UK), 20 ng/ml human epidermal growth factor (EGF, Peprotech, London, UK), 10 ng/ml human platelet-derived growth factor-AA (PDGF-AA, Peprotech, London, UK), 10 ng/ml human platelet-derived growth factor-BB (PDGF-BB, Peprotech, London, UK), and 2 µg/ml heparin (Vrije University Medical Center Pharmacy, Amsterdam, The Netherlands)[23]. Short tandem repeat (STR) analysis was used for validation of the cell line. Before use, tumor cells were harvested, mechanically dissociated with accutase and washed with phosphate buffered saline (PBS, Fresenius Kabi GmbH, Graz Austria). Luciferase expression was assessed with a luminometer (Lumat, Berthold Technologies GmbH & Co KG, Bad Wildbad, Germany).

### ***Xenograft model***

Animal experiments were conducted in accordance with Dutch national regulation guidelines on animal experimentation, as well as with EU Directive 2010/63/EU. The protocol was approved by the committee on animal experimentation of the Vrije University (VU) (AVD114002017841). Female athymic nude-foxn1nu mice (total n = 69: n=63 with xenograft and n=6 without xenograft), 6 weeks of age (Envigo-Harlan Laboratories, Horst, The Netherlands), were kept under filter top conditions with a 12 h artificial light/dark cycle. Mice received food and water ad libitum. Prior to surgery (n=63), mice received 0.067 mg/ml of carprofen (Rimadyl®, Zoetis, Rotterdam, The Netherlands) in drinking water for 24 h. Thirty minutes prior to intracranial injection (i.c.) mice received 0.05-0.1 mg/kg of buprenorphine hydrochloride (Temgesic®, Indivior UK Ltd, Berkshire, United Kingdom). Anesthesia was induced with isoflurane (1-3 % and 2 l/min of O<sub>2</sub>, Zoetis, Rotterdam, The Netherlands) and mice were fixed in a stereotactic frame. The depth of anesthesia was determined by the absence of palpebral, withdrawal, and corneal reflexes. Topical administration of 2 % of lidocaine was applied before incision along the midline, after which a burr hole was drilled 1.0 mm lateral and 0.8 mm posterior to the lambda using a high-speed drill. A Hamilton syringe (Hamilton Company, Reno, NV, USA) was used to inject 5 µl of 5 x 10<sup>5</sup> HSJD-DIPG-07 cells in PBS into the pons at a depth of 4.5 mm, with an infusion rate of 2 µl/min. After injection, the needle was left in place for 2 min before being slowly removed to avoid a vacuum

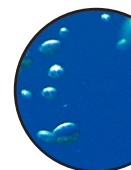
and cell accumulation into the needle tract. The wound was then closed using topical skin adhesive (Dermflex, Vygon, Ecouen, France) and the animals were allowed to awaken under a heating lamp. All animals awoke within 15 to 30 min following surgery and did not present any signs of distress. Carprofen in drinking water was removed 24 h following surgery. Mice received supplemented food (Nutrigel, Portland, ME, USA) for 24 to 48 h after treatment. Mice were regularly weighted and neurologically assessed[24]. Neurological assessment was based on motor score (ranging from no deficit to walking with obvious asymmetry to no movements) and abnormal movements such as tilted head and axial body rotation. Bioluminescence imaging (BLI) was performed once a week to monitor the growth rate of the orthotopic tumors. For BLI, mice were intraperitoneally (i.p.) injected with 150  $\mu$ l of D-luciferin Potassium Salt (100mM solution in PBS, Goldbio, St. Louis, MO, USA) 10 min before imaging. Animals were anaesthetized with isoflurane (3 % and 2 l/min O<sub>2</sub>) 5 min prior to imaging. BLI was performed with a Bruker In-Vivo Extreme Capture System (Bruker Corporation, Billerica, MA, USA) with an exposure time of 30 s. For each mouse, a region of interest (ROI) defined the luminescent area of the tumor and the mean intensity of the ROI (photon/sec/m<sup>2</sup>) was calculated using Molecular Imaging Software (Bruker Corporation, Billerica, MA, USA).

### ***Focused ultrasound***

The imaged-guided focused ultrasound method was previously described in Haumann et al.[25]. In brief, mice received 0.05-0.1 mg/kg of buprenorphine 15-30 min before anesthesia with isoflurane (1-3 % and 2 l/min of O<sub>2</sub>). The depth of anesthesia was determined by the absence of palpebral, withdrawal, and corneal reflexes. A 26 G catheter (Neoflon, Becton Dickinson, Helsingborg, Sweden) was placed in the tail vein and flushed with 50  $\mu$ l of heparin (Vrije University Medical Center Pharmacy) to prevent blood clotting. Mice were then mounted on a 3D printed platform and fixed with bite and ear bars, after which they received 150  $\mu$ l of D-luciferin via subcutaneous (s.c.) injection 10 min prior to treatment. BLI and X-ray was performed to localize the tumor and to guide the transducer to the tumor in the pons. A hydrophone was placed behind the ear of the mouse and coupled with a 1 MHz monoelement transducer using ultrasound gel. Microbubbles (SonoVue, Bracco International BV, Amsterdam) were prepared according to the manufacture's description. A 19 G needle was used to take up the microbubbles and fill up the catheter. Microbubbles were injected in two boli of 60  $\mu$ l. Focused ultrasound was then performed at a frequency of 1.5 Hz to a total exposure time of 160 s, consisting of 40 repetitions over 6 points with a total 240 sonications. The safety of the procedure was monitored with passive cavitation detection.

### ***BBB opening***

To ascertain optimal acoustic power in the HSJD-DIPG-07 xenograft model, different acoustic pressures were used, (Figure 1: BBB opening). Mice received either 200 kPa (n = 3) or 400 kPa (n = 3). Directly after FUS, mice received Evans blue (100  $\mu$ l, Sigma Aldrich, St. Louis, MO, USA). After 30 min mice were sacrificed and transcardially perfused with saline before brains were excised for analysis.





## ***Survival analysis***

HSJD-DIPG-07 xenografts were established in 54 mice. Tumor engraftment was monitored with weekly BLI measurements (Figure 1: survival). Upon increase of the BLI signal (indication of engraftment), at day 37 after implantation, mice were evenly stratified into nine groups of each 6 mice: (A) Control, (B) FUS only, (C) Vehicle liposomes + FUS, (D) doxorubicin + FUS, (E) systemic doxorubicin, (F) Caelyx<sup>®</sup> + FUS, (G) systemic Caelyx<sup>®</sup>, (H) 2B3-101 + FUS, and (I) systemic 2B3-101 (n=6 per group). At day 40, mice received 5 mg/kg doxorubicin (5 mg/kg, Vrije University Medical Center Pharmacy, Amsterdam, The Netherlands), Caelyx<sup>®</sup> (5 mg/kg, Vrije University Medical Center Pharmacy, Amsterdam, The Netherlands), 2B3-101 (5 mg/kg, kindly provided by dr. Pieter Gaillard) or control liposomes (PEG liposomes without doxorubicin) (kindly provided by prof. Gert Storm). The polyethylene glycol (PEG)-coated liposomal formulations of doxorubicin, Caelyx<sup>®</sup> and 2B3-101 as well as control liposomes were intravenously administered 60 min before sonoporation. Mice were regularly weighed and neurologically assessed. After treatment, BLI was performed twice a week for two weeks and followed by once a week to monitor tumor growth. At experimental endpoints, animals were deeply anaesthetized with a ketamine (2.4 mg, Alfasan Woerden, The Netherlands) and sedazine (0.24 mg, AST FARMA, Oudewater, The Netherlands) mixture and transcardially perfused with saline before brains were excised for analysis. In brief, once the animal was sedated and no reflexes were observed, an incision was made along the midline of the chest, and the resulting cavity was held open with retractors. A small incision was made to the left ventricle and right atrium and a blunt tip needle was then inserted through the left ventricle into the anterior aorta and held in place with surgical clamps before 50 ml of saline was circulated through the vascular system using a syringe. Following perfusion, brains were excised and cut along the sagittal plane. One sagittal half was fixed in 4 % formaldehyde (Merck, Darmstadt, Germany) and the other half was snap frozen in liquid nitrogen.

## ***Histology and immunohistochemistry***

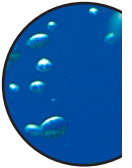
PEG staining was done to visualize the localization of PEGylated liposomes (Figure 1: immunofluorescence imaging). The staining was performed on both non-tumor bearing mice (n=3) and tumor bearing mice receiving Caelyx<sup>®</sup> (n=3) or 2B3-101 (n=3). Mice received focused ultrasound at 400 kPa. After 24 h, mice were transcardially perfused and brains were frozen in liquid nitrogen. Frozen tissue was cut at 5  $\mu$ m. Tissue was fixed with ice cold methanol. Aldehyde groups were blocked with glycine (VWR, Fontenay-sous-Bois, France) after which the sections were incubated with primary anti-PEG-B-47 antibody (1:100) (Abcam, Cambridge, MA, USA) and rat anti-mouse CD31 (1:50) (BD Pharmingen, San Diego, CA, USA) in PBS containing 1 % bovine serum albumin (Sigma Aldrich, St. Louis, MO, USA) overnight at RT. After washing, slices were incubated with Alexa Fluor goat anti-rabbit 488 and Alexa Fluor goat anti-rat 633 (Life technologies, Eugene, OR, USA) secondary antibodies for 30 min at RT. Slices were then rinsed and mounted with Vectashield mounting medium containing DAPI (Vector laboratories, Burlingame, CA, USA) and kept in the dark until analyzed.

The following stainings were performed on tissue obtained from the BBB opening and survival studies. Formaldehyde fixed tissues were embedded in paraffin and sectioned into 5  $\mu$ m slices using a microtome. Detailed observations of cellular and tissue structures in the

brain were obtained by performing standard hematoxylin and eosin (HE) staining (Sigma Aldrich, St. Louis, MO, USA) on slide mounted brain samples. For paraffin embedded sections, slides were first deparaffinized in xylene, after which they were rehydrated in a series of alcohol baths. The sections were then stained with hematoxylin, rinsed and counterstained with eosin. Slices were dehydrated and mounted with mounting medium (Eukitt, Sigma Aldrich, Steinheim, Germany).

Vimentin staining was performed on paraffin embedded tissue by initially deparaffinizing and rehydrating sections, followed by blocking of endogenous peroxidases and permeabilization of the cell membrane with 0.3 % peroxide (Merck, Darmstadt, Germany) in methanol (VWR, Fontenay-sous-Bois, France) for 30 min at room temperature (RT). Antigen retrieval was performed using citrate buffer before incubation of the primary Mouse- $\alpha$ -Vimentin (1:4000, Monoclonal mouse anti-vimentin clone V9, Dako Denmark Glostrup, Denmark) for 1 h at RT. Vimentin was visualized with EnVision  $\alpha$ M/ $\alpha$ R and 3,3'-diaminobenzidine (DAB) (Dako, Glostrup, Denmark). The slices were counterstained with hematoxylin, dehydrated and mounted with a coverslip with mounting medium.

Blood vessels were visualized on both 5  $\mu$ m frozen (HSJD-DIPG-07, n=3) and paraffin embedded tissue (non-tumor bearing control mice, n=2). Frozen tissue was fixed with 2 % paraformaldehyde for 10 min. Slides were rinsed and aldehyde groups were blocked with glycine. Tissue was incubated with primary CD31 rat anti-mouse antibody (1:50) and rabbit anti-mouse laminin (1:500) (Abcam, Cambridge, MA, USA) overnight at room temperature. The following day, slides were washed and incubated with Alexa Fluor goat anti-rabbit 488 and Alexa Fluor goat anti-rat 633 secondary antibodies for 60 min at RT. After rinsing, tissue was mounted with Vectashield mounting medium containing DAPI and kept in the dark until analyzed. Paraffin embedded control tissue (mice without tumor) was deparaffinized and rehydrated before antigen retrieval with Tris-EDTA Buffer (10mM Tris Base, 1mM EDTA Solution, 0.05% Tween 20, pH 9.0). The tissue was then incubated with glycine for 10 min to block aldehyde groups. Slides were incubated with Lycopersicon esculentum (tomato) lectin (1:100, Vector laboratories, Burlingame, CA, USA) for 60 min at RT. Slides were rinsed and mounted with Vectashield mounting medium containing DAPI and stored in the dark.



## **Statistics**

Survival analysis using Kaplan Meier and Log Rank test was performed in R (R Core Team (2017). R: A language and environment for statistical computing. R Foundation for Statistical Computing, Vienna, Austria. URL <https://www.R-project.org/>). Statistical significance was determined at  $p < 0.05$ .

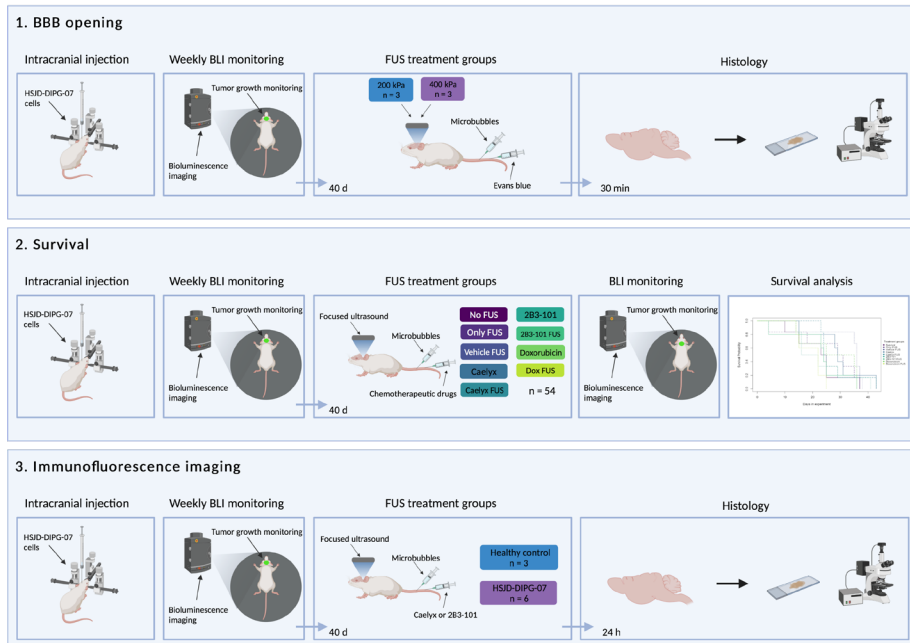


**Figure 1. | Experimental design.** BBB opening after FUS was determined in HSJD-DIPG-07 tumor-bearing mice which received 200 kPa (n=3) and 400 kPa (n=3) to observe the extent of BBB opening. Mice received 400 kPa during treatment in all subsequent experiments. Survival analysis was performed on HSJD-DIPG-07 xenograft models (n=54). Mice were regularly monitored with BLI and upon increase of the signal, mice received treatment with focused ultrasound. After treatment, mice were monitored and sacrificed at humane endpoints. Immunofluorescence histology was performed on non-tumor bearing mice (n=3) and tumor bearing mice (HSJD-DIPG-07) (n=6) to determine the presence of liposomal formulations of doxorubicin in the brain parenchyma. At 24 h after treatment mice were sacrificed and brains were frozen until analysis. (Created with Biorender)

## Results

### BBB opening

To optimize safe drug delivery, different pressures (200 kPa and 400 kPa) were applied to determine the extent of BBB opening in HSJD-DIPG-07 xenograft-bearing mice. Figure 2A shows the detection of microbubbles after the first and second i.v. administration, followed by the rapid gradual clearance of the microbubbles from the vasculature (indicated by arrows). The frequency spectrum that monitored the stable and inertial cavitation of the microbubbles did not show inertial cavitation which can be observed by a sudden increase in noise floor (Figure 2B). Rather, only a third harmonic was observed, indicative of stable cavitation. Treatment planning was performed using a combination of X-ray and BLI, targeting the pontine region (Figure 2C)[25].

Both pressures were well tolerated with no observation of bleeding or tissue damage, as shown with histology (Figure 3). Moreover, the image-guided targeting of FUS resulted in the local opening of the BBB in the pontine region, as visualized with Evans Blue, the golden standard to show BBB opening. However, we observed that the extent of BBB opening

following 200 kPa was remarkably lower, exemplified by lower Evans Blue extravasation and inadequate coverage of the tumor region defined by human vimentin staining, 400 kPa was chosen for treatment (Figure 3).

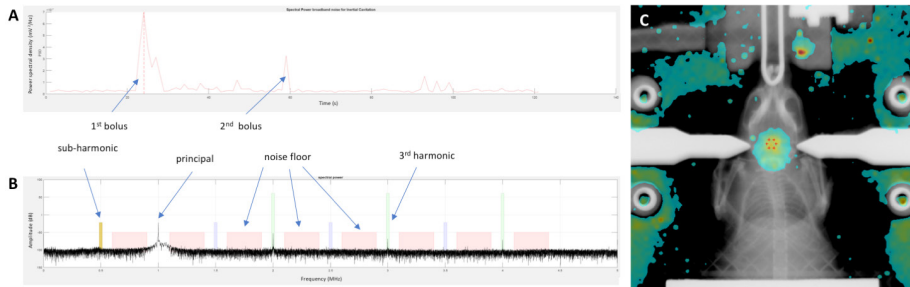
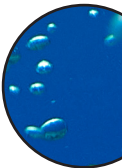


**Figure 2. | Cavitation detection and targeting.** A: The acoustic energy of the microbubbles reflected to the transducer recorded over 240 sonications. The two bolus ejections (blue arrows) can be observed followed by rapid clearance of the microbubbles. B: Integrated power spectrum of the 3rd harmonic over time, indicating stable cavitation. No sudden increase in noise floor was observed. C: Overlay of X-ray and BLI of mouse brain indicating the tumor in the red/yellow area. The target area is indicated with a hexagon (6 red dots).



### Survival Analysis

BLI signal exponentially increased at day 37 after i.c. injections (Figure 4A). Although BLI is not an exact measure for tumor size, it is a reliable indication of tumor growth and hence this was used to stratify mice into nine groups: (A) Control, (B) FUS only, (C) Vehicle liposomes + FUS, (D) systemic doxorubicin + FUS, (E) systemic doxorubicin, (F) Caelyx® + FUS, (G) systemic Caelyx®, (H) 2B3-101 + FUS, and (I) systemic 2B3-101 (n=6 per group). At day 40, mice were treated and received 5 mg/kg doxorubicin, 5 mg/kg Caelyx®, 5 mg/kg 2B3-101 or 5 mg/kg control liposomes. Mice maintained a stable weight directly after treatment, although weight decline was observed over time that correlated with increasing tumor growth measured with BLI (Supplemental Figure 1). After treatment, mice underwent BLI twice weekly for two weeks and thereafter once a week until humane endpoint was reached. BLI monitoring did not reveal a decrease in signal intensity after treatment (Supplemental Figure 2), which indicates that tumor growth was not stalled or reduced. The survival curves of the different treatment groups overlap. Survival analysis, using Kaplan Meier and Log Rank, showed no significant differences between the different treatment groups ( $p = 0.3$ , Figure 4B and Supplemental figure 3).

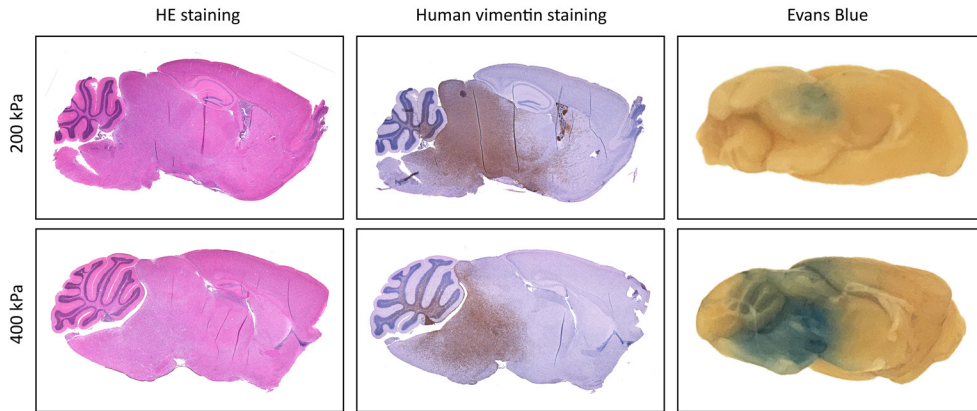


**Figure 3.** | Sagittal brain sections of FUS treated HSJD-DIPG-07 xenograft-bearing mice showing safety and BBB opening. Left: HE stainings indicating no tissue damage after FUS at 200 and 400 kPa. Middle: Human vimentin staining showing the diffuse growth pattern of HSJD-DIPG-07 xenograft. Right: Evans Blue extravasation after FUS showing an overlap with the human vimentin (tumor) staining at 400 kPa while at 200 kPa the tumor area is not covered.

### ***Liposome extravasation into the brain parenchyma***

Since no significant difference in survival was observed, the presence of doxorubicin-loaded liposomes in the vasculature and brain parenchyma was investigated with immunofluorescence stainings. Therefore, sagittal slices of mouse brain were incubated with an anti-PEG antibody to determine the local extravasation of liposomes in the pontine area (Figure 5). In non-tumor bearing mice (control), PEGylated liposomes were clearly extravasated and retained in the pontine area at 24 h after FUS treatment. PEGylated liposomes were observed in the brain parenchyma, in close vicinity of the blood vessels, resulting in only a partial exposure. However, two out of three brains of tumor bearing mice treated with Caelyx® and FUS stained positive for liposomes in the blood vessels after 24 h but not in the brain parenchyma (Supplemental Figure 4). One Caelyx® FUS and three 2B3-101 FUS-treated animals stained negative for PEG. The control groups also stained negative for liposomes.

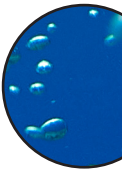
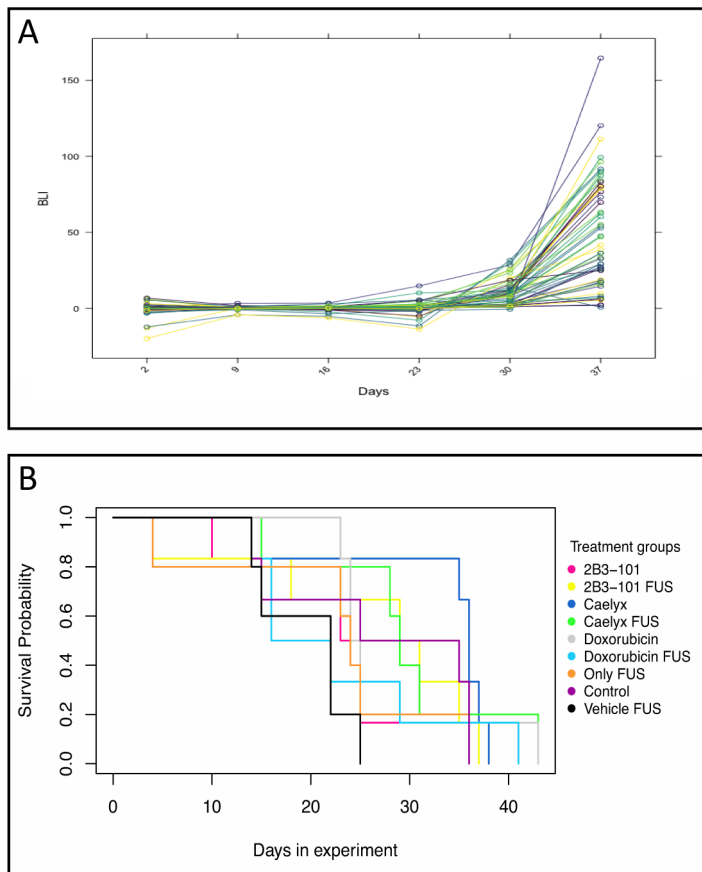


**Figure 4. | BLI monitored tumor engraftment and survival following treatment.** A: Weekly BLI (photon/sec/m<sup>2</sup>) monitoring as a measure of tumor engraftment. The mean intensity of the background was subtracted from the tumor BLI. Exponential growth was observed 37 days after tumor implantation. B: Survival analysis (Kaplan-Meier curve) of the different treatment groups. Day 0 is the start of treatment. “Days in experiment” represents the number of days after treatment. Differences in groups (n=6 mice per group) were not statistically significant (p = 0.3).

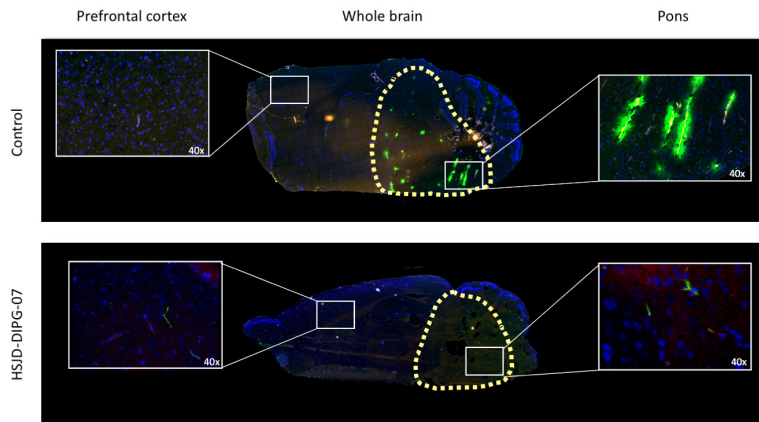


**Figure 5. | Immunofluorescent PEG staining on sagittal slices of FUS-treated mouse brains.** A positive staining of liposomes (in green) was detected in the pontine region of control (non-tumor bearing mice) (upper panel) who received Caelyx<sup>®</sup>. The pontine/tumor area delineated with a yellow dotted line. In contrast, only few liposomes were observed in the blood vessels of the HSJD-DIPG-07 xenograft model that received Caelyx<sup>®</sup> (lower panel). In both panels endothelial cells are indicated in red (CD31 staining), nuclei in blue (DAPI).

## Discussion

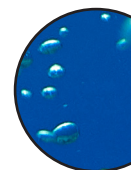
Current standard treatment for DIPG patients consist of radiotherapy in combination with adjuvant chemotherapy, resulting in a median overall survival of 11 months[1, 26]. However, after years of preclinical and clinical testing of new therapeutic approaches, the overall survival of DIPG patients remains unchanged [1, 27]. It is thought that most drugs do not reach and maintain high enough drug concentrations in the tumor area and thus result in a low efficacy in patients[28, 29]. Various formulations of doxorubicin have been used in phase I/II studies in both adult glioma and pediatric high-grade glioma population without clear benefit [30-32]. Most of these clinical studies have been initiated by promising *in vitro* results for many interesting drug candidates but *in vivo* do not show the same efficacy. One of the reasons could be that drug concentrations are low. The BBB, which is believed to remain intact in patients with DIPG, limits the exposure of the drugs to the brain[4, 5]. Since, only small molecules (< 500 Da) can enter the brain parenchyma, only a limited number of drugs are suitable for adjuvant treatment in DIPG [6]. As most drugs that have been developed do not readily cross the BBB, drug delivery methods are needed to circumvent the BBB and allow these drugs to enter the parenchyma[7].

Microbubble-mediated FUS has been used successfully in several orthotopic models. This drug delivery method has been shown to specifically target the tumor area and locally increase drug concentrations[33, 34]. More importantly, FUS is a minimally invasive procedure with fast recovery times and no serious side effects. To date, FUS has been successfully used in preclinical glioma models using temozolomide, bevacizumab, carboplatin, BCNU, etoposide, and doxorubicin[18, 33-40]. In both a 9-L glioma rat model as well as a U87 mouse model temozolomide significantly increased median survival[33, 38]. Bevacizumab

combined with FUS showed an increase in median survival in a U87 mouse model and normalization of the tumor vasculature was observed due to the bevacizumab-related block of vascular endothelial growth factor (VEGF)[34]:[41]. FUS with carboplatin also showed improvement in survival in a U87 mouse model but had a non-significant result in a patient-derived cell line (6240 LN)[39]. Furthermore, BCNU and etoposide showed a significant survival benefit, respectively in C6 glioma rats and a syngeneic mouse model (MGPP3 harboring PDGF<sup>+</sup>, Pten<sup>-/-</sup>, P53<sup>-/-</sup>)[37, 40]. However, the compounds that have been studied most in adult glioma models in combination with FUS are doxorubicin and liposomal doxorubicin[36, 42, 43]. Combining free doxorubicin with FUS resulted in an increase of drug concentration in the brain and improved overall survival in SMA 560 and GL261 glioma mouse models[36]. Furthermore, FUS in combination with a liposomal formulation of doxorubicin has shown improvement of survival in a 9L rat glioma model[18]:[44]. However, here improvement in survival was accompanied by severe side effects common to doxorubicin such as skin toxicity, impaired activity, damage to surrounding brain tissue, tissue loss at the tumor site, and intratumoral hemorrhage[44].

Since FUS has been successful in treating different adult glioma models, we aimed to explore the use of this technique for the treatment of pediatric DIPG in a preclinical animal model. *In vitro*, doxorubicin was found to be effective on primary cell cultures, including HSJD-DIPG-07[17, 45]. Since doxorubicin was found to be effective *in vitro* against DIPG cell lines and FUS in combination with (liposomal) doxorubicin has shown a survival benefit in glioma xenograft models, doxorubicin could be a good candidate for treatment of preclinical DIPG mouse model[17]. Ishida and colleagues recently showed that while FUS was able to enhance delivery of free doxorubicin into the brain, the combined use did not have the desired improvement in survival in a DIPG xenograft model[14]. Initially, Ishida and colleagues used 5 mg/kg of doxorubicin *in vivo*, which led to severe toxicity. Subsequently, a cumulative dose of 3 mg/kg (1.5 mg/kg weekly over 2 weeks) was used. However, unexpected toxicity was once again observed while survival benefits were not realized[14].

We hypothesized that the use of FUS with various formulations of PEGylated liposomal doxorubicin would reduce toxicity and expose the tumor for a prolonged period of time to doxorubicin. Contrary to Ishida et al., 5 mg/kg of free doxorubicin did not result in severe toxicity in our mouse model. Previous experiments showed that 5 mg/kg doxorubicin was tolerated and not toxic to the animals (Sewing et al., and data not shown)[17]. However, we observed that longer treatment times with FUS (> 20 min) resulted in poor recovery and increased weight loss. Since MRI-guided FUS as used by Ishida has a longer treatment time than the BLI image-guided FUS we used in our study[25]. The use of doxorubicin in combination with MRI-guided FUS with long treatment times might have resulted in limiting toxicities. Besides differences in treatment times, in our study mice also received additional nutritional food supplement to aid recovery. Furthermore, the used mouse strain (NOD scid gamma (NSG) vs nude-foxn1<sup>nu</sup>), and tumor model (SU-DIPG-17 vs DIPG-HSJD-07) differed in these studies, as well as the method to visualize tumor growth. Since PEGylated liposomes can be visualized with immunofluorescence, we stained the liposomes in both healthy controls and xenograft tissue to confirm delivery into the brain. Remarkably, liposomes were clearly observed in non-tumor bearing mice (control) tissue but not in HSJD-DIPG-07 brain tissue. In only two mice treated with Caelyx<sup>®</sup> and FUS we observed areas with PEGylated liposomes within the blood vessels but not in the brain parenchyma at 24 hour after treat-

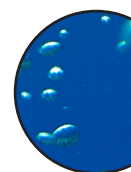




ment. These liposomes were not limited to the FUS treated area, which therefore might indicate local areas of poor cardiac perfusion. Hence, the lack of survival benefit might be a result of the lack of liposomes in the brain parenchyma, as observed already 24 h after treatment. The absence of liposomes might be caused by a high intratumoral pressure preventing accumulation of liposomes in the brain parenchyma[46]. Furthermore, the morphology and functionality of endothelial cells might be altered in the presence of a tumor, which can have a negative effect on liposomal binding in the endocytosis/transcytosis pathway, thus preventing liposomes to cross the BBB[47, 48]. Moreover, Alli et al. showed a 50-fold increase in doxorubicin concentration upon FUS treatment in non-tumor bearing mice, while Ishida et al. showed only a four-fold increase in a DIPG model[16, 49]. Therefore, the lack of accumulation of doxorubicin and doxorubicin liposomes might be intrinsic to the presence of a tumor or certain tumor type. These hypotheses should be further explored to explain the absence of liposomes 24 h after FUS. However, the analysis of liposomes in the brain is problematic since conventional analytical methods such as mass spectrometry or high-pressure liquid chromatography (HPLC) cannot distinguish between blood vessel and brain parenchyma, consequently making it impossible to determine the exact location of the liposomes. Additionally, liposomes are packed with multiple doxorubicin molecules and therefore determination of doxorubicin concentration is not a good measure to calculate the concentration of the drug in the brain. Microdialysis would have enabled us to determine the presence of liposomes over time in the brain, but this technique requires a metal canula that will interfere with FUS and therefore was not suited for our experiments. Visualization of liposomes in the brain and tumor regions following FUS treatment has also been unachievable for other groups, which relied heavily on HPLC and MS in showing doxorubicin concentration rather than presence of liposomes[18, 43].

Another possible explanation for the lack of efficacy observed in both our study and in Ishida et al. are the pharmacokinetics and –dynamics of (liposomal) doxorubicin in rodents, in relationship to the exposure needed to reach an effective local tissue area under the curve (AUC) *in vivo* that can compare with *in vitro* IC50. For the cell line used in our study, the IC50 was previously ascertained to be 40 nM at 96 hours. In published data, after administration of 5 mg/kg doxorubicin in rodents a Cmax of 10 µg/ml (18.4 µM) was reached just after injection but swiftly decreased to plasma concentrations between 0.1 and 0.01 µg/ml at 72 hours, corresponding to 184 nM and 18.4 nM respectively[50]. Alli et al. found a local brainstem tissue concentration of 824 nM, two hours after FUS and injection of 5 mg/kg doxorubicin in NGS mice[16]. If and how local tissue concentrations stay above the *in vitro* AUC can be debated. Potentially, the plasma wash-out goes hand in hand with decreasing local drug concentrations after FUS. With regard to the pharmacokinetics of liposomal formulations, important differences are observed compared to free doxorubicin, with an up to 2.6 – 6.8 increased plasma AUC[51]. Of note however in this respect is the fact that this AUC mainly reflects the presence of encapsulated doxorubicin, which is released over a longer time frame, with free drug slowly released from the liposomes, long after the BBB has closed after FUS. Furthermore, in patients often lower single doses of doxorubicin are administered, ranging between 1 – 1.6 mg/kg, which further limits the translatability of our study towards clinical trials. Yet, a clinical study that evaluates the safety of Caelyx® in combination with transcranial MRI-guided FUS for adult brain tumor patients is currently planned as a basis for later studies to evaluate clinical efficacy (NCT02343991). Here, we aimed to compare the effects of Caelyx® and 2B3-101 – which both have been approved for

clinical use – in combination with FUS to determine if there would be a treatment benefit of any of those compounds. 2B3-101 has been designed specifically for the treatment of brain tumor patients and has been shown to have a 5-times higher drug delivery into the brain than Caelyx<sup>®</sup> (in the absence of FUS)[52], while the slightly smaller size of Caelyx<sup>®</sup> might enhance brain distribution after passing the BBB. However, since in our experiments no difference in survival was observed and both liposomes could not be visualized in the treated animals, we cannot draw any conclusions about the difference between Caelyx<sup>®</sup> and 2B3-101 after FUS treatment. Regarding the programmed clinical trial, however, it should be noted that in various preclinical studies there is a clear difference in survival benefit between adult glioma and pediatric DIPG models. Both etoposide and doxorubicin have been used in preclinical models of glioma and DIPG[14, 36, 37, 53]. While etoposide and doxorubicin prolonged survival in adult glioma models, these compounds did not improve survival in preclinical models of DIPG, even after multiple treatments[37, 53]. This raises the question why is there a difference in efficacy, especially since etoposide was used in the same tumor model, with the only difference being the anatomical location of implantation. While there is little information on the permeability of the heterogenous BBB, there are indications that the BBB in the pontine region is more tightly regulated than other areas of the brain[4]. This might result in different BBB opening dynamics with FUS. Furthermore, we observed that the liposomes do not diffuse far into the tissue and remain in the vicinity of the blood vessels exposing only a small pontine area to the drug. In a recent study in our group, we found that the number of blood vessels are reduced in DIPG patients compared to healthy controls[54]. This would limit the exposure of drugs after treatment with FUS due to the low blood vessel density. To design an effective treatment for DIPG, we therefore hypothesize that a combination of FUS with other modalities could be beneficial. For example, low-frequency FUS has been shown to induce an immune response, such as an increased expression of pro-inflammatory cytokines, chemokines and infiltration of immune cells in the brain parenchyma[55]. However, more research is needed to investigate such combinations, as we could not determine the effects of FUS on the immune system in our (immune-deficient) xenografts. Of note, the HSJD-DIPG-07 mouse model used in our experiments showed a relatively high number of vessels compared to healthy controls (392.5 blood vessels/nm<sup>2</sup> versus 219.3 blood vessels/nm<sup>2</sup> respectively), and therefore blood vessel count does most likely not explain the ineffectiveness of the treatment described here. As such, there are still a lot of uncertainties before FUS can be translated into the clinic. Future research should investigate the exact reason why FUS in combination with various formulations of doxorubicin has been unsuccessful. Pharmacokinetic considerations are of high importance in the choice of drugs repurposed for FUS in this respect.



## Conclusion

In conclusion, FUS is a non-invasive technique that has been successfully used in preclinical glioma models. Here, we report a third study investigating FUS for the treatment of DIPG that shows safety, but does not show survival benefit after treatment with doxorubicin, 2B3-101, and Caelyx<sup>®</sup>. Further studies are needed to investigate the reason why FUS has a different response in DIPG xenograft models in order to translate into better treatments for this deadly pediatric brain cancer.

## Supplementary Materials

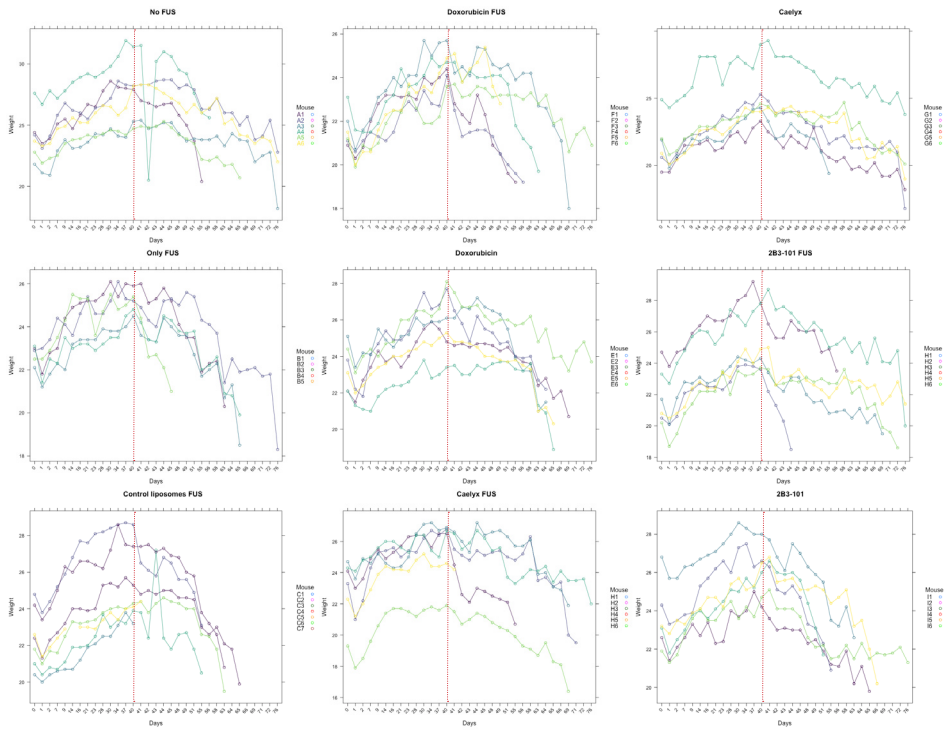


**Figure S1.** | Weight registration, Weight (grams, y-axis) was regularly monitored to assess animal well-being over time (days, x-axis). Overall mice weight remained stable around the treatment day, indicated by a red dotted line. With increasing tumor growth, weight also decreased.

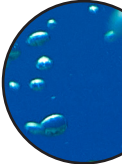
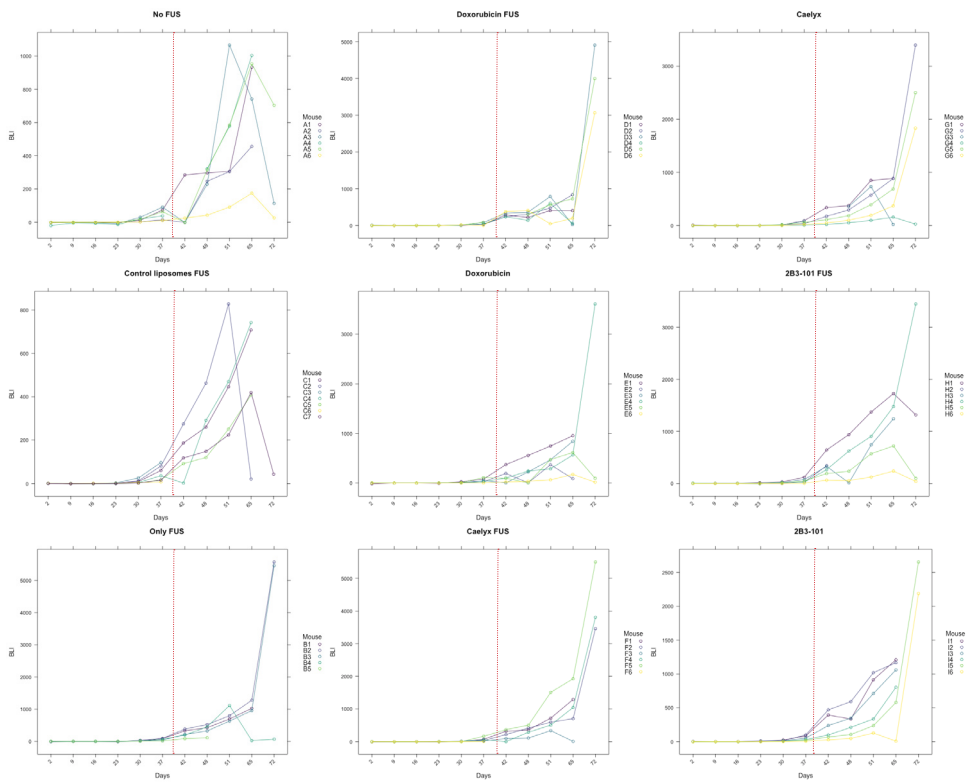


**Figure S2.** | BLI monitoring, BLI was measured twice a week for two weeks after treatment followed by once a week until humane endpoint was reached. For all mice, BLI signal did not decline after treatment, indicating tumor growth. Notably, in several cases BLI signal drastically dropped at humane endpoint. Dotted red line indicates time of treatment.

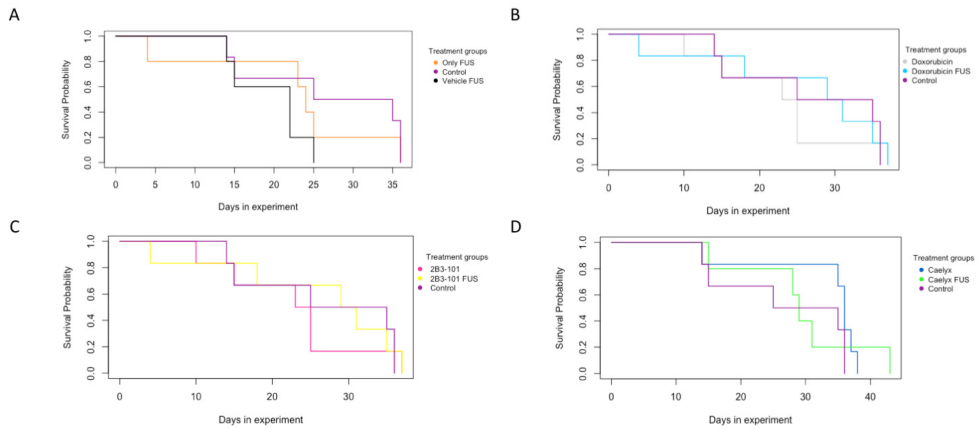


**Figure S3.** | Survival Analysis. Separated graphs from Figure 4 (Controls vs. Treatment). Day 0 is the start of treatment. “Days in experiment” represents the number of days after treatment. Figure 3A displays the survival curves of the control, vehicle FUS, and only FUS ( $p=0.2$ ). Here, graphs overlap indicating no difference between the control groups. The same holds true for the treatment groups displayed in Figure 3B (survival curves of control, doxorubicin with FUS, and doxorubicin) ( $p=0.7$ ), 3C (control, Caelyx<sup>®</sup> with FUS, and Caelyx<sup>®</sup>) ( $p=0.5$ ) and 3D (control, 2B3-101 with FUS, and 2B3-101) ( $p=0.9$ ).

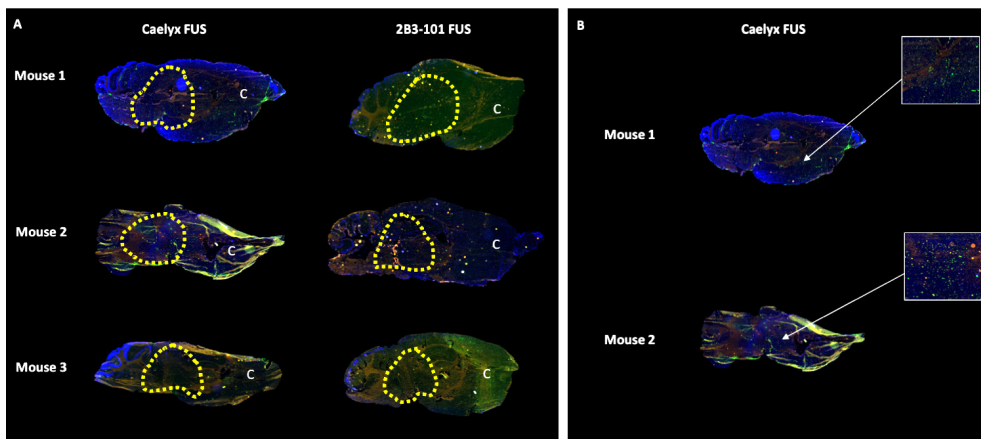
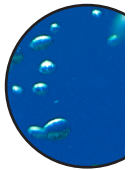


**Figure S4.** | Immunofluorescent (IF) staining on sagittal slices of mouse brains. A: IF of blood vessels (CD31 in red) and pegylated liposomes (anti-PEG in green) did not show the presence of liposomes 24 h after treatment except for mouse 1 and mouse 2 treated with Caelyx<sup>®</sup> and FUS. Yellow area indicates the tumor area. B: Enlarged picture shows the presence of Caelyx<sup>®</sup> liposomes in the cortex outside of the sonoporated area.

## References

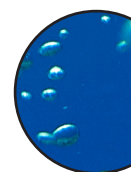
1. Hoffman, L.M., et al., *Clinical, radiologic, pathologic, and molecular characteristics of long-term survivors of diffuse intrinsic Pontine Glioma (DIPG): a collaborative report from the international and European Society for Pediatric Oncology DIPG registries*. Journal of Clinical Oncology, 2018. **36**(19): p. 1963–1972.
2. Wagner, S., et al., *Treatment options in childhood pontine gliomas*. Journal of neuro-oncology, 2006. **79**(3): p. 281-287.
3. Gokce-Samar, Z., et al., *Pre-radiation chemotherapy improves survival in pediatric diffuse intrinsic pontine gliomas*. Child's Nervous System, 2016. **32**(8): p. 1415-1423.
4. McCully, C.M., et al., *Model for concomitant microdialysis sampling of the pons and cerebral cortex in rhesus macaques (Macaca mulatta)*. Comparative medicine, 2013. **63**(4): p. 355-360.
5. Warren, K.E., *Beyond the blood: brain barrier: the importance of central nervous system (CNS) pharmacokinetics for the treatment of CNS tumors, including diffuse intrinsic pontine glioma*. Frontiers in oncology, 2018. **8**: p. 239.
6. Pardridge, W.M., *The blood-brain barrier: bottleneck in brain drug development*. NeuroRx, 2005. **2**(1): p. 3-14.
7. Haumann, R., et al., *Overview of Current Drug Delivery Methods Across the Blood–Brain Barrier for the Treatment of Primary Brain Tumors*. CNS drugs, 2020: **34**(11): 1121-1131.
8. Patel, M.M. and B.M. Patel, *Crossing the blood–brain barrier: recent advances in drug delivery to the brain*. CNS drugs, 2017. **31**(2): p. 109-133.
9. Agarwal, S., et al., *Active efflux of Dasatinib from the brain limits efficacy against murine glioblastoma: broad implications for the clinical use of molecularly targeted agents*. Mol Cancer Ther, 2012. **11**(10): p. 2183-2192.
10. Hynynen, K., et al., *Noninvasive MR imaging–guided focal opening of the blood-brain barrier in rabbits*. Radiology, 2001. **220**(3): p. 640-646.
11. McDannold, N., et al., *Temporary disruption of the blood–brain barrier by use of ultrasound and microbubbles: safety and efficacy evaluation in rhesus macaques*. Cancer research, 2012. **72**(14): p. 3652-3663.
12. Carpentier, A., et al., *Clinical trial of blood-brain barrier disruption by pulsed ultrasound*. Science translational medicine, 2016. **8**(343): p. 343re2-343re2.
13. Mainprize, T., et al., *Blood-Brain Barrier Opening in Primary Brain Tumors with Non-invasive MR-Guided Focused Ultrasound: A Clinical Safety and Feasibility Study*. Scientific reports, 2019. **9**(1): p. 321.



14. Ishida, J., et al., *MRI-guided focused ultrasound enhances drug delivery in experimental diffuse intrinsic pontine glioma*. *Journal of Controlled Release*, 2020.
15. Idbaih, A., et al., *Safety and feasibility of repeated and transient blood–brain barrier disruption by pulsed ultrasound in patients with recurrent glioblastoma*. *Clinical Cancer Research*, 2019. **25**(13): p. 3793-3801.
16. Alli, S., et al., *Brainstem blood brain barrier disruption using focused ultrasound: A demonstration of feasibility and enhanced doxorubicin delivery*. *Journal of Controlled Release*, 2018. **281**: p. 29-41.
17. Sewing, A.C.P., et al., *Preclinical evaluation of convection-enhanced delivery of liposomal doxorubicin to treat pediatric diffuse intrinsic pontine glioma and thalamic high-grade glioma*. *Journal of Neurosurgery: Pediatrics*, 2017. **19**(5): p. 518-530.
18. Treat, L.H., et al., *Improved anti-tumor effect of liposomal doxorubicin after targeted blood-brain barrier disruption by MRI-guided focused ultrasound in rat glioma*. *Ultrasound in medicine & biology*, 2012. **38**(10): p. 1716-1725.
19. Rafiyath, S.M., et al., *Comparison of safety and toxicity of liposomal doxorubicin vs. conventional anthracyclines: a meta-analysis*. *Exp Hematol Oncol*, 2012. **1**(1): p. 10.
20. Gaillard, P.J., et al., *Pharmacokinetics, brain delivery, and efficacy in brain tumor-bearing mice of glutathione pegylated liposomal doxorubicin (2B3-101)*. *PloS one*, 2014. **9**(1): p. e82331.
21. Birngruber, T., et al., *Enhanced doxorubicin delivery to the brain administered through glutathione PEGylated liposomal doxorubicin (2B3-101) as compared with generic Caelyx,®/Doxil®—a cerebral open flow microperfusion pilot study*. *Journal of Pharmaceutical Sciences*, 2014. **103**(7): p. 1945-1948.
22. Gabizon, A., H. Shmeeda, and Y. Barenholz, *Pharmacokinetics of pegylated liposomal doxorubicin*. *Clinical pharmacokinetics*, 2003. **42**(5): p. 419-436.
23. Meel, M.H., et al., *An efficient method for the transduction of primary pediatric glioma neurospheres*. *MethodsX*, 2018. **5**: p. 173-183.
24. Thomale, U., et al., *Neurological grading, survival, MR imaging, and histological evaluation in the rat brainstem glioma model*. *Child's Nervous System*, 2009. **25**(4): p. 433-441.
25. Haumann, R., et al., *A High-Throughput Image-Guided Stereotactic Neuronavigation and Focused Ultrasound System for Blood-Brain Barrier Opening in Rodents*. *J Vis Exp*, 2020(161).
26. Wagner, S., et al., *Treatment options in childhood pontine gliomas*. *Journal of Neuro-Oncology*, 2006. **79**(3): p. 281-287.
27. Hargrave, D., U. Bartels, and E. Bouffet, *Diffuse brainstem glioma in children: critical*

review of clinical trials. *Lancet Oncol*, 2006. **7**(3): p. 241-248.

28. Cohen, K.J., et al., *Temozolomide in the treatment of children with newly diagnosed diffuse intrinsic pontine gliomas: a report from the Children's Oncology Group*. *Neuro Oncol*, 2011. **13**(4): p. 410-416.
29. van Zanten, S.E.V., et al., *A phase I/II study of gemcitabine during radiotherapy in children with newly diagnosed diffuse intrinsic pontine glioma*. *Journal of neuro-oncology*, 2017. **135**(2): p. 307-315.
30. Chastagner, P., et al., *Phase I study of non-pegylated liposomal doxorubicin in children with recurrent/refractory high-grade glioma*. *Cancer Chemother Pharmacol*, 2015. **76**(2): p. 425-432.
31. Marina, N.M., et al., *Dose escalation and pharmacokinetics of pegylated liposomal doxorubicin (Doxil) in children with solid tumors: a pediatric oncology group study*. *Clin Cancer Res*, 2002. **8**(2): p. 413-8.
32. Wagner, S., et al., *Pegylated-liposomal doxorubicin and oral topotecan in eight children with relapsed high-grade malignant brain tumors*. *J Neurooncol*, 2008. **86**(2): p. 175-181.
33. Liu, H.-L., et al., *Pharmacodynamic and therapeutic investigation of focused ultrasound-induced blood-brain barrier opening for enhanced temozolomide delivery in glioma treatment*. *PloS one*, 2014. **9**(12): p. e114311.
34. Liu, H.-L., et al., *Focused ultrasound enhances central nervous system delivery of bevacizumab for malignant glioma treatment*. *Radiology*, 2016. **281**(1): p. 99-108.
35. Bunevicius, A., N.J. McDannold, and A.J. Golby, *Focused ultrasound strategies for brain tumor therapy*. *Operative Neurosurgery*, 2020. **19**(1): p. 9-18.
36. Kovacs, Z., et al., *Prolonged survival upon ultrasound-enhanced doxorubicin delivery in two syngenic glioblastoma mouse models*. *Journal of controlled release*, 2014. **187**: p. 74-82.
37. Wei, H.-J., et al., *Focused Ultrasound-Mediated Blood-Brain Barrier Opening Increases Delivery and Efficacy of Etoposide for Glioblastoma Treatment*. *International Journal of Radiation Oncology\* Biology\* Physics*, 2021, **110**(2): 539-550.
38. Wei, K.-C., et al., *Focused ultrasound-induced blood-brain barrier opening to enhance temozolomide delivery for glioblastoma treatment: a preclinical study*. *PloS one*, 2013. **8**(3): p. e58995.
39. Dréan, A., et al., *Temporary blood-brain barrier disruption by low intensity pulsed ultrasound increases carboplatin delivery and efficacy in preclinical models of glioblastoma*. *Journal of neuro-oncology*, 2019. **144**(1): p. 33-41.
40. Liu, H.-L., et al., *Blood-brain barrier disruption with focused ultrasound enhances de-*



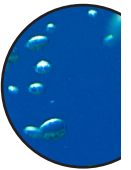


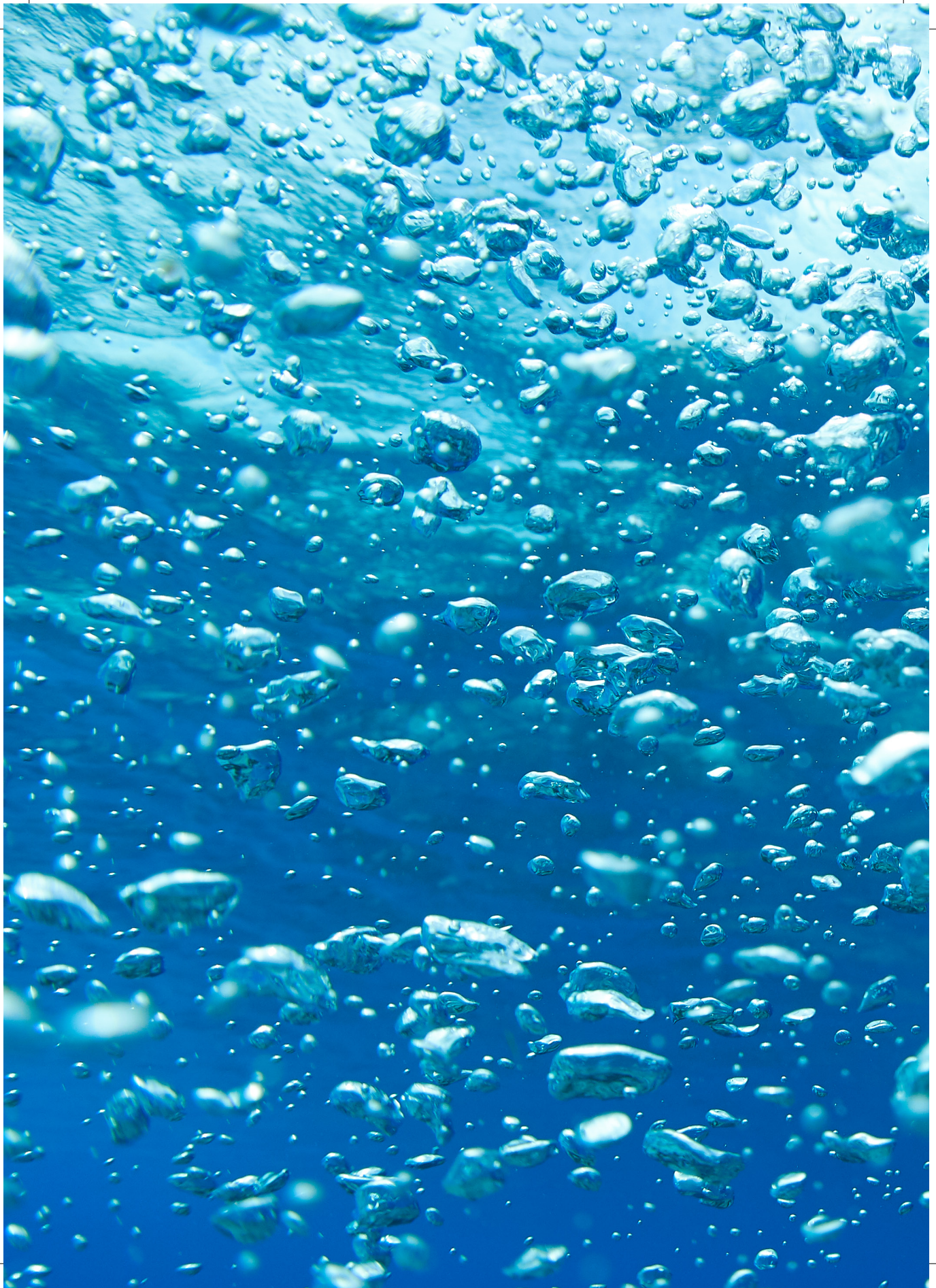
*livery of chemotherapeutic drugs for glioblastoma treatment*. *Radiology*, 2010. **255**(2): p. 415-425.

41. Zhao, C., et al., *Hypoxic glioblastoma release exosomal VEGF-A induce the permeability of blood-brain barrier*. *Biochemical and biophysical research communications*, 2018. **502**(3): p. 324-331.
42. Lin, Y.-L., M.-T. Wu, and F.-Y. Yang, *Pharmacokinetics of doxorubicin in glioblastoma multiforme following ultrasound-Induced blood-brain barrier disruption as determined by microdialysis*. *Journal of pharmaceutical and biomedical analysis*, 2018. **149**: p. 482-487.
43. Sun, T., et al., *Closed-loop control of targeted ultrasound drug delivery across the blood–brain/tumor barriers in a rat glioma model*. *Proceedings of the National Academy of Sciences*, 2017. **114**(48): p. E10281-E10290.
44. Aryal, M., et al., *Multiple treatments with liposomal doxorubicin and ultrasound-induced disruption of blood–tumor and blood–brain barriers improve outcomes in a rat glioma model*. *Journal of controlled release*, 2013. **169**(1-2): p. 103-111.
45. Ung, C., et al., *Doxorubicin-Loaded Gold Nanoarchitectures as a Therapeutic Strategy against Diffuse Intrinsic Pontine Glioma*. *Cancers*, 2021. **13**(6): p. 1278.
46. Harward, S., et al., *T2-weighted images are superior to other MR image types for the determination of diffuse intrinsic pontine glioma intratumoral heterogeneity*. *Child's Nervous System*, 2018. **34**(3): p. 449-455.
47. Hofman, P., et al., *Endothelial cell hypertrophy induced by vascular endothelial growth factor in the retina: new insights into the pathogenesis of capillary nonperfusion*. *Archives of ophthalmology*, 2001. **119**(6): p. 861-866.
48. Witmer, A.N., et al., *In vivo angiogenic phenotype of endothelial cells and pericytes induced by vascular endothelial growth factor-A*. *Journal of Histochemistry & Cytochemistry*, 2004. **52**(1): p. 39-52.
49. Ishida, J., et al., *MRI-guided focused ultrasound enhances drug delivery in experimental diffuse intrinsic pontine glioma*. *Journal of Controlled Release*, 2020. **330**(10): p. 1034-1045.
50. Lee, J.B., et al., *Interspecies prediction of pharmacokinetics and tissue distribution of doxorubicin by physiologically-based pharmacokinetic modeling*. *Biopharmaceutics & drug disposition*, 2020. **41**(4-5): p. 192-205.
51. Lu, W.-L., et al., *A pegylated liposomal platform: pharmacokinetics, pharmacodynamics, and toxicity in mice using doxorubicin as a model drug*. *Journal of pharmacological sciences*, 2004. **95**(3): p. 381-389.
52. Brandsma, D., et al., *Phase 1/2a study of glutathione pegylated liposomal doxorubicin (2b3-101) in patients with brain metastases (BM) from solid tumors or recurrent high*

*grade gliomas (HGG)*. *Annals of Oncology*, 2014. **25**: p. iv157.

53. Englander, Z.K., et al., *Focused ultrasound mediated blood–brain barrier opening is safe and feasible in a murine pontine glioma model*. *Scientific Reports*, 2021. **11**(1): p. 1-10.
54. El-Khouly, F.E., et al., *The neurovascular unit in diffuse intrinsic pontine gliomas*. *Free Neuropathology*, 2021. **2**: p. 17-17.
55. Kim, C., et al., *The roles of thermal and mechanical stress in focused ultrasound-mediated immunomodulation and immunotherapy for central nervous system tumors*. *J Neurooncol*, 2022.







## Chapter 5

### The Neurovascular Unit in Diffuse Intrinsic Pontine Gliomas

This chapter was originally published as El-Khouly, F. E., Haumann, R., Breur, M., van Zanten, S. E. V., Kaspers, G. J., Hendrikse, N. H., Hulleman, E., van Vuurden, D.G., Bugiani, M. The neurovascular unit in diffuse intrinsic pontine gliomas. *Free Neuropathology*, 2, 17-17 (2021).

## Abstract

Diffuse intrinsic pontine glioma (DIPG) is a childhood brainstem tumor with a median overall survival of eleven months. Lack of chemotherapy efficacy may be related to an intact blood-brain barrier (BBB). In this study we aim to investigate the neurovascular unit (NVU) in DIPG patients.

DIPG biopsy (n = 4) and autopsy samples (n = 6) and age-matched healthy pons samples (n = 20) were immunohistochemically investigated for plasma protein extravasation, and the expression of tight junction proteins claudin-5 and zonula occludens-1 (ZO-1), basement membrane component laminin, pericyte marker PDGFR- $\beta$ , and efflux transporters P-gp and BCRP. The mean vascular density and diameter were also assessed.

DIPGs show a heterogeneity in cell morphology and evidence of BBB leakage. Both in tumor biopsy and autopsy samples, expression of claudin-5, ZO-1, laminin, PDGFR- $\beta$  and P-gp was reduced compared to healthy pontine tissues. In DIPG autopsy samples, vascular density was lower compared to healthy pons. The density of small vessels (<10  $\mu\text{m}$ ) was significantly lower ( $P < 0.001$ ), whereas the density of large vessels ( $\geq 10 \mu\text{m}$ ) did not differ between groups ( $P = 0.404$ ). The median vascular diameter was not significantly different: 6.21  $\mu\text{m}$  in DIPG autopsy samples (range 2.25-94.85  $\mu\text{m}$ ), and 6.26  $\mu\text{m}$  in controls (range 1.17-264.77  $\mu\text{m}$ ).

Our study demonstrates evidence of structural changes in the NVU in DIPG patients, both in biopsy and autopsy samples, as well as a reduced vascular density in end-stage disease. Adding such a biological perspective may help to better direct future treatment choices for DIPG patients.

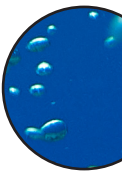
## Introduction

Diffuse intrinsic pontine gliomas (DIPGs) are rare and aggressive childhood malignancies of the brainstem. These tumors are characterized by a diffuse growth pattern closely interwoven within white matter tracts and grey matter structures, and an intrinsic nature, uttered by hypertrophy of the brainstem often encasing the basilar artery [1, 2]. With a median overall survival of eleven months, and a two-year survival rate of 10%, DIPGs are the leading cause of brain tumor-related deaths in children [3-7]. In the recent World Health Organization (WHO) classification of tumors of the central nervous system (CNS), DIPGs were reclassified as H3K27M mutated Diffuse Midline Glioma (DMG H3K27M) [8].

Though much research has been dedicated to DIPG, its poor outcome has remained unchanged for the past 40 years [9]. To date, radiotherapy remains the only (temporarily) effective, albeit palliative treatment, and no chemotherapy regimens prolonging survival have been identified yet. Since *in vitro* and *in vivo* drug testing on patient-derived tumor cells has shown sensitivity to conventional cytotoxic agents and novel drugs, the lack of efficacy in patients is hypothesized to be related to ineffective drug delivery due to an intact blood-brain barrier (BBB) [10-12].

The BBB is formed by endothelial cells interconnected and sealed by tight junctions. The abluminal surface of the endothelium is covered by a basement membrane in which pericytes are embedded. Pericytes control the cerebral blood flow by regulating capillary diameter and vessel stability. The basement membrane is enclosed by astrocyte end-feet, also important for brain homeostasis. Together, pericytes and astrocyte end-feet induce and maintain the integrity of the BBB [13, 14]. The BBB regulates transport of essential nutrients to the brain through active transport mechanisms, such as glucose transporters of the GLUT-family. The efflux of waste products and exogenous compounds is mediated through efflux transporters of the ATP-binding cassette family (e.g. P-gp, BCRP, MRP-1) [14, 15]. Additionally, the paracellular barrier capacities of the tight junctions limit transport of circulating monoamines and drugs across the BBB [14-16]. The intimate contact and interaction of the BBB complex, formed by endothelial cells, tight junctions, pericytes and astrocyte end-feet, with neurons and perivascular microglia form a dynamic functional unit, called the neurovascular unit (NVU) [13, 14, 16].

Some studies report different expression of tight junction proteins throughout the brain, suggestive of regional heterogeneity in BBB permeability [17, 18]. However, little research has been done on the BBB and NVU in the brainstem and particularly in the pons. Yet, better insight into the BBB and the NVU at these sites is needed to develop new treatment strategies for pediatric brainstem tumors. This especially holds true for DIPG, where the BBB is thought to be a major contributor to therapeutic inefficacy. In this study, we aim at determining and comparing the histological and immunohistochemical characteristics of the NVU of the pons in children with DIPG and age-matched controls.



## Patients and Methods

### *Patients and Samples*

DIPG pre-treatment biopsy samples (n = 4) were obtained from the Biobank of the Princess Máxima Center for Pediatric Oncology, Utrecht, the Netherlands, and processed as formalin-fixed paraffin-embedded tissue. End-stage disease DIPG autopsy samples (n = 6) were obtained from the 'VUmc Brain autopsy in children with DIPG' study [19]. This study was approved by the institutional review board of Amsterdam UMC, location VUmc (METc VUmc, study number: VUMC2009/237) and the Scientific Committee of the Dutch Childhood Oncology Group (DCOG). In this study, brain tissue was obtained within a post-mortem interval of less than six hours for Dutch patients and less than nine hours for patients from abroad, and was processed as formalin-fixed paraffin-embedded tissue or snap frozen. Biopsy samples were MRI-guided and taken from the tumor area displaying the highest hyper-intensity on T2-weighted image (Figure 1A). Autopsy samples were obtained from the non-necrotic tumor core in the pons (Figure 1B).

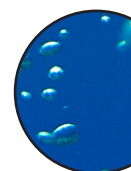
Age-matched, healthy pontine tissue samples (n = 20) were obtained from the NIH NeuroBioBank, Maryland, United States. Samples were selected based on (i) brain region (pons), (ii) clinical brain diagnosis (unaffected control/sudden deaths), (iii) post-mortem interval (<17 hours), and (iv) presence of formalin-fixed tissue and frozen tissue.

Table 1 shows patient and treatment characteristics of the DIPG patients. Median age at diagnosis was 7.7 years (range 1.3-17.0 years). All patients had a H3K27M mutated DIPG. All autopsy patients, except for the youngest, received radiotherapy at diagnosis. Of these, at disease progression, three out of six received different chemotherapy regimens and two patients did not proceed to further treatment. Median overall survival of patients that were autopsied was 19.5 months (range 5.5-24.0 months). Supplementary Table 1 shows the characteristics of the control group. Median age was 7.0 years (range 1.0-19.0 years). All controls were healthy and had an accidental death.

**Table 1. | DIPG patient characteristics**

	Gender	Age at diagnosis (y)	Type of sample	Genetics (WHO grading)	First-line treatment	Second-line treatment	OS (mo.)
1	F	3.5	Biopsy	DMG H3K27M (WHO IV)	n.a.	n.a.	n.a.
2	F	6.9	Biopsy	DMG H3K27M (WHO IV)	n.a.	n.a.	n.a.
3	M	7.9	Biopsy	DMG H3K27M (WHO IV)	n.a.	n.a.	n.a.
4	F	13.6	Biopsy	DMG H3K27M (WHO IV)	n.a.	n.a.	n.a.
5	M	14.4	Autopsy	DMG H3K27M (WHO IV)	RTx	Chemo	18.7
6	F	11.4	Autopsy	DMG H3K27M (WHO IV)	RTx	Chemo	24.0
7	F	17.0	Autopsy	DMG H3K27M (WHO IV)	Chemo-RTx	Chemo	24.7
8	F	1.3	Autopsy	DMG H3K27M (WHO IV)	Chemo	None	10.6
9	F	4.0	Autopsy	DMG H3K27M (WHO IV)	RTx	Chemo-RTx	20.2
10	M	7.5	Autopsy	DMG H3K27M (WHO IV)	RTx	None	5.5

*F: female; M: male; y: year; DMG H3K27M: H3K27M mutated diffuse midline glioma; WHO: World Health Organization; RTx: radiotherapy; Chemo-RTx: radiotherapy combined with chemotherapy; OS (mo.): overall survival (months); n.a.: not applicable.*



### **Immunohistochemistry**

Air-dried 5 µm-thick cryosections were fixed in 2% formaldehyde for 10 min at room temperature (RT). Aldehyde groups were blocked in 0.1 g glycine in 100 ml distilled water for 10 min at RT. Sections were incubated overnight at RT with a primary antibody: (i) tight junction protein claudin-5 (1:50, Invitrogen, Carlsbad, CA, USA); (ii) tight junction protein ZO-1 (1:50, Invitrogen, Carlsbad, CA, USA); (iii) basement membrane component laminin (1:500, Novus Biologicals, Abingdon UK); or (iv) pericyte marker PDGFR-β (1:500, Abcam, Cambridge, UK). The sections were co-stained with glial fibrillary acidic protein (GFAP; 1:1000, Merck, Darmstadt, Germany). The following day, the sections were incubated with Alexa Fluor®-labelled secondary antibodies, background was quenched with 0.1% Sudan black B, and sections were mounted in mounting medium (Vectashield with 4',6-diamidino-2-fenylindool (DAPI); Vector Laboratories Inc., Burlingame, California, USA).

Five-µm-thick formalin-fixed paraffin-embedded tissue sections were routinely stained with hematoxylin & eosin (H&E). A gross axial section through the pons and cerebellum was stained with Luxol fast blue-periodic acid-Schiff. For immunohistochemistry, sections were deparaffinized using xylene, and rehydrated through descending alcohol concentrations. Endogenous peroxidase activity was blocked by incubating the slides for 30 min in phosphate



buffered saline (PBS) containing 0.3 % H<sub>2</sub>O<sub>2</sub>. Heat-induced antigen retrieval was performed in 0.01 M citrate buffer (pH 6.0). After washing in PBS, the slides were incubated overnight at RT with primary antibodies against P-gp (1:20; Millipore, CA, USA), BCRP (1:40; Abcam, Cambridge, UK), pre-albumin (1:50,000, Dako, Glostrup, Denmark), fibrinogen (1:1,600, Dako, Glostrup, Denmark), IgG (1:800, Dako, Glostrup, Denmark) and hypoxia-inducible factor 1 $\alpha$  (HIF-1 $\alpha$ ; 1:40, Cayman Chemical, Michigan, USA). The next day, slides were incubated with ready-to-use EnVision™-HRP (Dako, Glostrup, Denmark) for 1 hour at RT and visualized with 3,3'-Diaminobenzidine (DAB+ DAKO; 1:50, Glostrup, Denmark) for 10 min. The slides were counterstained with hematoxylin for 1 min and mounted with Quick-D mounting medium (Klinipath, Duiven, The Netherlands).

### ***Data Analysis***

Sections were imaged using a Leica DM6000B microscope (400x magnification; Leica Microsystems BV, Rijswijk, The Netherlands). From each tissue slide, ten images were made. A semi-quantitative analysis of the BBB staining, comparing DIPG samples with control samples, was done by two independent reviewers (FE and RH) using the Leica Application Suite X: LAS X version 3.1.5.16308. The vascular density was assessed on claudin-5-stained tissue sections by counting the number of blood vessels per mm<sup>2</sup>. The luminal diameter of the blood vessels was measured with the Leica Application Suite X: LAS X version 3.1.5.16308.

### ***Statistics***

Data were analyzed using an independent samples t-test (p-value = 0.05) using IBM SPSS Statistics version 26. The Levene's Test of Equality of Variance was used to first test the assumption of homogeneity or variance between the groups (p-value = 0.05). When equal variances were assumed, pooled estimates were used for the independent t-test statistics. When equal variances were not assumed, un-pooled data and an adjustment to the degree of freedom (df) were used for the independent t-test statistics.

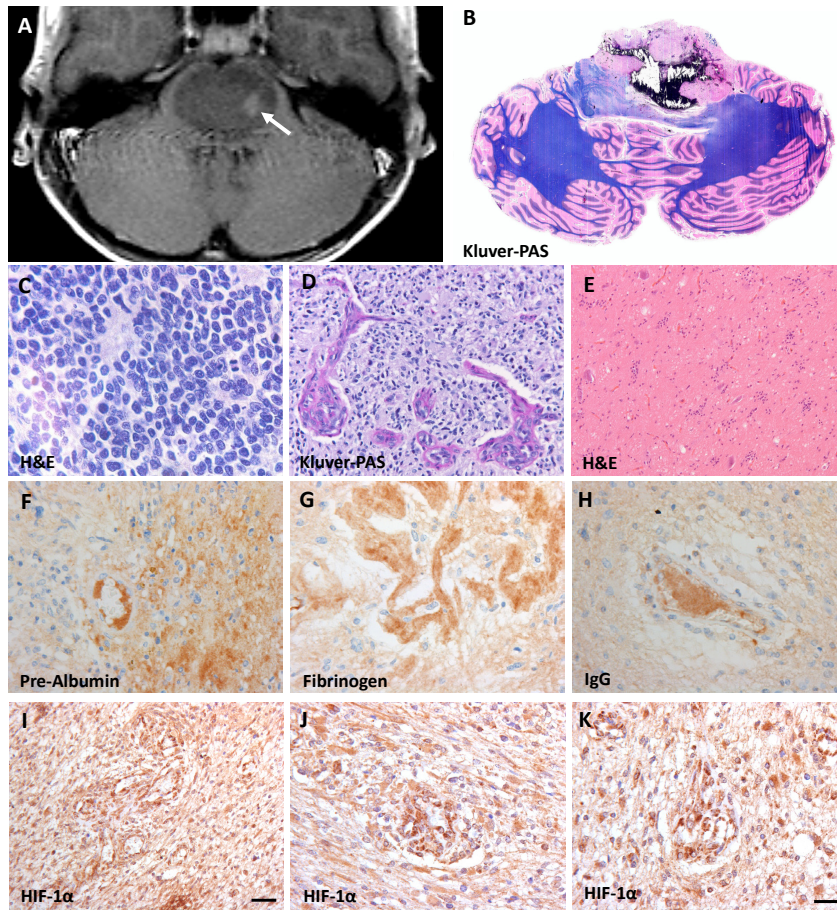


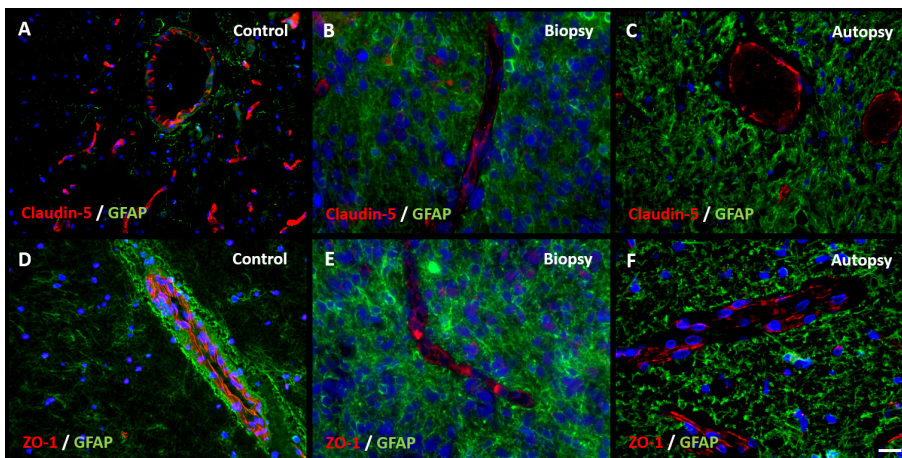
**Figure 1. | Characteristics of diffuse intrinsic pontine glioma (DIPG).** A: T2-weighted MRI-image of a DIPG patient showing an expanded tumor at the basis of the pons. The arrow indicates the biopsy sampling area; B: Gross axial section of the pons and cerebellum showing the presence of a diffuse infiltrating tumor in the pons, reaching the middle cerebellar peduncles. The box indicates the sampling location of autopsy tissue at the non-necrotic tumor site; C-E: hematoxylin and eosin (H&E) staining of the vital tumor bulk showing morphologic heterogeneity compatible with WHO grade IV tumors (C and D) and grade I tumors (E); H-F: stains against intravascular plasma proteins pre-albumin (F), fibrinogen (G) and IgG (H) showing extravasation of these protein into the DIPG tumor parenchyma; I-K: hypoxia inducible factor-1 $\alpha$  (HIF-1 $\alpha$ ) staining demonstrating a high expression of HIF1 $\alpha$ . (scale bar: 5  $\mu$ m)

## Results

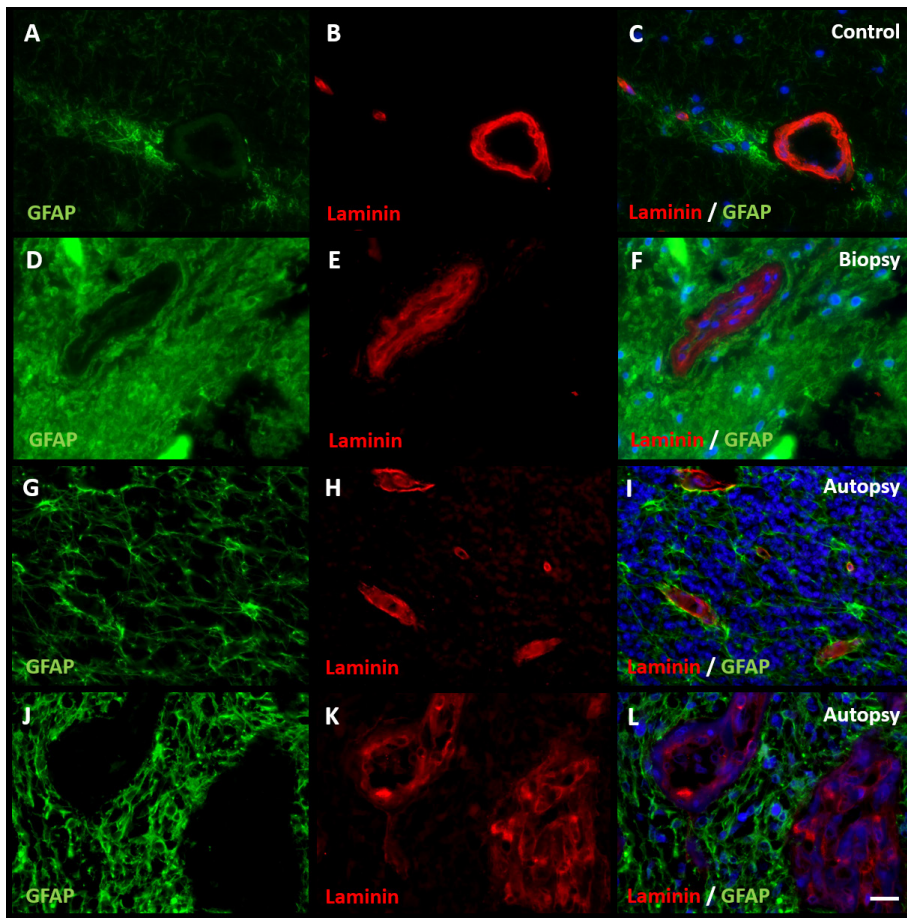
### Immunohistochemistry

Figure 1 shows typical DIPG MRI features with enlargement of the pons and contrast enhancement. Gross inspection confirms the presence of a partly necrotic and hemorrhagic tumor center in the pons. Microscopic examination shows variability of tumor cell morphology, ranging from grade I to grade IV according to the 2016 WHO classification of CNS tumors. Tumor areas were recognized based on cell density, the presence of (atypical) mitotic figures and features of high grade glioma, including necrosis and microvascular proliferation. In these tumors, the integrity of the BBB is compromised, as demonstrated by extravasation of pre-albumin, fibrinogen and IgG. This corresponds with expression of HIF-1 $\alpha$ , indicating tumor hypoxia. Notably, as expected for a heterogeneous tumor such as DIPG, the density of GFAP-expressing astrocytes varied throughout the tumor [20]. Additionally, tumor cells were differentiated from pre-existing astrocytes by their higher expression levels of GFAP, conceivably also related to their less differentiated state [20].

Immunohistochemical staining of claudin-5, ZO-1, laminin, PDGFR- $\beta$ , P-gp and BCRP were evaluable in all samples. Expression of tight junction proteins claudin-5 and ZO-1 was lower at inspection in all DIPG biopsy and autopsy samples compared to control samples (Figure 2). The expression of basement membrane protein laminin was lower at the glial basement membrane in DIPG biopsy and autopsy samples. Interestingly, this was observed in both pre-existent vessels within the tumor cells and in neovascular proliferation (Figure 3). Expression of pericyte marker PDGFR- $\beta$  was also reduced in both DIPG biopsy and autopsy samples (Figure 4). Efflux transporter P-gp expression was lower in DIPG biopsy and autopsy samples, whereas the expression of BCRP was not different in DIPG compared to controls (Figure 5).



**Figure 2. | Expression of tight junction proteins claudin-5 and zonula occludens-1 (ZO-1) in DIPG pre-treatment biopsy and post-mortem autopsy samples.** In controls, claudin-5 and ZO-1 are sharply defined and have a segmented pattern (A and D). Claudin-5 and ZO-1 show reduced expression in DIPG samples (B, C, E, F). Please note the non-activated state of GFAP-expressing astrocytes in control tissue. (blue: nuclei; green: astrocytes; red: claudin-5 or ZO-1; scale bar: 5  $\mu$ m).



**Figure 3. | Expression of basement membrane (laminin) in DIPG pre-treatment biopsy and post-mortem autopsy samples.** In controls (A-C), laminin shows a continuous pattern. Laminin expression was reduced at the glial basement membrane in both DIPG biopsy (D-F) and autopsy samples (G-I). This was also observed in neovascularization in autopsy samples (J-L). Of note: neovascular proliferation was not detected in biopsy samples (blue: nuclei; green: astrocytes; red: laminin; scale bar: 5  $\mu$ m).

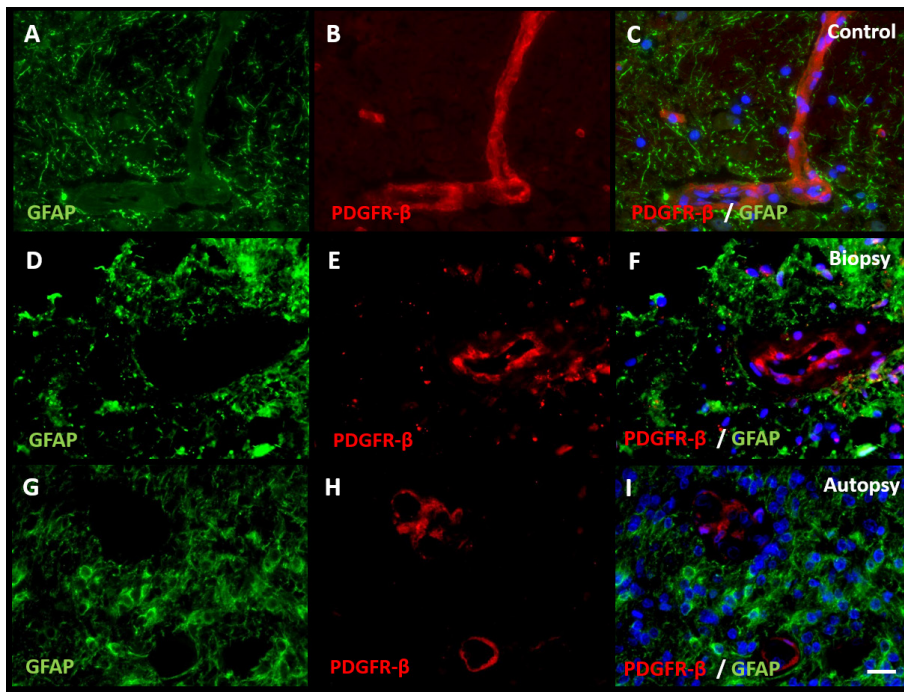


**Figure 4. | Expression of pericytes (PDGFR- $\beta$ ) in DIPG pre-treatment biopsy and post-mortem autopsy samples.** In controls (A-C), PDGFR- $\beta$  shows a continuous pattern. Expression of PDGFR- $\beta$  was reduced in both DIPG biopsy (D-F) and autopsy samples (G-I). (blue: nuclei; green: astrocytes; red: PDGFR- $\beta$ ; scale bar: 5  $\mu$ m).

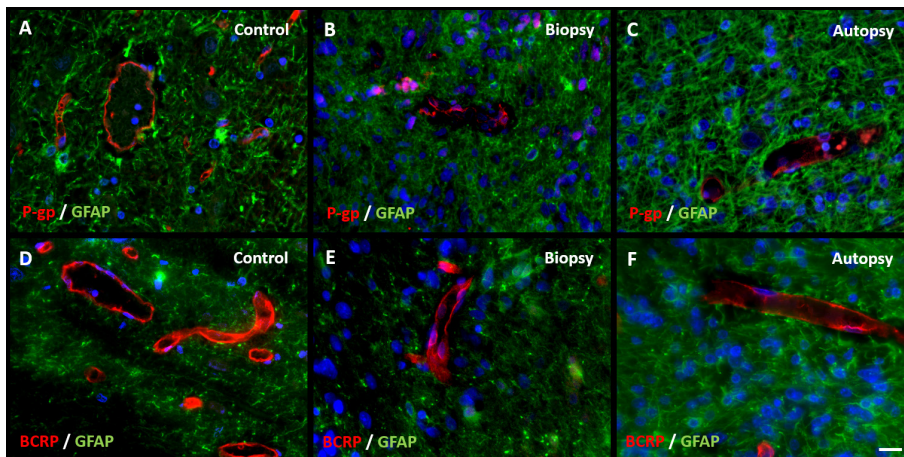


**Figure 5. | Expression of efflux transporters P-gp and BCRP in DIPG pre-treatment biopsy and post-mortem autopsy samples.** P-gp and BCRP are sharply defined and have a segmented pattern in controls (A and D). Expression of P-gp was reduced in both DIPG samples (B and C). BCRP expression was unchanged (E and F). (blue: nuclei; green: astrocytes; red: P-gp or BCRP; scale bar: 5  $\mu$ m).

## Vascular Density

Vascular density per  $\text{mm}^2$  was measured in non-necrotic biopsy and autopsy tissue. It was significantly reduced in DIPG autopsy samples compared to controls ( $1.5 \pm 1.2/\text{mm}^2$  versus  $17.5 \pm 9.5/\text{mm}^2$ , respectively;  $t_{113,890} = 6.831$ ,  $p$ -value  $< 0.001$ ; Figure 6A). Notably, the density of small blood vessels ( $< 10 \mu\text{m}$ ) was significantly lower in DIPG autopsy samples than in controls ( $t_{180,609} = -4.303$ ,  $p$ -value  $< 0.001$ ), whereas the density of large blood vessels ( $\geq 10 \mu\text{m}$ ) did not differ between groups ( $t_{597} = -0.835$ ,  $p$ -value =  $0.404$ ). Most blood vessels in DIPG autopsy and control samples had a diameter smaller than  $10 \mu\text{m}$ . The median vascular diameter was  $6.21 \mu\text{m}$  in DIPG autopsy samples (range  $2.25$ - $94.85 \mu\text{m}$ ), versus  $6.26 \mu\text{m}$  in controls (range  $1.17$ - $264.77 \mu\text{m}$ ; Figure 6B). Due to the very small size of the biopsy samples, it was not possible to statistically analyze the vascular density and diameter in these tissue samples. Visual inspection of three patients, however, showed a mean vascular density of  $7.5$  vessels per  $\text{mm}^2$ , and a median vascular diameter of  $8.23 \mu\text{m}$  (data not shown).

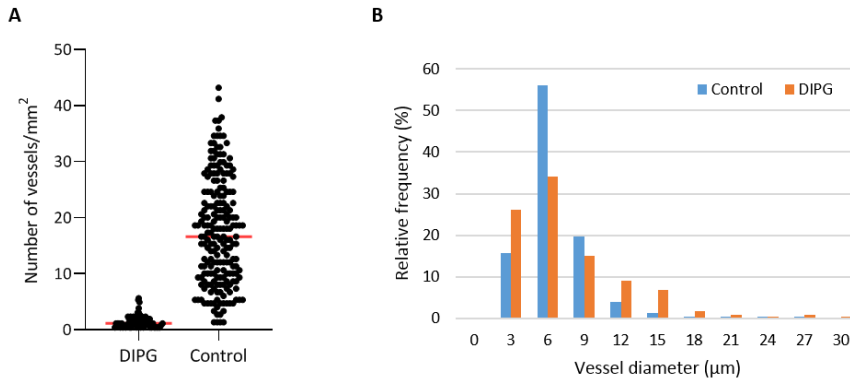
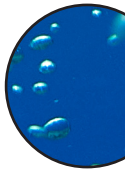


**Figure 6. | Vascular density and diameter in DIPG post-mortem autopsy and healthy control samples.** A: vascular density in DIPG post-mortem autopsy samples and healthy control samples. Mean vascular density was  $1.5 \pm 1.2/\text{mm}^2$  in DIPG versus  $17.5 \pm 9.5/\text{mm}^2$  in controls (red line). B: Vascular size distribution in DIPG post-mortem samples and healthy control samples.

## Discussion

Little research has been done to identify the NVU in DIPG, while it is hypothesized that treatment failure is caused by an intact BBB. As summarized by Figure 7, our study demonstrates structural changes in the NVU of DIPG patients that are already present at diagnosis, suggesting these to be tumor-related and not only due to treatment.

All studied DIPG patients harbored a H3K27M mutation, thus fulfilling the diagnosis of DMG H3K27M according to the revised WHO classification [8]. Up to 85% of DIPG patients harbor this mutation [21, 22]. Since three out of six DIPG autopsy patients were long-term survivors, the median overall survival of the patients in this group was longer than known



from literature, 19.5 months versus 11 months, respectively [7]. Whether neuropathological grading (WHO II-IV), tumor location or the presence of a H3K27M mutation have an impact on survival is still not clear [22-24].

The barrier properties of the NVU strongly depend on the complex interaction between endothelial cells and their tight junctions, pericytes, basement membranes and astrocytes. In physiological conditions, tight junctions are formed by inter-endothelial connections between transmembrane proteins of the claudin-family (claudin-1, 3, 5, and 12), which regulate the function of these tight junctions [25, 26]. Claudins are anchored into the endothelial cells by proteins from the zonula occludens-family (ZO-1, 2, and 3) that regulate adherens junctions and influence cytoskeletal organization, angiogenic potential and cell migration [27]. Moreover, ZO-1 is responsible for the spatial organization of claudin-5 by linking it to the actin cytoskeleton [25]. Downregulation of ZO-1 can lead to tight junction disruption and a larger intercellular distance between endothelial cells and thus pathologically increased paracellular transport [27]. Claudin-5 is most abundant in brain vessels (600-times higher expression than other claudins), where it has a heterogeneous distribution [26]. The highest claudin-5 expression is seen in capillaries and small post-capillary venules [25, 28]. In a claudin-5 knockout mouse model, an increased leakage of molecules up to 800 Da was observed [29], whereas the permeability of normal BBB only allows passage of molecules up to 500 Da [30, 31]. When additional tight junction proteins are downregulated, a size-dependent increase in paracellular transport is seen of molecules with a size up to 10,000 Da [29, 32]. In our study, a reduced expression of claudin-5 and ZO-1 was observed in DIPG patients both pre-treatment and post-mortem, indicating a barrier defect, increasing paracellular transport across the BBB [27]. Nevertheless, there are more tight junction proteins of the zonula occludens and claudin-family expressed by brain endothelial cells. Whether possible downregulation of claudin-5 and ZO-1 is compensated by overexpression of other tight junction proteins remains unknown.

Endothelial cells are surrounded by a basement membrane that contains laminin produced by pericytes and astrocytes [33, 34]. Laminin is essential for basement membrane assembly and maintenance of NVU integrity [35]. In our study, employing a pan-laminin antibody, we found that expression of laminin was lower at the glial basement membrane in both DIPG biopsy and autopsy samples. This was observed in pre-existent vessels amongst the tumor cells and in neovascular proliferation. Our results suggest a pathological involvement of pericytes and astrocytes in DIPG that could have consequences on the behavior of the endothelial cells, thus also disrupting the integrity of the NVU [34]. Immunohistochemistry showed also a lower expression of PDGFR- $\beta$  in DIPG biopsy and autopsy samples, suggesting a reduction in pericytic coverage in DIPG NVU. Besides contributing to secretion of basement membrane components [33, 34], pericytes are essential for regulating capillary diameter and vessel stability [13]. The possible reduction of pericytic coverage observed in our study may explain the possible downregulation of laminin at the glial basement membrane in DIPG patients.

Under physiological conditions, P-gp and BCRP are the most dominantly expressed efflux transporters in de BBB [36, 37]. Our study shows a decreased P-gp expression and unchanged BCRP expression in DIPG pre-treatment and post-mortem samples. This is in line with previous work showing a “moderate expression” of P-gp and intense staining of BCRP in DIPG tumor vasculature [10].

Overall, our results show alterations of the NVU in DIPG patients, which could result in or reflect a more leaky NVU. This hypothesis of a leaky NVU is supported by the demonstrated extravasation of some intravascular proteins, such as pre-albumin, fibrinogen and IgG. Theoretically, this might positively influence influx of chemotherapeutic agents into the tumor based on passive diffusion. Clinical data, however, do not support this possibility [38, 39]. A possible explanation for this discrepancy might be the markedly reduced vascular density in DIPG that could overrule the effects of a leaky NVU. Whether the reduction of vascular density in DIPG that could overrule the effects of a leaky NVU. Whether the reduction of vascular density is also present at diagnosis remains to be investigated.

Lack of therapy efficacy in DIPG has been linked to an intact BBB. Here, we demonstrated structural changes of the NVU together with a lower vascular density in these tumors. These findings have consequences for drug administration, since coverage of the whole tumor, including the migrating/diffusely growing tumor cells, is essential. Our findings suggest that drug administration techniques that mostly rely on vascular density for drug distribution, including conventional systemic administration and microbubble mediated focused ultrasound, might show limited efficacy in DIPG [12]. In contrast, convection-enhanced delivery might be a more suitable technique, in which drug distribution across the tumor relies on a positive pressure gradient instead of passive diffusion [12, 40, 41]. Adding such a biological NVU perspective may help to better direct treatment choices for DIPG patients in the future.

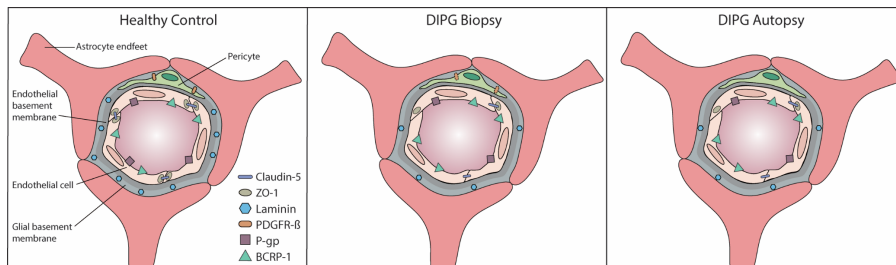


**Figure 7. | Graphical overview of the structural capillary changes observed in DIPG pre-treatment biopsy and post-mortem autopsy samples:** lower expression of tight junction proteins claudin-5 and ZO-1, basement membrane component laminin, pericyte marker PDGFR- $\beta$  and efflux transporter P-gp in DIPG biopsy and autopsy samples; unchanged expression of efflux transporter BCRP-1 in DIPG biopsy and autopsy samples.



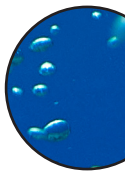
## Supplementary Material

Supplementary Table 1. | Characteristics of age-matched healthy controls

Case	Gender	Age (y)
1	M	1
2	M	2
3	F	2
4	M	2
5	M	2
6	M	2
7	M	2
8	F	3
9	F	3
10	M	6
11	M	8
12	M	12
13	F	13
14	M	13
15	F	14
16	F	16
17	M	18
18	M	19
19	F	13
20	M	17

## References

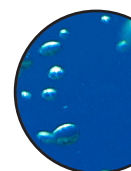
1. Epstein, F. and E.L. McCleary, *Intrinsic brain-stem tumors of childhood: surgical indications*. J Neurosurg, 1986. **64**(1): p. 11-15.
2. Yoshimura, J., et al., *Clinicopathological Study of Diffuse Type Brainstem Gliomas : Analysis of 40 Autopsy Cases*. Neurol Med Chir (Tokyo), 2003. **43**: p. 375-382.
3. Broniscer, A. and A. Gajjar, *Supratentorial high-grade astrocytoma and diffuse brainstem glioma: two challenges for the pediatric oncologist*. Oncologist, 2004. **9**(2): p. 197-206.
4. Hargrave, D., U. Bartels, and E. Bouffet, *Diffuse brainstem glioma in children: critical review of clinical trials*. The lancet oncology, 2006. **7**(3): p. 241-248.
5. Jansen, M.H., et al., *Survival prediction model of children with diffuse intrinsic pontine glioma based on clinical and radiological criteria*. Neuro Oncol, 2015. **17**(1): p. 160-166.
6. Veringa, S.J.E., et al., *In vitro drug response and efflux transporters associated with drug resistance in pediatric high grade glioma and diffuse intrinsic pontine glioma*. PLoS one, 2013. **8**(4): p. e61512-e61512.
7. Hoffman, L.M., et al., *Clinical, Radiologic, Pathologic, and Molecular Characteristics of Long-Term Survivors of Diffuse Intrinsic Pontine Glioma (DIPG): A Collaborative Report From the International and European Society for Pediatric Oncology DIPG Registries*. . Journal of Clinical Oncology, 2018. **36**(19): p. 1963–1972.
8. Louis, D.N., et al., *The 2016 World Health Organization Classification of Tumors of the Central Nervous System: a summary*. Acta Neuropathol, 2016. **131**(6): p. 803-820.
9. Sewing, A.C., et al., *Convection enhanced delivery of carmustine to the murine brainstem: a feasibility study*. J Neurosci Methods, 2014. **238**: p. 88-94.
10. Veringa, S.J., et al., *In vitro drug response and efflux transporters associated with drug resistance in pediatric high grade glioma and diffuse intrinsic pontine glioma*. PLoS One, 2013. **8**(4): p. e61512.
11. Grasso, C.S., et al., *Functionally defined therapeutic targets in diffuse intrinsic pontine glioma*. Nat Med, 2015. **21**(6): p. 555-559.
12. Haumann, R., et al., *Overview of Current Drug Delivery Methods Across the Blood-Brain Barrier for the Treatment of Primary Brain Tumors*. CNS Drugs, 2020. **34**(11): p. 1121-1131.
13. Obermeier, B., R. Daneman, and R.M. Ransohoff, *Development, maintenance and disruption of the blood-brain barrier*. Nat Med, 2013. **19**(12): p. 1584-1596.
14. Serlin, Y., et al., *Anatomy and physiology of the blood-brain barrier*. Semin Cell Dev Biol, 2015. **38**: p. 2-6.



15. Abbott, N.J., L. Ronnback, and E. Hansson, *Astrocyte-endothelial interactions at the blood-brain barrier*. Nat Rev Neurosci, 2006. **7**(1): p. 41-53.
16. Liebner, S., et al., *Functional morphology of the blood-brain barrier in health and disease*. Acta Neuropathol, 2018. **135**(3): p. 311-336.
17. Wilhelm, I., et al., *Heterogeneity of the blood-brain barrier*. Tissue Barriers, 2016. **4**(1): p. e1143544.
18. Villabona-Rueda, A., et al., *The Evolving Concept of the Blood Brain Barrier (BBB): From a Single Static Barrier to a Heterogeneous and Dynamic Relay Center*. Front Cell Neurosci, 2019. **13**: p. 405.
19. Caretti, V., et al., *Implementation of a multi-institutional diffuse intrinsic pontine glioma autopsy protocol and characterization of a primary cell culture*. Neuropathol Appl Neurobiol, 2013. **39**(4): p. 426-436.
20. Bugiani, M., et al., *Deceptive morphologic and epigenetic heterogeneity in diffuse intrinsic pontine glioma*. Oncotarget, 2017. **8**(36): p. 60447-60452.
21. Castel, D., et al., *Histone H3F3A and HIST1H3B K27M mutations define two subgroups of diffuse intrinsic pontine gliomas with different prognosis and phenotypes*. Acta Neuropathol, 2015. **130**(6): p. 815-827.
22. Karremann, M., et al., *Diffuse high-grade gliomas with H3 K27M mutations carry a dismal prognosis independent of tumor location*. Neuro Oncol, 2018. **20**(1): p. 123-131.
23. Wagner, S., et al., *Treatment options in childhood pontine gliomas*. J Neurooncol, 2006. **79**(3): p. 281-287.
24. von Bueren, A.O., et al., *A suggestion to introduce the diagnosis of "diffuse midline glioma of the pons, H3 K27 wildtype (WHO grade IV)"*. Acta Neuropathol, 2018. **136**(1): p. 171-173.
25. Greene, C., N. Hanley, and M. Campbell, *Claudin-5: gatekeeper of neurological function*. Fluids Barriers CNS, 2019. **16**(1): p. 1-15.
26. Jia, W., et al., *The role of claudin-5 in blood-brain barrier (BBB) and brain metastases (review)*. Mol Med Rep, 2014. **9**(3): p. 779-785.
27. Tornavaca, O., et al., *ZO-1 controls endothelial adherens junctions, cell-cell tension, angiogenesis, and barrier formation*. J Cell Biol, 2015. **208**(6): p. 821-838.
28. Paul, D., et al., *Novel 3D analysis of Claudin-5 reveals significant endothelial heterogeneity among CNS microvessels*. Microvasc Res, 2013. **86**: p. 1-10.
29. Nitta, T., et al., *Size-selective loosening of the blood-brain barrier in claudin-5-deficient mice*. J Cell Biol, 2003. **161**(3): p. 653-660.
30. El-Khouly, F.E., et al., *Effective Drug Delivery in Diffuse Intrinsic Pontine Glioma: A Theo-*

*retical Model to Identify Potential Candidates.* Front Oncol, 2017. **7**: p. 254.

31. Pike, V.W., *PET radiotracers: crossing the blood-brain barrier and surviving metabolism.* Trends in pharmacological sciences, 2009. **30**(8): p. 431-440.
32. Keane, J., et al., *Autoregulated paracellular clearance of amyloid- $\beta$  across the blood-brain barrier.* Science Advances, 2015. **1**(8): p. e1500472.
33. Gautam, J., X. Zhang, and Y. Yao, *The role of pericytic laminin in blood brain barrier integrity maintenance.* Sci Rep, 2016. **6**: p. 36450.
34. Yao, Y., et al., *Astrocytic laminin regulates pericyte differentiation and maintains blood brain barrier integrity.* Nat Commun, 2014. **5**: p. 1-12.
35. Givant-Horwitz, V., B. Davidson, and R. Reich, *Laminin-induced signaling in tumor cells.* Cancer Lett, 2005. **223**(1): p. 1-10.
36. Al-Majdoub, Z.M., et al., *Proteomic Quantification of Human Blood-Brain Barrier SLC and ABC Transporters in Healthy Individuals and Dementia Patients.* Mol Pharm, 2019. **16**(3): p. 1220-1233.
37. Uchida, Y., et al., *Quantitative targeted absolute proteomics of human blood-brain barrier transporters and receptors.* J Neurochem, 2011. **117**(2): p. 333-345.
38. El-Khouly, F.E., et al., *Diagnostics and treatment of diffuse intrinsic pontine glioma: where do we stand?* J Neurooncol, 2019. **145**(1): p. 177-184.
39. Veldhuijzen van Zanten, S.E., et al., *A twenty-year review of diagnosing and treating children with diffuse intrinsic pontine glioma in The Netherlands.* Expert Rev Anticancer Ther, 2015. **15**(2): p. 157-164.
40. Barua, N.U., et al., *A novel implantable catheter system with transcutaneous port for intermittent convection-enhanced delivery of carboplatin for recurrent glioblastoma.* Drug Deliv, 2016. **23**(1): p. 167-173.
41. Lewis, O., et al., *Chronic, intermittent convection-enhanced delivery devices.* J Neurosci Methods, 2016. **259**: p. 47-56.







## Chapter 6

### The Blood-brain Barrier in Xenograft Models of Diffuse Midline Glioma H3 K27M: A Pilot Study

## **Abstract**

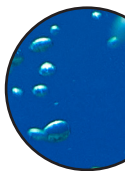
Diffuse midline glioma (DMG) H3 K27M, a pediatric brain tumor, has a dismal prognosis with an overall survival of only 11 months. Previous research showed that the blood-brain barrier (BBB) is affected in human biopsy and autopsy samples. In this pilot study we aim to investigate the BBB in several DMG H3 K27M xenograft models. Six human xenograft models and three mouse xenograft models were immunohistochemically stained for BBB markers claudin-5, zonula occludens-1, laminin, PDGFR- $\beta$ , P-gp, and BCRP. BBB markers were differentially expressed in the investigated xenograft models. A major limitation of this study is that only one sample per xenograft model was stained. In order to determine if the tumor cell line is responsible for the changes in BBB, more samples need to be investigated.

## Introduction

Diffuse midline glioma (DMG) H3 K27M is an aggressive pediatric brain tumor with a median survival of 11 months [1]. So far, radiotherapy has been the only treatment that has prolonged survival with merely a few months [2]. Even though, *in vitro* research showed sensitivity of tumor cells to several drugs, *in vivo* these drugs did not significantly increase survival [3, 4]. The lack of a significant increase in survival is most likely at least partly due to low efficacy as a result of the blood-brain barrier (BBB). The BBB is a protective barrier that prevents drugs from entering and actively exports drugs out of the brain parenchyma [4-6].

Endothelial cells, astrocytes, pericytes, basal lamina and microglia form the BBB. Brain endothelial cells are closely connected by tight junctions [7, 8]. These tight junctions are formed by occludins, tricellulins, claudins, and junctional adhesion molecules preventing large molecules from entering the brain parenchyma by paracellular transport [7, 9]. Furthermore, endothelial cells contain efflux transporters (P-glycoprotein 1 (P-gp), multidrug-associated proteins (MRPs), and the breast cancer resistance protein (BCRP)), which actively transports molecules out of the brain parenchyma limiting drug efficacy [10]. Endothelial cells are connected to astrocytes through astrocytic endfeet. Astrocytes are vital for BBB formation and maintenance [7, 11]. The endfeet produce proteins that regulate the composition of the extracellular matrix, immune cell infiltration, BBB permeability, and BBB integrity [7, 11, 12]. The BBB is further regulated by pericytes which are key regulators of BBB permeability, vascular function, vessel formation and vessel maturation [7, 8, 11]. Pericytes and endothelial cells are surrounded by basal lamina which influences the BBB function [11]. Furthermore, immune cells - microglia - are present that protect the brain from blood-borne substances and inflammatory stimuli [13]. The BBB can be impaired by the presence of tumor cells that influences its integrity [6].

The influence of DMG H3 H27M on the integrity of the BBB has not been studied extensively. Similarly, little is known about the BBB in the brainstem. One study showed that the BBB is heterogenous throughout the brain with a stronger barrier in the brainstem compared to the cortex [14, 15]. Another study investigated the expression of BBB efflux transporters in a DMG H3 H27M xenograft model which showed that P-gp, BCRP1 and MRP1 were present in endothelial cells while MRP1 was also expressed in DMG H3 H27M cells [16]. Recently we published a study in which we characterized the BBB in DMG H3 H27M in both biopsy and autopsy samples. Here, the BBB showed differences in expression of important BBB markers, such as claudin-5 and zonula-occludence-1 (ZO-1) [17]. Since there is only a limited number of studies on the BBB in DMG H3 H27M, much remains unknown. Therefore, more research is needed both preclinically and clinically. Here, we have stained several DMG H3 H27M xenograft models for BBB markers. This is relevant since preclinical research is often translated into the clinic and differences or similarities in BBB integrity might help to predict results in the clinic.





## Materials and Method

### *Tissue Samples*

Tissue samples of xenograft tumors were obtained from the achieved collection of the Hullemans group at VU University Medical Center, Amsterdam and Princess Máxima Center for Pediatric Oncology, Utrecht, the Netherlands. Human DMG H3 H27M cell lines were obtained at biopsy or autopsy of DMG H3 H27M patients [18-21]. Mouse cell lines were obtained from in utero electroporation and were made available by Dr. T.N. Phoenix [22]. In previous studies, mice received intracranial injections as described by Caretti et al. (2015) [18]. In short, cells were cultured and concentrated to  $1 \times 10^5$  -  $2 \times 10^5$  cells per  $\mu\text{l}$ . Cells were intracranially injected at 0.8 mm posterior to the lambda, 1.0 mm lateral from lambda, and at a depth of 4 mm with an infusion rate of 2  $\mu\text{l}/\text{min}$ . Tumor growth was monitored by bioluminescence imaging (BLI) which was performed once a week. Mice were regularly weighted and neurologically assessed until they reached humane endpoints. After sacrifice, tissue was formalin-fixed with various fixation times (24 h to weeks) followed by paraffin embedding. Control samples were obtained from other studies where mice had no intracranial tumors.

### *Immunohistochemistry*

Formalin-fixed paraffin-embedded tissue was sectioned at 5  $\mu\text{m}$ . Sections were deparaffinized using xylene, and rehydrated through descending alcohol concentrations. Tissue was stained with human vimentin for the identification of human tumor cells. Tissue was blocked by endogenous peroxidases and permeabilized with 0.3 % peroxide (Merck, Darmstadt, Germany) in methanol (VWR, Fontenay-sous-Bois, France) for 30 min at room temperature (RT). Citrate buffer was used for antigen retrieval after which primary Mouse- $\alpha$ -Vimentin was used (1:4000, Monoclonal mouse anti-vimentin clone V9, Dako Denmark Glostrup, Denmark) for 1 h at RT. Vimentin was visualized with EnVision  $\alpha\text{M}/\alpha\text{R}$  and 3,3'-diaminobenzidine (DAB) (Dako, Glostrup, Denmark). The slices were counterstained with hematoxylin, dehydrated and mounted with a coverslip with mounting medium.

After identification of tumor cells in the sections, slides were stained for BBB markers. First, aldehyde groups were blocked with 0.1 g glycine in 100 ml distilled water for 10 min at RT. After blocking, heat-induced antigen retrieval was performed in tris-EDTA buffer (10mM Tris Base, 1mM EDTA Solution, 0.05% Tween 20, pH 9.0) in the autoclave for 2.5 h. Slides were cooled down in ice, washed with PBS, and incubated overnight at RT with primary antibodies against claudin-5 (1:50, Invitrogen, Carlsbad, CA, USA), ZO-1 (1:50, Invitrogen, Carlsbad, CA, USA), laminin (1:500, Novus Biologicals, Abingdon UK), PDGFR- $\beta$  (1:500, Abcam, Cambridge, UK), P-gp (1:20; Millipore, CA, USA), or BCRP (1:40; Abcam, Cambridge, UK). After 24 h, the sections were washed and incubated with Alexa Fluor<sup>®</sup>-labelled secondary antibody. After washing, slides were incubated with Lycopersicon Esculentum Tomato Lectin (LEL, TL), DyLight<sup>®</sup> 594 (Vector Laboratories Inc., Burlingame, California, USA) for 1 h at RT. The background was quenched with 0.1% Sudan black B in ethanol. Finally, sections were mounted in mounting medium with 4',6-diamidino-2-fenylindol (DAPI) (Vector Laboratories Inc., Burlingame, California, USA).

## Data analysis

Sections were imaged using a Leica DM6000 microscope (40x magnification; Leica Microsystems BV, Rijswijk, The Netherlands). Ten images were made of each section. The Leica Application Suite X: LAS X version 3.1.5.16308 was used for analysis.

## Results

### Diffuse growth pattern DMG H3 H27M

Mice were sacrificed at humane end point just before tumor burden was too harmful. After sacrifice, brains were extracted and stained with human vimentin. Human vimentin expression is maintained in the different DMG H3 H27M xenograft models (Figure 1). However, the growth pattern is unique for each cell line. HSJD-DIPG-07 shows the most spread throughout the entire brain, while VUMC-DIPG-11, VUMC-DIPG-08, and VUMC-DIPG-F also spread throughout the brain but have a more pronounced tumor core. JHH-DIPG-01 is maintained in distal part of the pons while SU-DIPG-21 is only observed outside the pontine area.

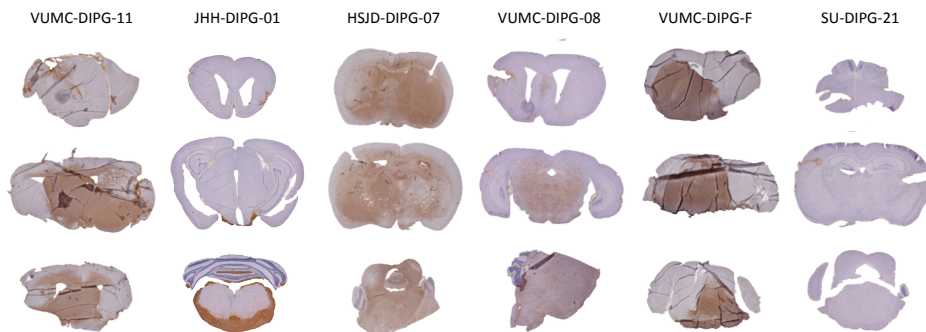
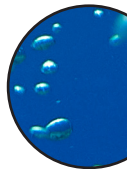
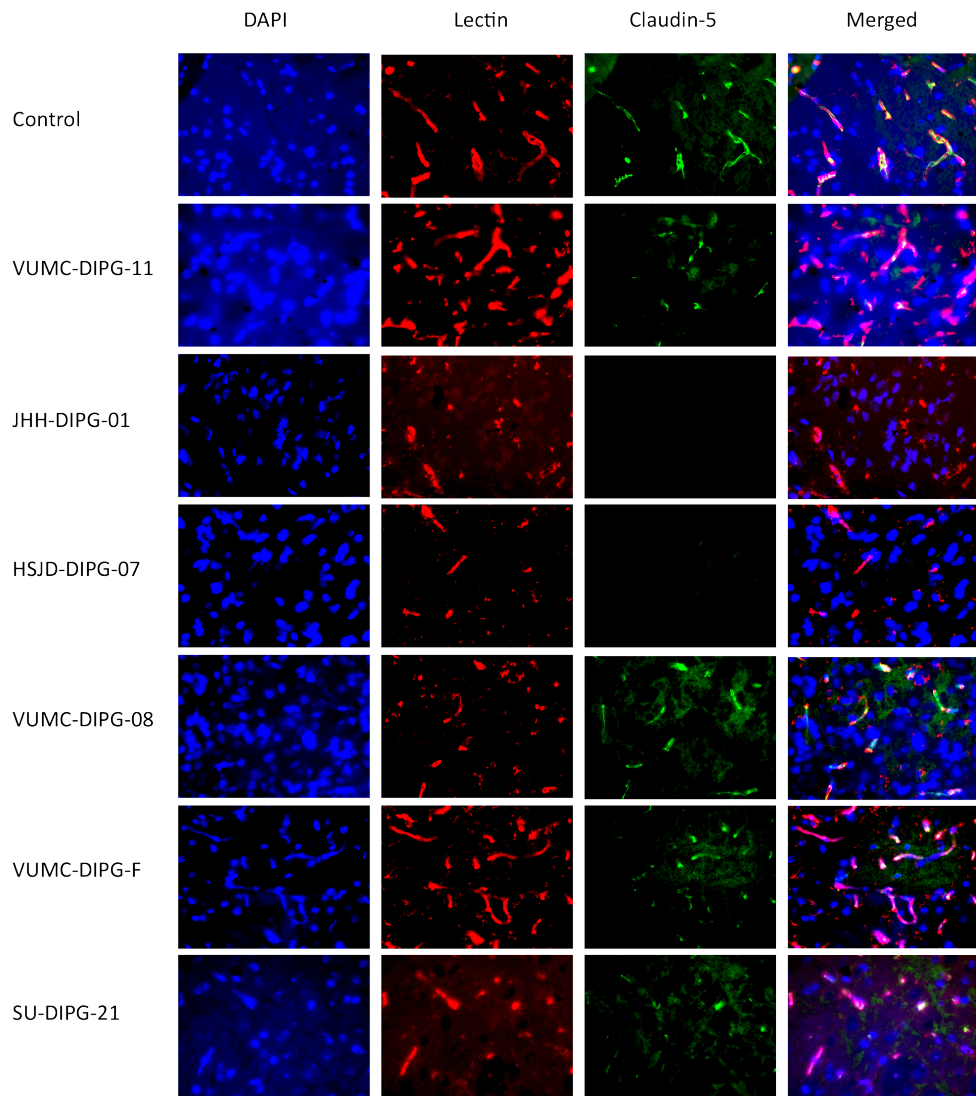


**Figure 1. | Human vimentin staining.** Human vimentin is expressed by human tumor cells. Human vimentin staining shows the diffuse growth pattern of xenograft models of DIPG. HSJD-DIPG-07 is the most diffusely grown tumor while VUMC-DIPG-11, VUMC-DIPG-08, VUMC-DIPG-F, and JHH-DIPG-01 have a more pronounced tumor core with tumor cells spread throughout the brain. SU-DIPG-21 shows the least positive tumor cells.

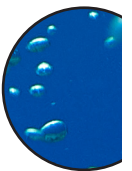


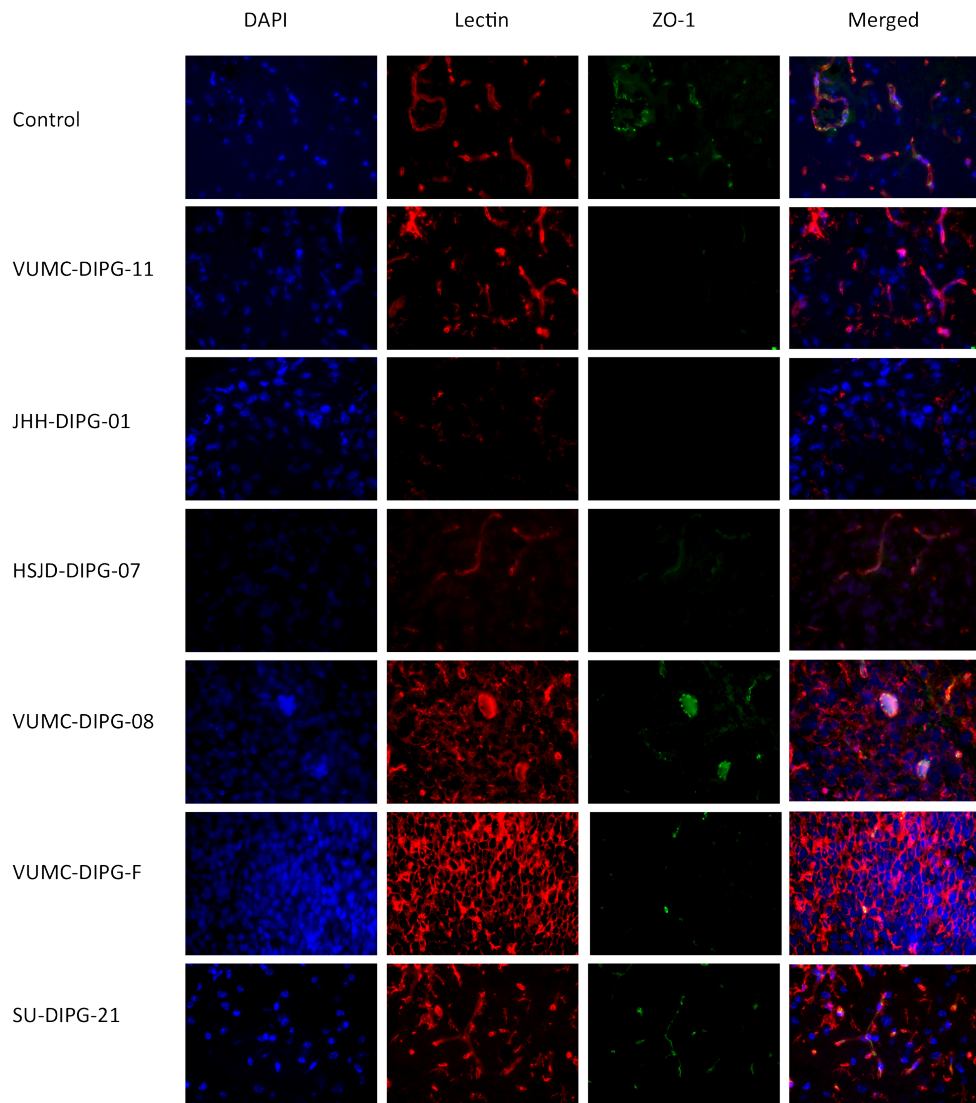
### ***Blood-brain barrier of human DMG H3 H27M xenografts***

Claudin-5, ZO-1, laminin, and P-gp immunohistochemical stainings were evaluable on archived DMG H3 H27M slides while PDGFR- $\beta$  and BCRP stainings were not successful. Tight junction protein claudin-5 is sharply defined in control mouse brain (Figure 2). In DMG H3 H27M sections, claudin-5 was absent in JHH-DIPG-01 and HSJD-DIPG-07 in both the pontine area as well as in the internal control of the cortex area (Figure S1). In VUMC-DIPG-11 claudin-5 was heterogeneously expressed in the blood vessels with areas of claudin-5 and areas where claudin-5 was absent. VUMC-DIPG-08, VUMC-DIPG-F, and SU-DIPG-21 have a lower expression of claudin-5. In control samples, ZO-1 is sharply defined and segmented similar to VUMC-DIPG-08 and SU-DIPG-21 (Figure 3). Strikingly, SU-DIPG-21 internal control showed a lower expression of ZO-1 (Figure S2). In VUMC-DIPG-11, JHH-DIPG-01, and HSJD-DIPG-07 ZO-1 was absent while Internal controls of VUMC-DIPG-11 and JHH-DIPG-01 showed a lower expression of ZO-1. VUMC-DIPG-F had a lower expression of ZO-1 in both the pontine area as well as in the cortex. The basement membrane protein laminin shows a continuous pattern in control samples (Figure 4). In all samples, except for HSJD-DIPG-07, laminin was similar to controls. In HSJD-DIPG-07 laminin was absent. Internal control of JHH-DIPG-01 showed a less defined line and lower expression of laminin around the blood vessel (Figure S3). In controls, P-gp shows a continuous expression in the blood vessels (Figure 5). No changes in P-gp expression was observed in VUMC-DIPG-11 and VUMC-DIPG-F while P-gp was absent in JHH-DIPG-01, HSJD-DIPG-07, VUMC-DIPG-08 and SU-DIPG-21. However, P-gp was observed in internal controls of JHH-DIPG-01 and VUMC-DIPG08 (Figure S4).

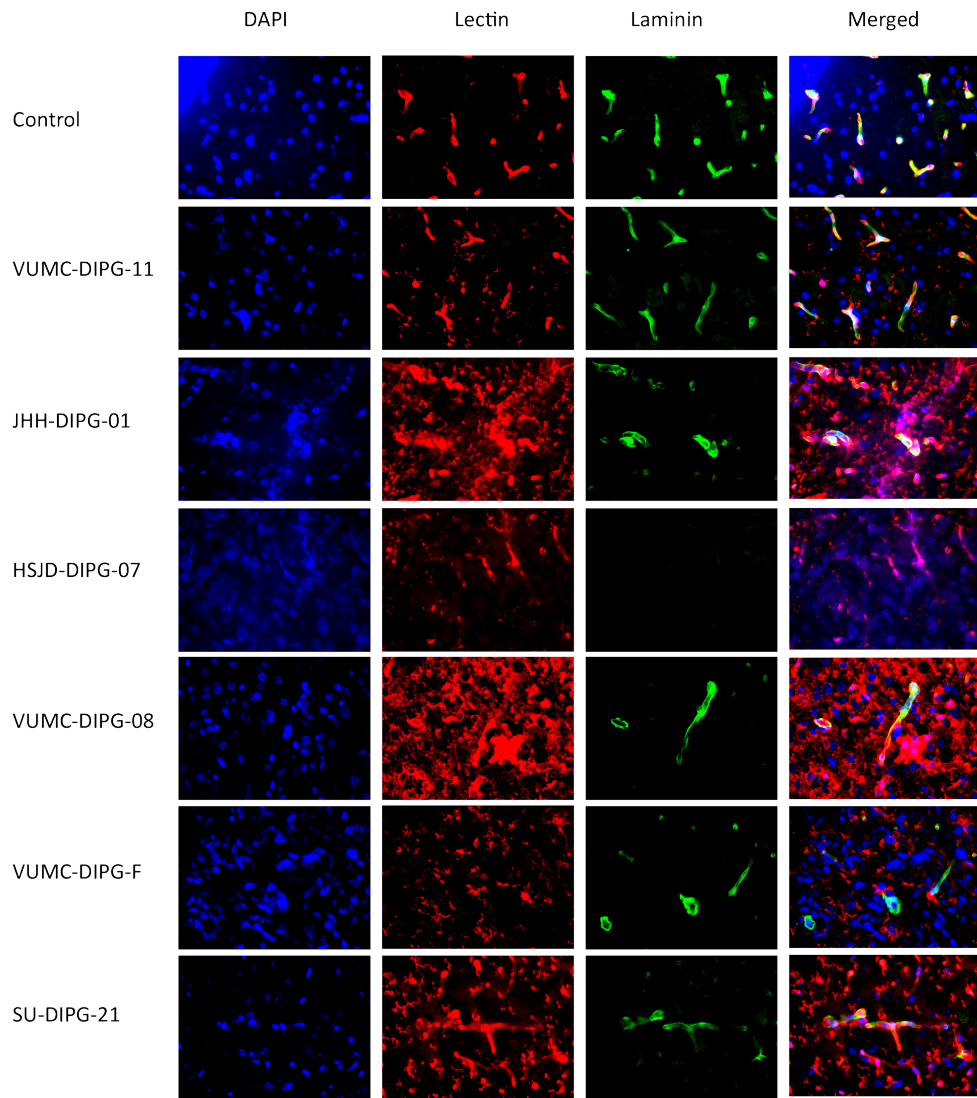


**Figure 2. | Claudin-5 expression in DMG H3 H27M xenograft models.** Claudin-5 is sharply defined in controls. JHH-DIPG-01 and HSJD-DIPG-07 showed no expression of claudin-5. VUMC-DIPG-11 showed a heterogenous expression of claudin-5 with areas of claudin-5 and areas where claudin-5 is absent. A lower expression of claudin-5 is observed in VUMC-DIPG-08, VUMC-DIPG-F, and SU-DIPG-21.

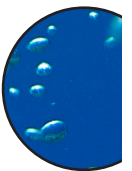


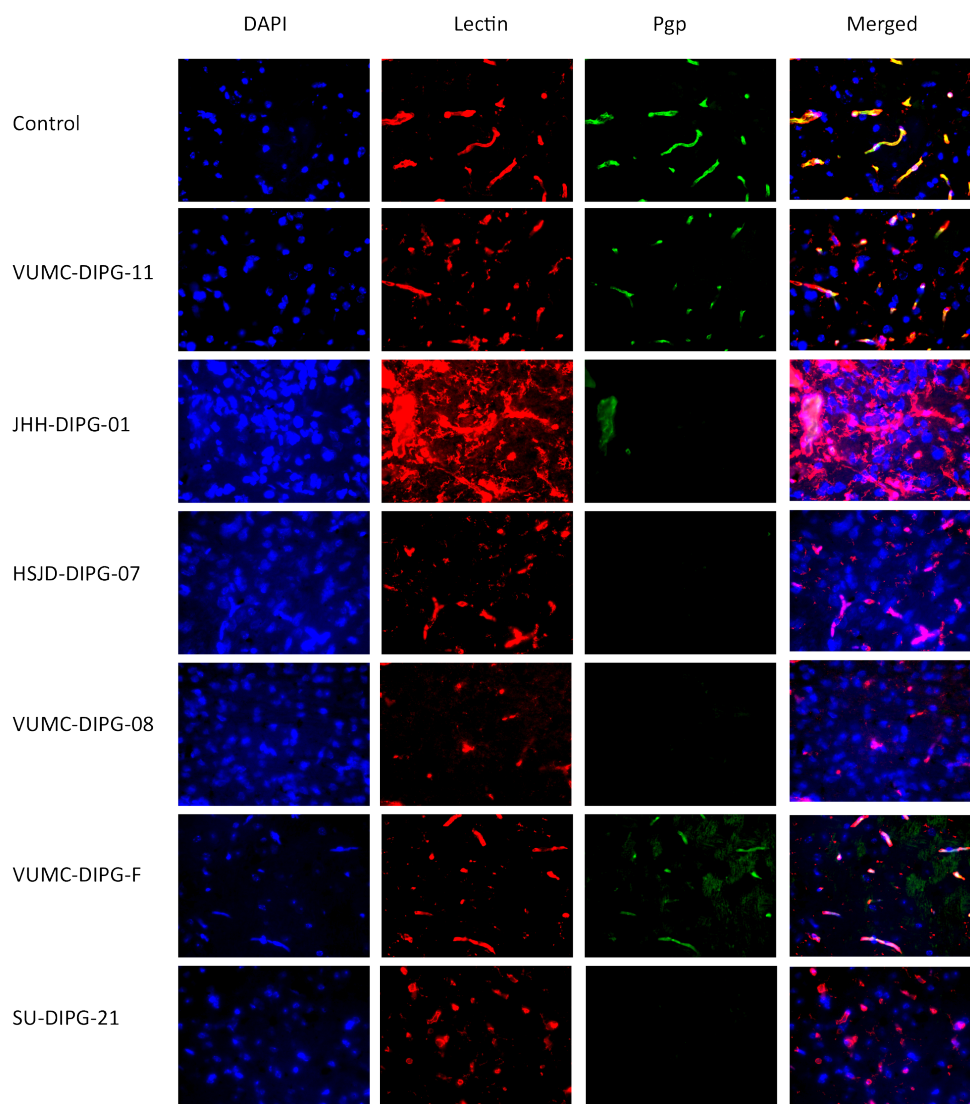


**Figure 3. | ZO-1 expression in DMG H3 H27M xenograft models.** ZO-1 is sharply defined and segmented in controls. VUMC-DIPG-08 and SU-DIPG-21 also showed sharply defined and segmented ZO-1. ZO-1 was absent in VUMC-DIPG-11, JHH-DIPG-01, and HSJD-DIPG-07 ZO-1 while VUMC-DIPG-F had a lower expression of ZO-1.



**Figure 4. | Laminin expression in DMG H3 H27M xenograft models.** Laminin shows a continuous pattern in controls and in all samples except for HSJD-DIPG-07. Laminin was absent in HSJD-DIPG-07.

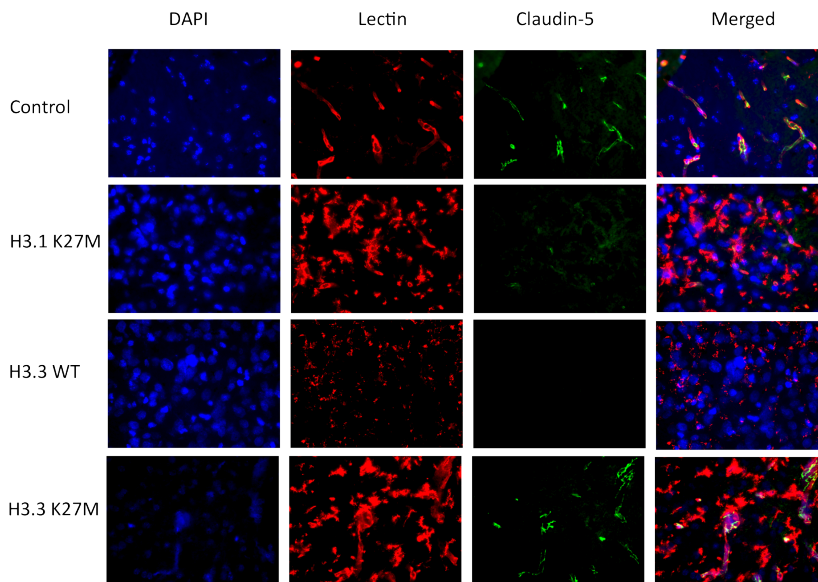




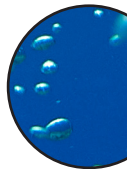
**Figure 5. | P-gp expression in DMG H3 H27M xenograft models.** P-gp shows a continuous pattern in controls and VUMC-DIPG-11 and VUMC-DIPG-F. P-gp was absent in JHH-DIPG-01, HSJD-DIPG-07, VUMC-DIPG-08 and SU-DIPG-2.

### **Blood-brain barrier of mouse DMG H3 H27M xenografts**

In mouse DMG H3 H27M xenografts claudin-5 is sharply defined in H3.3 K27M while claudin-5 H3.1 K27M, and H3.3 WT claudin-5 was absent (Figure 6). Internal control of H3.1 K27M showed sharply defined claudin-5 expression in the cortex. Tight junction protein ZO-1 was absent in H3.1 K27M, and H3.3 WT (Figure 7). While H3.3 K27M showed a lower expression of ZO-1. Internal controls showed sharply defined ZO-1 expression in H3.1 K27M and H3.3 K27M. The basement membrane protein laminin was absent in H3.3 WT and had a lower expression in H3.3 K27M. H3.1 K27M showed no changes of laminin compared to controls (Figure 8). Finally, efflux transporter P-gp was absent in H3.1 K27M and H3.3 WT (Figure 9). In A H3.3 K27M P-gp showed a lower expression compared to controls.



**Figure 6. | Claudin-5 expression in mouse DMG H3 H27M xenograft models.** Claudin-5 is sharply defined in control and H3.3 K27M. Claudin-5 was not observed in H3.1 K27M, and H3.3 WT.





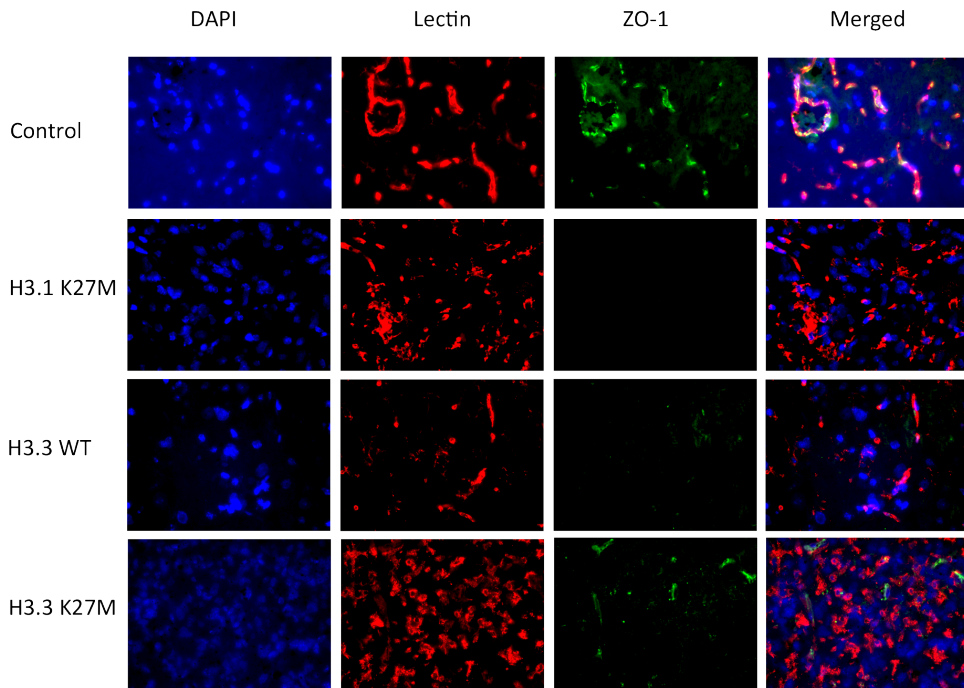


**Figure 7. | ZO-1 expression in mouse DMG H3 H27M xenograft models.** ZO-1 is sharply defined and segmented in controls. A lower expression of ZO-1 was observed in H3.3 K27M. H3.1 K27M and H3.3 WT lacked ZO-1 expression.

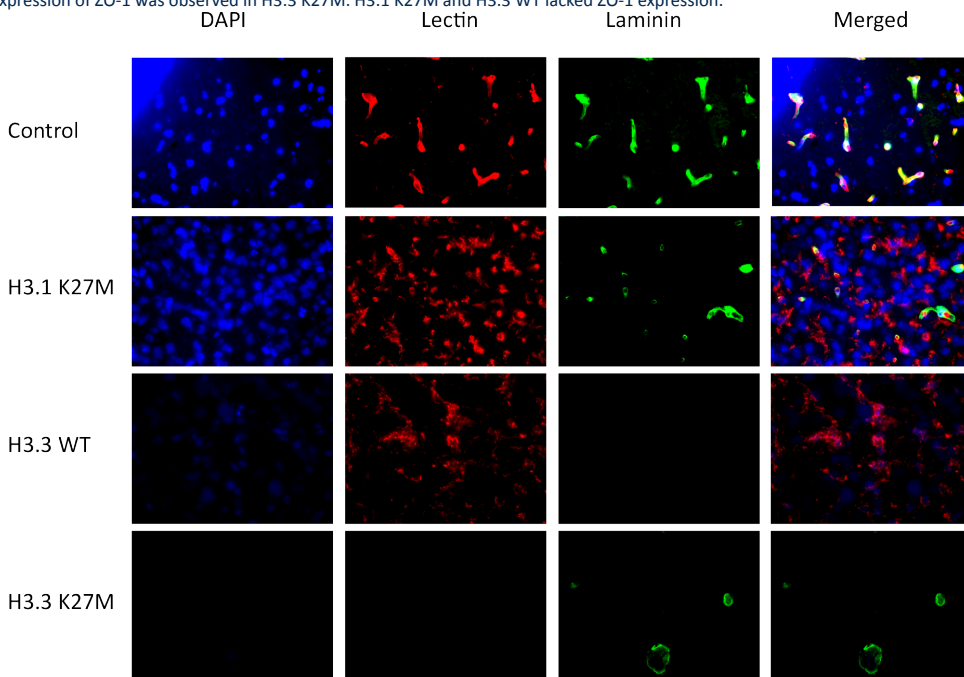


**Figure 8. | Laminin expression in mouse DMG H3 H27M xenograft models.** Laminin shows a continuous pattern in control and H3.1 K27M. Laminin was absent in H3.3 WT and had a lower expression in H3.3 K27M.

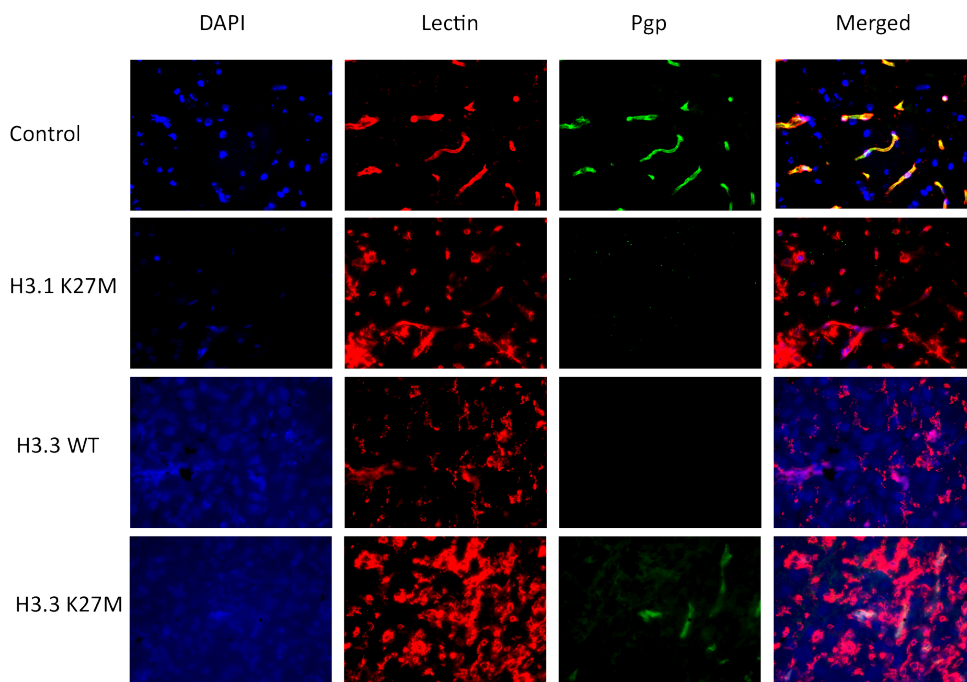
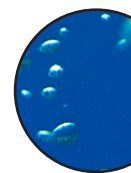


**Figure 9. | P-gp expression in mouse DMG H3 H27M xenograft models.** P-gp is sharply defined in controls. P-gp was not observed in H3.1 K27M and H3.3 WT while H3.3 K27M P-gp showed a lower expression compared to controls.



## Discussion

Only a few studies investigated the BBB in the healthy brainstem and in DMG H3 H27M affected brainstem. Previous research of our group showed structural differences in both biopsy and autopsy samples of DMG H3 H27M patients. In this pilot study, multiple xenograft models of DMG H3 H27M were characterized of archived *in vivo* samples.

Human xenograft models studied here all harbor the H3.3 K27M mutation that is characteristic for DMG H3 H27M (Table S1). However, the expression of BBB markers was not comparable between the tumor models. Tight junction proteins claudin-5 and ZO-1 were not preserved in the human models. Most cell lines showed absence or a lower expression of these tight junction proteins. Tight junction protein ZO-1 was only preserved in SU-DIPG-21. In mouse models only H3.3 K27M showed preservation of claudin-5. In physiological conditions claudin-5 prevents paracellular transport of molecules larger than 500 Da [23, 24]. Loss of claudin-5 results in an increased leakage of molecules up to 800 Da [25]. In xenograft models, loss of claudin-5 can have an effect on drug delivery studies when investigating small molecules with a size up to 800 Da. ZO-1 also influences the paracellular transport of molecules [26]. Larger drugs such as antibodies or nanoparticles will not be affected with a change in claudin-5 and ZO-1 expression.

The basement membrane protein laminin was affected in HSJD-DIPG-07, H3.3 K27M, and H3.3 WT while in all other xenograft models this protein was not affected. Laminin is important for the BBB integrity since laminin reduces caveoli-1 regulating transcytosis, induces tight junction proteins, maintains tight junctions, and inhibits pericyte differentiation [27, 28]. Loss of laminin might increase transcytosis and affects the tight junctions and thus paracellular transport. Furthermore, loss of laminin might result in hemorrhage but this was not observed in our sections [27].

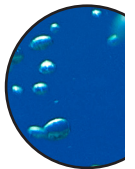
Most DMG H3 H27M xenograft models showed an absence of the drug efflux transporter P-gp. However, previous studies showed that P-gp expression in human section was reduced but was not absent [17, 29]. P-gp transporters actively transport a wide variety of molecules from the brain parenchyma to the blood stream reducing the concentration of the molecule in the brain [10]. A reduction of P-gp expression aids in effective drug treatment because drugs are not actively transported out of the brain parenchyma but also toxic substances will accumulate in the brain. A discrepancy of P-gp expression between preclinical models and clinical samples might result in inconsistency in clinical translation.

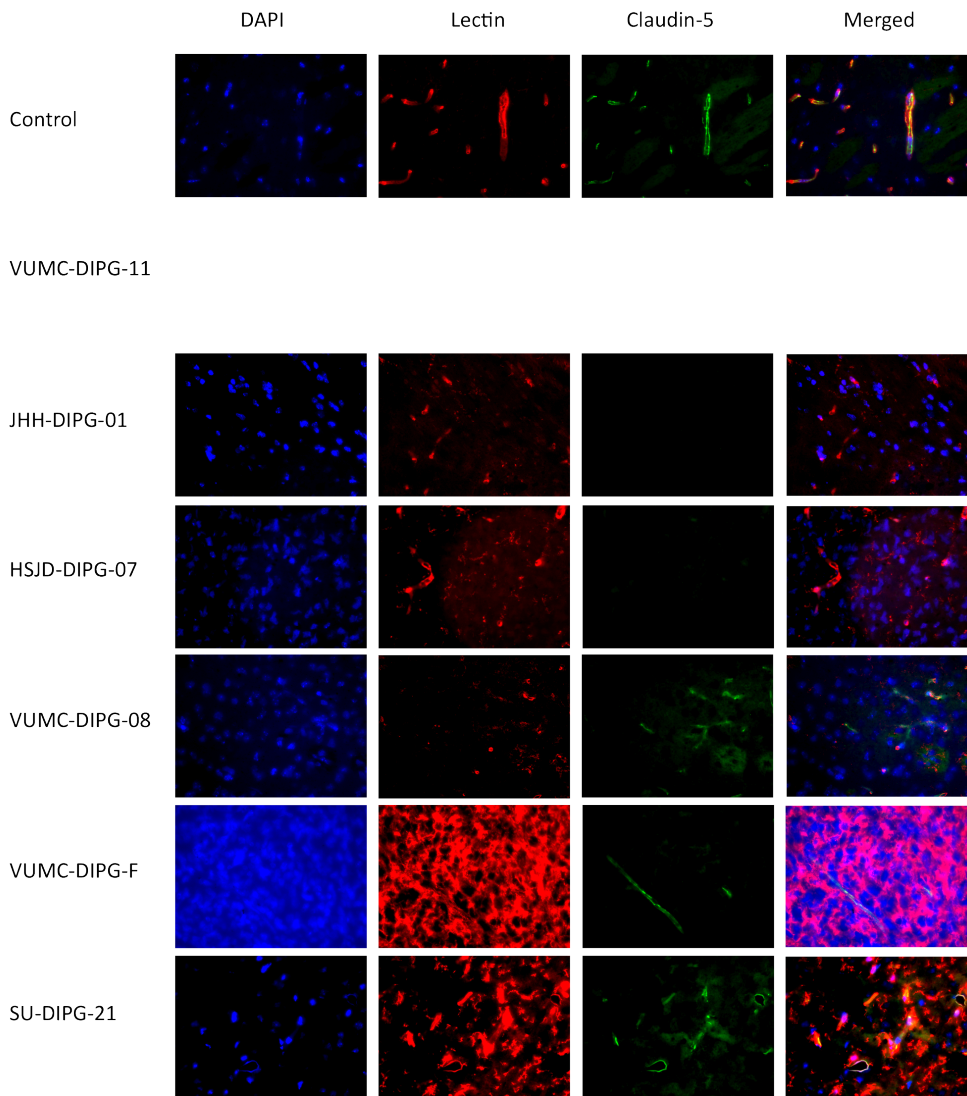
In this pilot study, where we investigated only one brain per model, we observed important differences in protein expression between DMG H3 H27M tumor models that harbor the same mutation. Of relevance, differences in protein expression between preclinical DMG H3 H27M models was not investigated. This pilot study showed interesting differences in BBB markers, but since only a limited number of samples was investigated, future more extensive studies are required to more conclusively determine the effect of DMG H3 H27M on the BBB integrity.

## Supplemental Figures

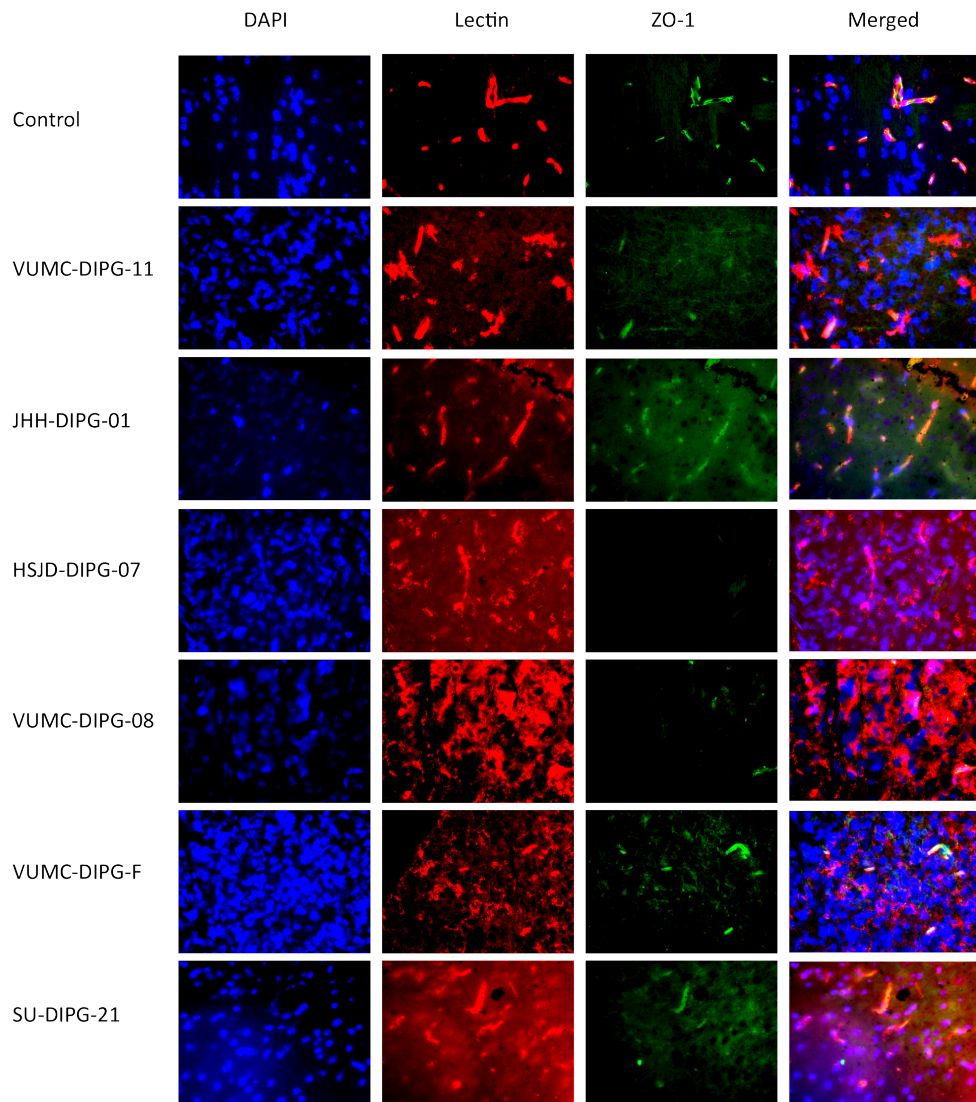
**Tabel S1. | BBB stainings xenograft models.** Characterization of the expression of BBB markers in DMG H3 H27M xenograft models and internal controls (ic).

	<b>Claudin-5</b>	<b>ZO-1</b>	<b>Laminin</b>	<b>Pgp</b>	<b>Mutation[30]</b>
VUMC-DIPG-11	Heterogenous	Absent	No changes	No changes	H3.3 K27M
JHH-DIPG-01	Absent	Absent	No changes, lower expression ic	Absent, present in ic	H3.3 K27M
HSJD-DIPG-07	Absent	Absent/lower	Absent	Absent	H3.3 K27M
VUMC-DIPG-08	Lower	No changes	No changes	Absent, present ic	H3.3 K27M
VUMC-DIPG-F	Lower	lower	No changes	Less sharply defined	H3.3 K27M
SU-DIPG-21	Lower	No changes, lower expression ic	No changes	Absent	H3.3 K27M
H3.1 K27M	Absent, sharply defined ic	Absent, sharply defined ic	No changes	Absent	H3.1 K27M
H3.3 WT	Absent	Absent	Absent	Absent	H3.3 WT
H3.3 K27M	Sharply defined	Lower expression, sharply defined ic	Low expression and heterogeneously expressed	Low expression	H3.3 K27M

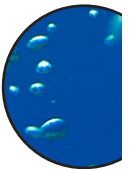




**Figure S1. | Claudin-5 expression in internal controls of DMG H3 H27M xenograft models.** In the cortex of control brains claudin-5 is sharply defined. Claudin-5 is also sharply defined in VUMC-DIPG-F and SU-DIPG-21. A lower expression of claudin-5 was observed in the cortex of VUMC-DIPG-08. Claudin-5 is absent in HSJD-DIPG-07 and JHH-DIPG-01.



**Figure S2. | ZO-1 expression in internal controls of DMG H3 H27M xenograft models. ZO-1 is sharply defined and segmented in the cortex of controls and VUMC-DIPG-F. A lower expression of ZO-1 was observed in VUMC-DIPG-11, JHH-DIPG-01, and SU-DIPG-21. ZO-1 was absent in HSJD-DIPG-07 and VUMC-DIPG-08.**



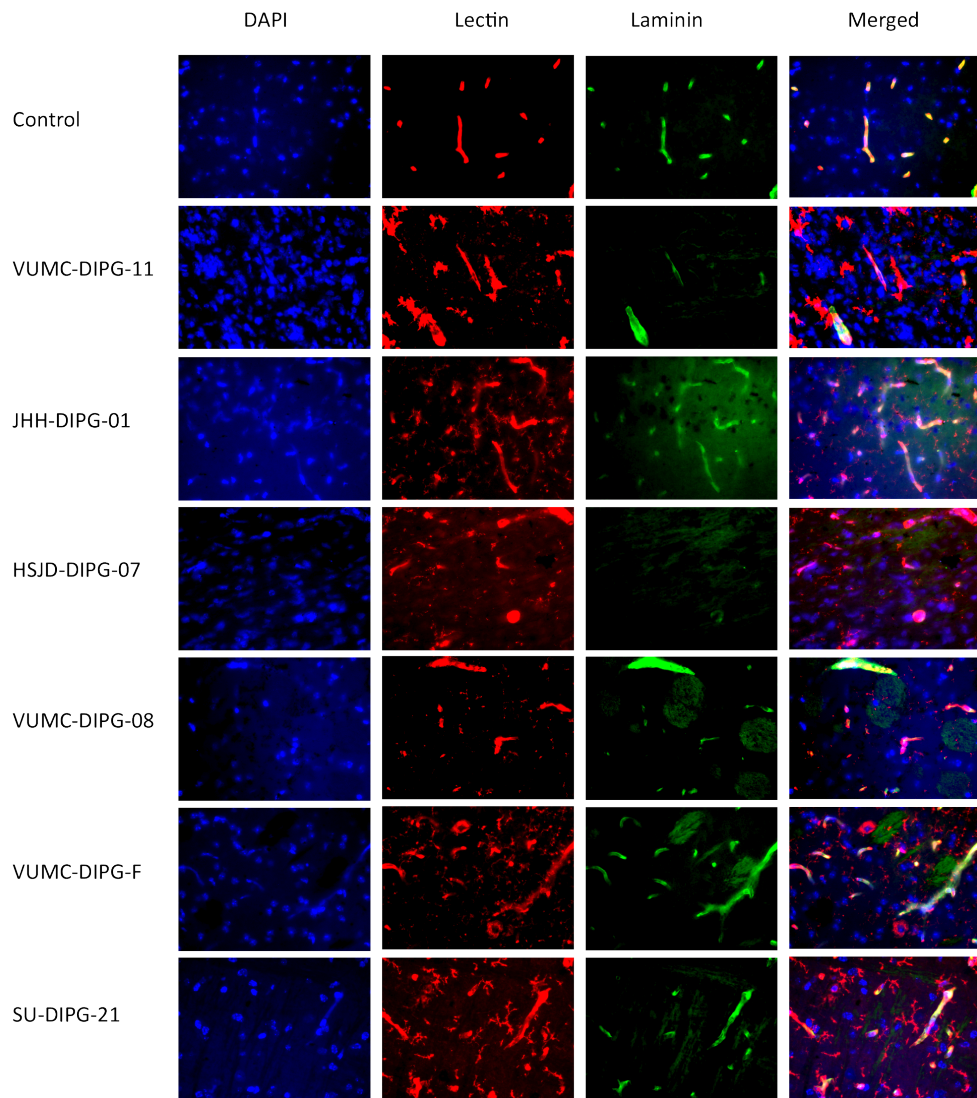


**Figure S3. | Laminin expression in internal controls of DMG H3 H27M xenograft models.** Laminin has a continuous expression in the cortex of the control section. VUMC-DIPG-11, VUMC-DIPG-08, VUMC-DIPG-F and SU-SIPG-21 showed a similar expression of laminin compared to control. HSJD-DIPG-07 did not stain positive for laminin while a lower expression was observed in JHH-DIPG-01.

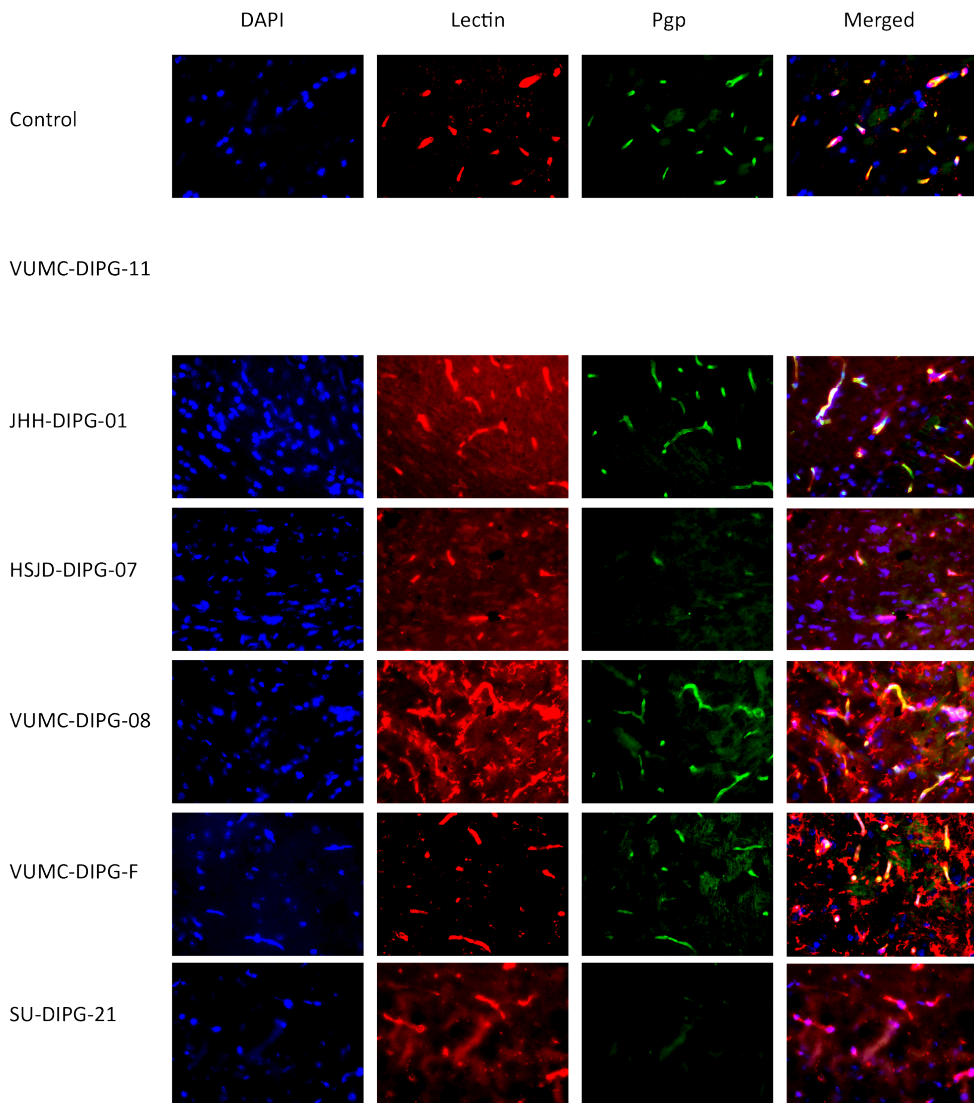
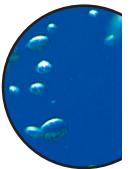


**Figure S4. | P-gp expression in internal controls of DMG H3 H27M xenograft models.** P-gp is sharply defined in controls. In the cortex of JHH-DIPG-01, VUMC-DIPG-08, and VUMC-DIPG-F showed a sharply defined P-gp expression. P-gp had a lower expression in HSJD-DIPG-07 and was absent in SU-DIPG-21.

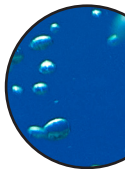


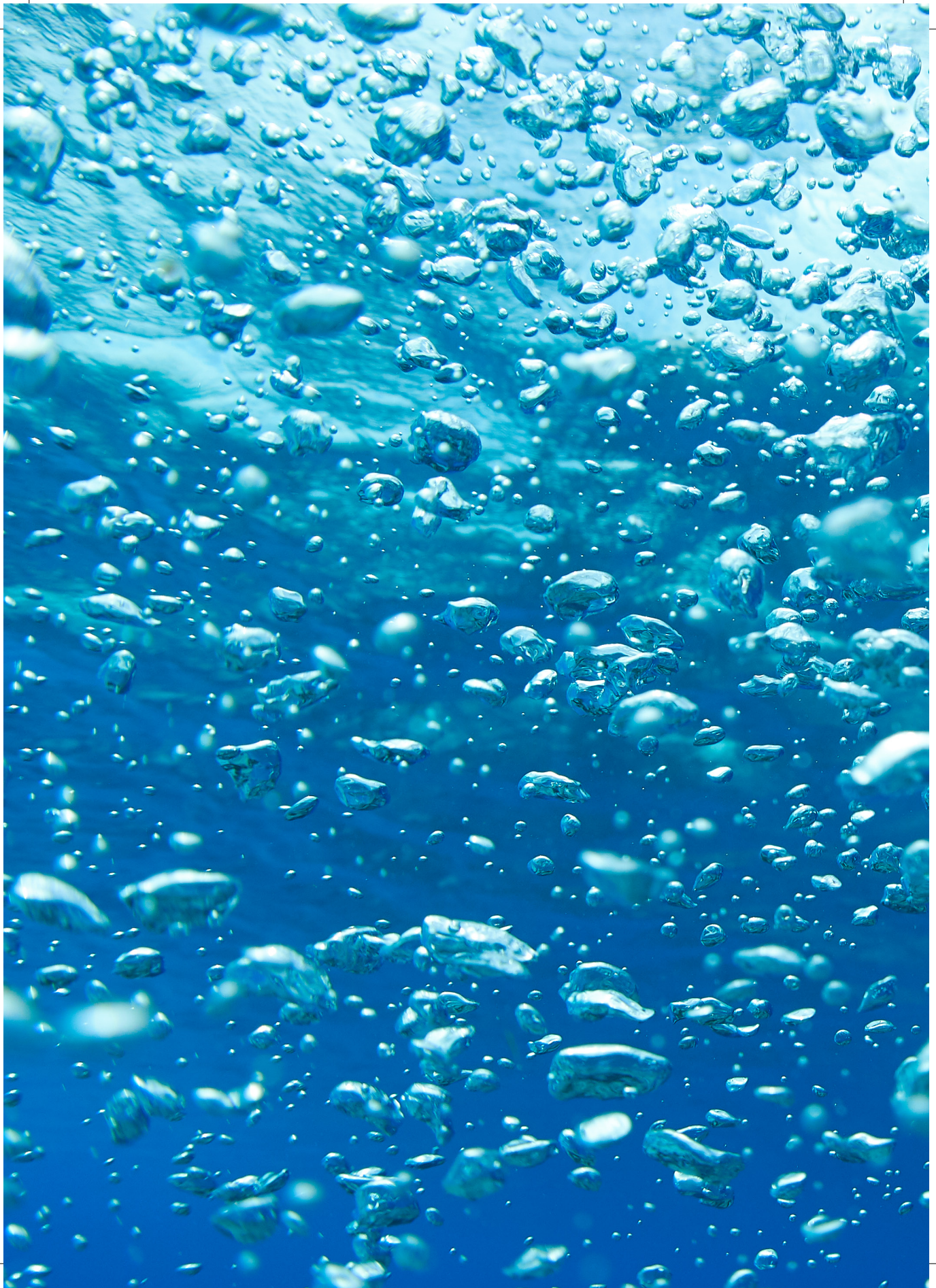


## References

1. Hoffman, L.M., et al., *Clinical, radiologic, pathologic, and molecular characteristics of long-term survivors of diffuse intrinsic Pontine Glioma (DIPG): a collaborative report from the international and European Society for Pediatric Oncology DIPG registries*. Journal of Clinical Oncology, 2018. **36**(19): p. 1963.
2. Langmoen, I.A., et al., *Management of pediatric pontine gliomas*. Child's Nervous System, 1991. **7**(1): p. 13-15.
3. Grasso, C.S., et al., *Functionally defined therapeutic targets in diffuse intrinsic pontine glioma*. Nature medicine, 2015. **21**(6): p. 555-559.
4. Veringa, S.J., et al., *In vitro drug response and efflux transporters associated with drug resistance in pediatric high grade glioma and diffuse intrinsic pontine glioma*. PLoS One, 2013. **8**(4): p. e61512.
5. Grasso, C.S., et al., *Functionally defined therapeutic targets in diffuse intrinsic pontine glioma*. Nat Med, 2015. **21**(6): p. 555-559.
6. Haumann, R., et al., *Overview of Current Drug Delivery Methods Across the Blood-Brain Barrier for the Treatment of Primary Brain Tumors*. CNS Drugs, 2020. **34**(11): p. 1121-1131.
7. Langen, U.H., S. Ayloo, and C. Gu, *Development and cell biology of the blood-brain barrier*. Annual review of cell and developmental biology, 2019. **35**: p. 591-613.
8. Daneman, R. and B. Engelhardt, *Brain barriers in health and disease*. Neurobiology of Disease, 2017. **Volume 107**: p. 1-3.
9. Partridge, W., *The blood-brain barrier: bottleneck in brain development*. J. Am. Soc. Exp. Neuro Ther, 2005. **2**: p. 3-14.
10. Löscher, W. and H. Potschka, *Blood-brain barrier active efflux transporters: ATP-binding cassette gene family*. NeuroRx, 2005. **2**(1): p. 86-98.
11. Arvanitis, C.D., G.B. Ferraro, and R.K. Jain, *The blood–brain barrier and blood–tumour barrier in brain tumours and metastases*. Nature Reviews Cancer, 2019: p. 1-16.
12. Bart, J., et al., *The blood-brain barrier and oncology: new insights into function and modulation*. Cancer treatment reviews, 2000. **26**(6): p. 449-462.
13. Liebner, S., et al., *Functional morphology of the blood–brain barrier in health and disease*. Acta neuropathologica, 2018: p. 1-26.
14. McCully, C.M., et al., *Model for concomitant microdialysis sampling of the pons and cerebral cortex in rhesus macaques (Macaca mulatta)*. Comparative medicine, 2013. **63**(4): p. 355-360.
15. Warren, K.E., *Beyond the blood: brain barrier: the importance of central nervous system (CNS) pharmacokinetics for the treatment of CNS tumors, including diffuse intrinsic pon-*

- tine glioma*. *Frontiers in oncology*, 2018. **8**: p. 239.
16. Veringa, S.J., et al., *In vitro drug response and efflux transporters associated with drug resistance in pediatric high grade glioma and diffuse intrinsic pontine glioma*. *PLoS one*, 2013. **8**(4).
  17. El-Khouly, F.E., et al., *The neurovascular unit in diffuse intrinsic pontine gliomas*. *Free Neuropathology*, 2021. **2**: p. 17-17.
  18. Caretti, V., et al., *Human pontine glioma cells can induce murine tumors*. *Acta neuropathologica*, 2014. **127**(6): p. 897-909.
  19. Jansen, M.H., et al., *Bevacizumab targeting diffuse intrinsic pontine glioma: results of 89Zr-bevacizumab PET imaging in brain tumor models*. *Molecular cancer therapeutics*, 2016. **15**(9): p. 2166-2174.
  20. Taylor, K.R., et al., *Recurrent activating ACVR1 mutations in diffuse intrinsic pontine glioma*. *Nature genetics*, 2014. **46**(5): p. 457-461.
  21. Monje, M., et al., *Hedgehog-responsive candidate cell of origin for diffuse intrinsic pontine glioma*. *Proceedings of the National Academy of Sciences*, 2011. **108**(11): p. 4453-4458.
  22. Patel, S.K., et al., *Generation of diffuse intrinsic pontine glioma mouse models by brain-stem-targeted in utero electroporation*. *Neuro-oncology*, 2020. **22**(3): p. 381-392.
  23. El-Khouly, F.E., et al., *Effective Drug Delivery in Diffuse Intrinsic Pontine Glioma: A Theoretical Model to Identify Potential Candidates*. *Front Oncol*, 2017. **7**: p. 254.
  24. Pike, V.W., *PET radiotracers: crossing the blood-brain barrier and surviving metabolism*. *Trends in pharmacological sciences*, 2009. **30**(8): p. 431-40.
  25. Nitta, T., et al., *Size-selective loosening of the blood-brain barrier in claudin-5-deficient mice*. *J Cell Biol*, 2003. **161**(3): p. 653-60.
  26. Tornavaca, O., et al., *ZO-1 controls endothelial adherens junctions, cell-cell tension, angiogenesis, and barrier formation*. *J Cell Biol*, 2015. **208**(6): p. 821-38.
  27. Gautam, J., et al., *Loss of mural cell-derived laminin aggravates hemorrhagic brain injury*. *Journal of neuroinflammation*, 2020. **17**(1): p. 1-16.
  28. Yao, Y., et al., *Astrocytic laminin regulates pericyte differentiation and maintains blood brain barrier integrity*. *Nature communications*, 2014. **5**(1): p. 1-12.
  29. Veringa, S.J., et al., *In vitro drug response and efflux transporters associated with drug resistance in pediatric high grade glioma and diffuse intrinsic pontine glioma*. *PLoS one*, 2013. **8**(4): p. e61512.
  30. Meel, M.H., et al., *MELK inhibition in diffuse intrinsic pontine glioma*. *Clinical Cancer Research*, 2018. **24**(22): p. 5645-5657.







# Chapter 7

## Discussion



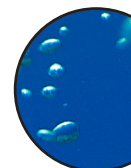
## General discussion

DMG H3 K27M has one of the worst prognoses in pediatric cancer with an overall survival of only 11 months. In the last few decades, palliative radiotherapy has been the only course of treatment [1, 2]. Even though DMG H3 K27M cells are sensitive to drugs tested *in vitro* [7-9], multiple clinical trials that were based on preclinical results have not shown a significant improvement in survival so far [3-6]. Since different types of drugs, such as conventional chemotherapy and targeted drugs have not been successful, it has been proposed that the blood-brain barrier (BBB) hampers the accumulation of drugs in the brain tumors. The BBB prevents drugs from entering the brain parenchyma due to the tightly aligned endothelial cells that prevent paracellular transport and the presence of efflux transporters that pump out drugs. These properties result in a low exposure of the brain tumor to these drugs [7-9]. In order to reach a sufficient drug concentration in the brain tumor, the BBB can be circumvented with several drug delivery methods [10, 11]. Here, we investigated microbubble-mediated focused ultrasound as a drug delivery method for the treatment of DMG H3 K27M. This research is the first step to investigate if microbubble-mediated focused ultrasound is feasible for clinical translation.

## Drug delivery

Several drug delivery methods have been investigated for DMG H3 K27M, such as systemic drug delivery, use of nanoparticles, convection enhanced delivery (CED), and microbubble-mediated focused ultrasound. Systemic drug delivery is achieved by administering drugs to the bloodstream. Molecules with a molecular weight of < 500 Dalton (Da) and a high lipophilicity are able to cross the BBB through transcellular diffusion [12]. However, most drugs have unsuitable chemical properties, such as the number of hydrogen bonds, Log P (a measure for lipophilicity), and molecular weight that prevent the molecules from crossing the BBB [13]. For systemic drug delivery to be successful, molecules can be chemically modified in order to satisfy the chemical rules for BBB crossing [14]. However, this is a costly and difficult process. Alternatively, nanoparticles can be used to package drugs to make them more suitable for BBB crossing. Nanoparticles can traverse the BBB in a number of ways such as endocytosis, receptor-mediated transcytosis, or the enhanced permeability and retention (EPR) effect [15-17]. Moreover, nanoparticles often have an increased plasma half-life resulting in a prolonged exposure of the drug to the tumor [18]. *In vivo* it was shown by other researchers that nanoparticles loaded with various drugs such as doxorubicin did not improve survival in H3 K27M [19, 20]. The low efficacy can partially be explained by an intact BBB which prevents delivery through the EPR effect [15-17]. Another application is targeted nanoparticles in which nanoparticles are designed in such a way that these nanoparticles can specifically target the brain tumor where the encapsulated drugs are released [19]. However, this has not been extensively studied for the treatment of DMG H3 K27M and further research is needed.

Other drug delivery methods can be employed to deliver drugs directly into the brain, thus circumventing the BBB. An example of a technique circumventing the BBB is CED. CED is a drug delivery method that bypasses the BBB by infusing drugs directly into the tumor. However, CED has had variable outcomes ranging from no significant improvement in survival



to an improvement by 4 months [21-23]. One of the limitations of CED is the heterogeneous pressure gradient in the tumor which results in a non-uniform drug distribution and inhomogeneous drug concentrations in the treated area. In addition, catheter-induced tissue damage and reflux can be seen alongside the catheter [24]. Optimization of the CED procedure with different types of drugs might result in an effective combination that does reduce tumor growth, but this requires further studies.

### ***Microbubble-mediated focused ultrasound***

Previous preclinical research in our group showed that systemic delivery, nanoparticles, and CED have not yet led to a significant improvement of survival. Recently, microbubble-mediated focused ultrasound has been successfully used as a drug delivery technique in preclinical adult glioma mouse models [25-35]. This promising method is both non-invasive as well as a precise technique that can specifically target the tumor area. Moreover, this technique can be used in combination with Food and Drug Administration (FDA) and European Medicines Agency (EMA) approved drugs which could result in quick translation into the clinic. Therefore, we investigated the use of microbubble-mediated focused ultrasound for the treatment of DMG H3 K27M.

### ***Microbubble-mediated focused ultrasound – drug selection***

Doxorubicin is a FDA and EMA approved drug that is used for several types of tumors including breast, lung, and pediatric tumors [36]. Doxorubicin is an anthracycline antibiotic isolated from *Streptomyces peucetius var. caesioides* [36]. This cytotoxic drug induces DNA damage resulting into cell death [36]. Doxorubicin was found to be effective in DMG H3 K27M cell cultures [20, 37]. In our group doxorubicin was previously used in combination with CED in the brainstem. However, doxorubicin caused severe toxicity in pontine DMG H3 K27M xenograft mouse models [38]. In adult glioma xenograft models, doxorubicin in combination with microbubble-mediated focused ultrasound showed a survival benefit. Therefore, this combination could potentially be beneficial for DMG H3 K27M. Here we used doxorubicin, Caelyx and 2B3-101 in combination with microbubble-mediated focused ultrasound. Liposomal formulations of doxorubicin such as Caelyx and 2B3-101 release doxorubicin slowly over time, thus reducing toxicity [39]. The difference between Caelyx and 2B3-101 is that 2B3-101 is conjugated with the brain-targeting ligand glutathione (GSH) showing a better brain distribution compared to non-targeted Caelyx [40, 41].

### ***Microbubble-mediated focused ultrasound – DMG H3 K27M xenograft mouse model***

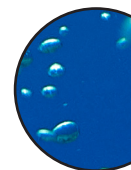
While the research described in this thesis was in progress, the ‘Toronto focused ultrasound research group’ showed that 5 mg/kg doxorubicin in combination with microbubble-mediated focused ultrasound was well tolerated in non-tumor bearing Nod/Scid/Gamma (NSG) mice [42]. More importantly, they showed that the concentration of doxorubicin in the targeted area of the brainstem increased more than 50-fold compared to non-treated brain-

stem in mice. This research group proceeded further with their treatment procedure on a DMG H3 K27M mouse model (SU-DIPG-17) [43]. Strikingly, toxicity was observed at 5 mg/kg of doxorubicin delivered with microbubble-mediated focused ultrasound showing that non-tumor bearing mice tolerate doxorubicin better than this xenograft model. One of the major differences was the use of a different focused ultrasound platform and imaging modality. The image-guided focused ultrasound platform, described in chapter 3, is suitable for high-throughput animal studies. The major advantage of this system is that mice are only sedated for a short period of time since X-ray and bioluminescence are fast imaging techniques. The Toronto group used MRI as an imaging modality which yields substantially longer treatment times. However, in another study, toxicity of 5 mg/kg of doxorubicin was also observed with direct infusion of doxorubicin in the brainstem with CED [38]. Therefore, the treatment time is most likely not of major influence on treatment burden of the mice. Since, the CED study showed that no toxicity was observed after administration of 5 mg/kg doxorubicin in a thalamic E98-FM glioma model the authors concluded that the anatomic location determines the severity of toxicity. The results of the Toronto group could also lead to the conclusion that not the anatomical location but the presence of DMG H3 K27M in the brainstem determines the severity of toxicity since in non-tumor bearing mice no toxicity was observed. This is further illustrated with research published on etoposide in combination with microbubble-mediated focused ultrasound. Etoposide in combination with microbubble-mediated focused ultrasound prolonged survival in adult glioma models where it did not improve survival in a DMG H3 K27M mouse model [44, 45]. Since both doxorubicin and etoposide have a different result in DMG H3 K27M models we hypothesize that the difference in effect is due to the tumor location.

In order to reach a higher drug concentration in the brain without increasing toxicity, we hypothesized that liposomal versions of doxorubicin would reduce toxicity and increase the drug concentration in the brain since liposomes release the drug over a longer period of time. Strikingly, we did not observe liposomes in the brain 24 hours after focused ultrasound in HSJD-DIPG-07 xenograft model while in non-tumor bearing mice liposomes were observed. We have to speculate why the liposomes were not present in the tumor-bearing mice. An explanation might be a high interstitial pressure caused by the tumor [46]. Another explanation might be an altered morphology of the endothelial cells in the brain which might have a negative effect on liposomal binding in the endocytosis/transcytosis pathway [47, 48]. However, there is only little known about the influence of the tumor on drug accumulation in the brainstem.

### **The BBB and vasculature of the brainstem**

In order to bridge this knowledge gap, we explored the effect of DMG H3 K27M on the BBB and vasculature in the brainstem. Here, we used human pontine samples and DMG H3 K27M pontine samples to study the BBB and vasculature. We stained these tissues for several BBB markers and observed structural differences in the BBB. One of the differences was the expression of tight junction proteins claudin-5 and ZO-1. Tight junction proteins claudin-5 and ZO-1 are required for barrier formation because these proteins influence the cytoskeletal organization [49-51]. These proteins were downregulated which could lead to an increase of paracellular transport of across the BBB in a size-dependent manner up to 10 000 Da [51-53]. Furthermore, we observed differences in efflux transporter expression. We





showed a decreased P-gp expression while BCRP was not affected in DMG H3 K27M tissue. Microbubble-mediated focused ultrasound itself also suppresses P-gp expression which implies that drugs are retained in the brainstem [54]. In chapter 6, we also stained multiple DMG H3 K27M xenograft models for BBB markers. In this pilot study we observed differences in BBB expression between the xenograft models. In order to draw conclusions from this research, more samples need to be stained in order to quantify the structural changes. In chapter 5, we also investigated the vasculature and observed a reduced vascular density in DMG H3 K27M.

The observed structural differences have an impact on the effectiveness of drug delivery methods. For example, microbubble-mediated focused ultrasound uses systemic delivery of microbubbles, and therefore vascular density has a major influence on the area of tissue that is exposed to the drug while CED does not use the vasculature for drug delivery and is less dependent on the vasculature. Arvanitis *et al.* showed that doxorubicin remains in close vicinity of the blood vessels [55]. Our stainings of liposomes also showed that liposomes remain in closed vicinity of the blood vessel. Therefore, clinical translation of microbubble-mediated focused ultrasound in combination with doxorubicin might be problematic since doxorubicin possibly will not cover the entire tumor area. Drugs that diffuse further into the tissue might be of interest but more research is needed to determine which drugs might be more suitable.

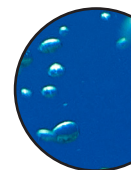
## Closing remarks

Here we showed that microbubble-mediated focused ultrasound did not lead to an improvement of survival in a DMG H3 K27M xenograft model. Design of drug delivery techniques often do not consider physiological aspects such as the BBB and the vasculature that can have a major influence on treatment success. In case of DMG H3 K27M, a lot is still unknown and therefore more research is needed to close the knowledge gap.

Furthermore, the approach of designing new techniques should not only focus on the technique itself, but also consider physiological aspects. For DMG H3 K27M it might be necessary to reduce the tumor size by radiotherapy first. Then a drug delivery approach that is not dependent on the vasculature could be used, such as CED. However, CED needs further research in order to have an effect on tumor growth. Alternatively, microbubble-mediated focused ultrasound could be explored further. This technique in combination with other drugs might improve survival in DMG H3 H27M. One of the requirements is that drugs should diffuse far from the blood vessel into the tissue since the vascular density is low in DMG H3 K27M. Development of an effective treatment for DMG H3 K27M is clearly a complex process and will require many more preclinical and clinical studies.

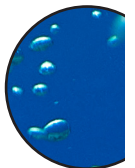
## References

1. Veldhuijzen van Zanten, S.E., et al., *A twenty-year review of diagnosing and treating children with diffuse intrinsic pontine glioma in The Netherlands*. Expert review of anti-cancer therapy, 2015. **15**(2): p. 157-164.
2. Vanan, M.I. and D.D. Eisenstat, *DIPG in Children - What Can We Learn from the Past?* Front Oncol, 2015. **5**: p. 237.
3. Grill, J., et al., *DIPG-35. Biological medicine for diffuse intrinsic pontine glioma (DIPG) eradication: results of the three arm biomarker-driven randomized BIOMEDE 1.0 trial*. Neuro-Oncology, 2020. **22**(Suppl 3): p. iii293.
4. Bernier-Chastagner, V., et al., *Topotecan as a radiosensitizer in the treatment of children with malignant diffuse brainstem gliomas: results of a French Society of Paediatric Oncology Phase II Study*. Cancer: Interdisciplinary International Journal of the American Cancer Society, 2005. **104**(12): p. 2792-2797.
5. Bartels, U., et al., *Phase 2 study of safety and efficacy of nimotuzumab in pediatric patients with progressive diffuse intrinsic pontine glioma*. Neuro-oncology, 2014. **16**(11): p. 1554-1559.
6. Tinkle, C.L., et al., *Phase 1 study using crenolanib to target PDGFR kinase in children and young adults with newly diagnosed DIPG or recurrent high-grade glioma, including DIPG*. Neuro-Oncology Advances, 2021. **3**(1).
7. Warren, K.E., *Beyond the blood: brain barrier: the importance of central nervous system (CNS) pharmacokinetics for the treatment of CNS tumors, including diffuse intrinsic pontine glioma*. Frontiers in oncology, 2018. **8**: p. 239.
8. Warren, K.E., *Novel therapeutic delivery approaches in development for pediatric gliomas*. CNS oncology, 2013. **2**(5): p. 427-435.
9. McCully, C.M., et al., *Model for concomitant microdialysis sampling of the pons and cerebral cortex in rhesus macaques (Macaca mulatta)*. Comparative medicine, 2013. **63**(4): p. 355-360.
10. Abbott, N.J., et al., *Structure and function of the blood-brain barrier*. Neurobiology of disease, 2010. **37**(1): p. 13-25.
11. Liu, X., et al., *Development of a computational approach to predict blood-brain barrier permeability*. Drug metabolism and disposition, 2004. **32**(1): p. 132-139.
12. Pardridge, W.M., *CNS drug design based on principles of blood-brain barrier transport*. Journal of neurochemistry, 1998. **70**(5): p. 1781-1792.
13. Pardridge, W.M., *The blood-brain barrier: bottleneck in brain drug development*. NeuroRx, 2005. **2**(1): p. 3-14.



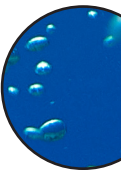
14. Pardridge, W.M., *Blood-brain barrier delivery*. Drug Discov Today, 2007. **12**(1-2): p. 54-61.
15. Vieira, D.B. and L.F. Gamarra, *Getting into the brain: liposome-based strategies for effective drug delivery across the blood–brain barrier*. International journal of nanomedicine, 2016. **11**: p. 5381–5414.
16. Allen, T.M. and P.R. Cullis, *Drug delivery systems: entering the mainstream*. Science, 2004. **303**(5665): p. 1818-1822.
17. Zhao, M., et al., *Nanocarrier-based drug combination therapy for glioblastoma*. Theranostics, 2020. **10**(3): p. 1355.
18. Alexis, F., et al., *Factors affecting the clearance and biodistribution of polymeric nanoparticles*. Molecular pharmaceutics, 2008. **5**(4): p. 505-515.
19. Bukchin, A., et al., *Amphiphilic polymeric nanoparticles modified with a protease-resistant peptide shuttle for the delivery of SN-38 in diffuse intrinsic pontine glioma*. ACS Applied Nano Materials, 2021. **4**(2): p. 1314-1329.
20. Ung, C., et al., *Doxorubicin-Loaded Gold Nanoarchitectures as a Therapeutic Strategy against Diffuse Intrinsic Pontine Glioma*. Cancers, 2021. **13**(6): p. 1278.
21. Souweidane, M.M., et al., *A phase I study of convection enhanced delivery (CED) of 124I-8H9 radio-labeled monoclonal antibody in children with diffuse intrinsic pontine glioma (DIPG)*. 2017, American Society of Clinical Oncology.
22. Heiss, J.D., et al., *Phase I trial of convection-enhanced delivery of IL13-Pseudomonas toxin in children with diffuse intrinsic pontine glioma*. Journal of Neurosurgery: Pediatrics, 2018. **23**(3): p. 333-342.
23. Szychot, E., et al., *Clinical experience of convection-enhanced delivery (CED) of carboplatin and sodium valproate into the pons for the treatment of diffuse intrinsic pontine glioma (DIPG) in children and young adults after radiotherapy*. International Journal of Clinical Oncology, 2021. **26**(4): p. 647-658.
24. Bidros, D.S. and M.A. Vogelbaum, *Novel drug delivery strategies in neuro-oncology*. Neurotherapeutics, 2009. **6**(3): p. 539-546.
25. Kovacs, Z., et al., *Prolonged survival upon ultrasound-enhanced doxorubicin delivery in two syngenic glioblastoma mouse models*. Journal of controlled release, 2014. **187**: p. 74-82.
26. Treat, L.H., et al., *Improved anti-tumor effect of liposomal doxorubicin after targeted blood-brain barrier disruption by MRI-guided focused ultrasound in rat glioma*. Ultrasound Med Biol, 2012. **38**(10): p. 1716-25.
27. Liu, H.-L., et al., *Pharmacodynamic and therapeutic investigation of focused ultrasound-induced blood-brain barrier opening for enhanced temozolomide delivery in glioma*.

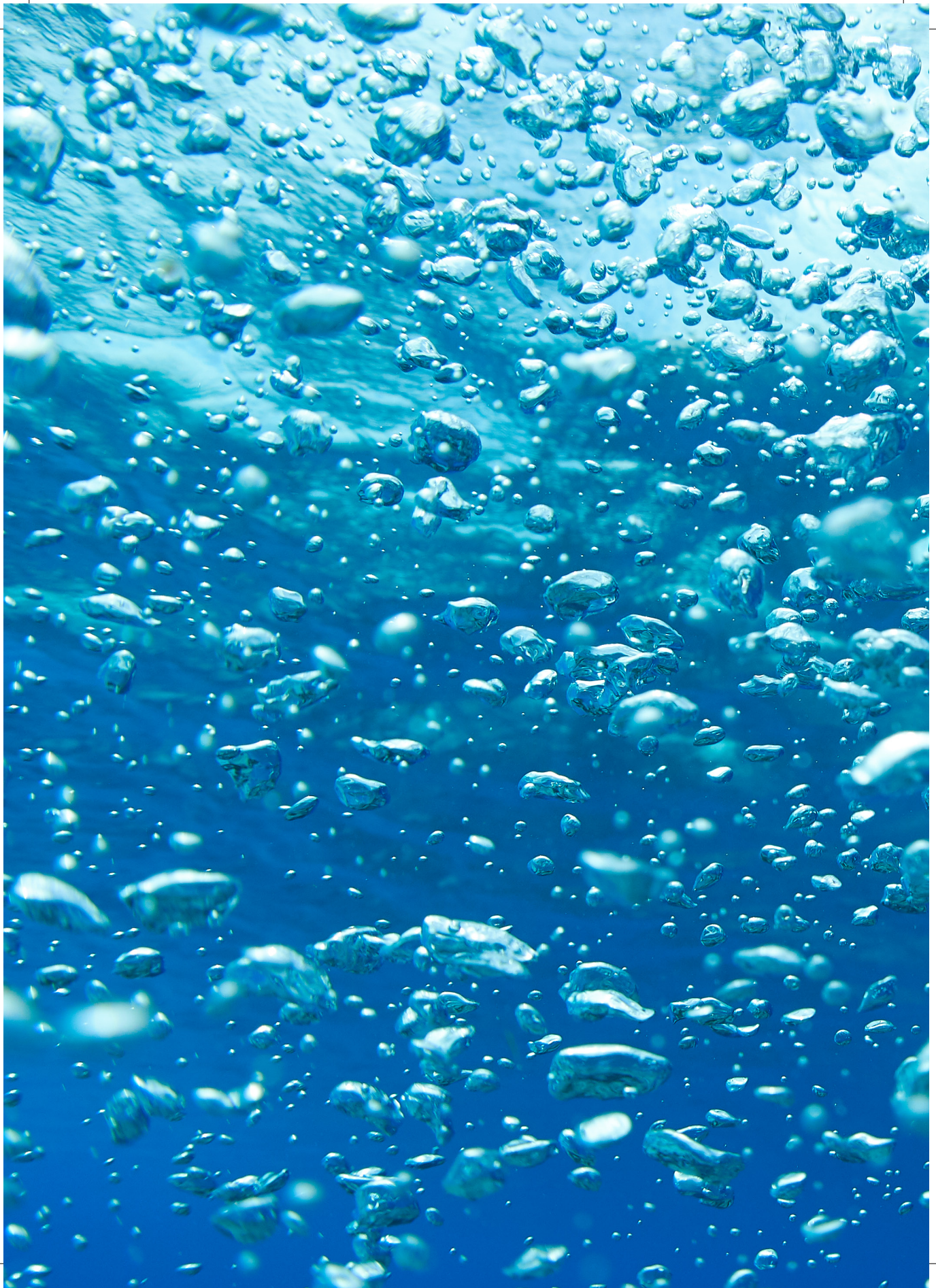
- ma treatment*. PloS one, 2014. **9**(12): p. e114311.
28. Wei, K.-C., et al., *Focused ultrasound-induced blood–brain barrier opening to enhance temozolomide delivery for glioblastoma treatment: a preclinical study*. PloS one, 2013. **8**(3): p. e58995.
  29. Liu, H.-L., et al., *Focused ultrasound enhances central nervous system delivery of bevacizumab for malignant glioma treatment*. Radiology, 2016. **281**(1): p. 99-108.
  30. Bunevicius, A., N.J. McDannold, and A.J. Golby, *Focused ultrasound strategies for brain tumor therapy*. Operative Neurosurgery, 2020. **19**(1): p. 9-18.
  31. Treat, L.H., et al., *Improved anti-tumor effect of liposomal doxorubicin after targeted blood-brain barrier disruption by MRI-guided focused ultrasound in rat glioma*. Ultrasound in medicine & biology, 2012. **38**(10): p. 1716-1725.
  32. Wei, H.-J., et al., *Focused Ultrasound-Mediated Blood-Brain Barrier Opening Increases Delivery and Efficacy of Etoposide for Glioblastoma Treatment*. International Journal of Radiation Oncology\* Biology\* Physics, 2020. **110**(2): p. 539-550.
  33. Dréan, A., et al., *Temporary blood–brain barrier disruption by low intensity pulsed ultrasound increases carboplatin delivery and efficacy in preclinical models of glioblastoma*. Journal of neuro-oncology, 2019. **144**(1): p. 33-41.
  34. Liu, H.-L., et al., *Blood-brain barrier disruption with focused ultrasound enhances delivery of chemotherapeutic drugs for glioblastoma treatment*. Radiology, 2010. **255**(2): p. 415-425.
  35. Aryal, M., et al., *Multiple treatments with liposomal doxorubicin and ultrasound-induced disruption of blood–tumor and blood–brain barriers improve outcomes in a rat glioma model*. Journal of controlled release, 2013. **169**(1-2): p. 103-111.
  36. Thorn, C.F., et al., *Doxorubicin pathways: pharmacodynamics and adverse effects*. Pharmacogenetics and genomics, 2011. **21**(7): p. 440.
  37. Sewing, A.C.P., et al., *Preclinical evaluation of convection-enhanced delivery of liposomal doxorubicin to treat pediatric diffuse intrinsic pontine glioma and thalamic high-grade glioma*. Journal of Neurosurgery: Pediatrics, 2017. **19**(5): p. 518-530.
  38. Sewing, A.C.P., et al., *Preclinical evaluation of convection-enhanced delivery of liposomal doxorubicin to treat pediatric diffuse intrinsic pontine glioma and thalamic high-grade glioma*. Journal of Neurosurgery: Pediatrics, 2017. **19**(5): p. 518-530.
  39. van Dalen, E.C., et al., *Different anthracycline derivatives for reducing cardiotoxicity in cancer patients*. Cochrane Database of Systematic Reviews, 2006(4).
  40. Gaillard, P.J., et al., *Pharmacokinetics, brain delivery, and efficacy in brain tumor-bearing mice of glutathione pegylated liposomal doxorubicin (2B3-101)*. PloS one, 2014. **9**(1): p. e82331.



41. Birngruber, T., et al., *Enhanced doxorubicin delivery to the brain administered through glutathione PEGylated liposomal doxorubicin (2B3-101) as compared with generic Caelyx,®/Doxil®—a cerebral open flow microperfusion pilot study*. Journal of Pharmaceutical Sciences, 2014. **103**(7): p. 1945-1948.
42. Alli, S., et al., *Brainstem blood brain barrier disruption using focused ultrasound: A demonstration of feasibility and enhanced doxorubicin delivery*. Journal of Controlled Release, 2018. **281**: p. 29-41.
43. Ishida, J., et al., *MRI-guided focused ultrasound enhances drug delivery in experimental diffuse intrinsic pontine glioma*. Journal of Controlled Release, 2020. **330**(10): p. 1034-1045.
44. Wei, H.-J., et al., *Focused Ultrasound-Mediated Blood-Brain Barrier Opening Increases Delivery and Efficacy of Etoposide for Glioblastoma Treatment*. International Journal of Radiation Oncology\* Biology\* Physics, 2020. **110**(2): p. 539-550.
45. Englander, Z.K., et al., *Focused ultrasound mediated blood–brain barrier opening is safe and feasible in a murine pontine glioma model*. Scientific Reports, 2021. **11**(1): p. 1-10.
46. Harward, S., et al., *T2-weighted images are superior to other MR image types for the determination of diffuse intrinsic pontine glioma intratumoral heterogeneity*. Child's Nervous System, 2018. **34**(3): p. 449-455.
47. Hofman, P., et al., *Endothelial cell hypertrophy induced by vascular endothelial growth factor in the retina: new insights into the pathogenesis of capillary nonperfusion*. Archives of ophthalmology, 2001. **119**(6): p. 861-866.
48. Witmer, A.N., et al., *In vivo angiogenic phenotype of endothelial cells and pericytes induced by vascular endothelial growth factor-A*. Journal of Histochemistry & Cytochemistry, 2004. **52**(1): p. 39-52.
49. Daneman, R. and B. Engelhardt, *Brain barriers in health and disease*. Neurobiology of Disease, 2017. **Volume 107**: p. 1-3.
50. Liebner, S., et al., *Functional morphology of the blood–brain barrier in health and disease*. Acta neuropathologica, 2018: p. 1-26.
51. Tornavaca, O., et al., *ZO-1 controls endothelial adherens junctions, cell-cell tension, angiogenesis, and barrier formation*. J Cell Biol, 2015. **208**(6): p. 821-38.
52. Keane, J., et al., *Autoregulated paracellular clearance of amyloid-b across the blood-brain barrier*. Science Advances, 2015. **1**(8): p. e1500472.
53. Nitta, T., et al., *Size-selective loosening of the blood-brain barrier in claudin-5-deficient mice*. J Cell Biol, 2003. **161**(3): p. 653-660.
54. Aryal, M., et al., *Effects on P-glycoprotein expression after blood-brain barrier disruption using focused ultrasound and microbubbles*. PLoS One, 2017. **12**(1).

55. Arvanitis, C.D., et al., *Mechanisms of enhanced drug delivery in brain metastases with focused ultrasound-induced blood–tumor barrier disruption*. Proceedings of the National Academy of Sciences, 2018. **115**(37): p. E8717-E8726.





The background of the page is a vibrant blue underwater scene filled with numerous bubbles of various sizes, creating a sense of depth and movement. A large, dark blue circle is superimposed on the right side of the page, serving as a backdrop for the text.

## Chapter 8

### Summary

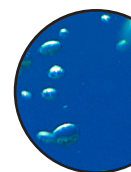




## Summary

Life expectancy of children diagnosed with cancer has increased in the past few decades. This is illustrated by a five-year survival of nearly 80 % for most cancers. However, this has not been observed for pediatric brain tumors which account for 40 % of the cancer-related deaths in children. The most fatal pediatric brain cancer is high-grade glioma (HGG) with an overall survival of less than 5 %. The HGG subtype diffuse midline glioma (DMG), H3 K27M localized in the midline structure of the brain, has one of the worst prognoses with a median survival of only 11 months. Resection of these tumors is usually not possible due to their location. DMG H3 K27M is located in the midline structures such as brainstem and thalamus which are important for vital functions since it regulates for example cardiac function, respiratory function, and sleep. Radiotherapy, albeit palliative, is the only method that can relieve symptoms for a short period of time. Conventional chemotherapy has not prolonged survival since the efficacy of chemotherapeutics is low, at least in part due to the presence of the blood-brain barrier (BBB). This protective barrier prevents drugs from entering the brain parenchyma and actively exports drugs back into the bloodstream. In order to circumvent the BBB, alternative drug delivery methods have been proposed that deliver drugs into the brain tumor. In **Chapter 2** we discuss the use of nanoparticles, microbubble-mediated focused ultrasound, convection enhanced delivery (CED), intranasal delivery, and intra-arterial delivery to increase the concentration of drugs in the brain. These drug delivery methods have been used in (pre)clinical trials with various results.

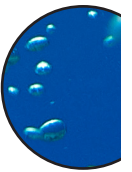
DMG H3 K27M that resides in the brainstem requires a non-invasive method to circumvent the BBB since the brainstem is a delicate structure regulating vital functions. Microbubble-mediated focused ultrasound is such a non-invasive method that can specifically target the tumor area for local drug delivery into the brain tumor. Upon the application of ultrasound waves, microbubbles start to oscillate against the endothelial cell wall of blood vessels. This initiates transcytosis and disruption of the tight junctions between the endothelial cells, allowing for paracellular transport of drugs. Microbubble-mediated focused ultrasound is a reversible process because within several hours the BBB returns to its original state. In **Chapter 3**, we describe the in-house built focused ultrasound system for high-throughput small animal studies. Here, we used bioluminescence (BLI) and X-ray to guide the transducer to the brain tumor. Microbubble vibrations, an indication of safety, were monitored with integrative cavitation detection monitoring. The system has been validated for DMG H3 K27M mouse models. We used this system for the treatment of DMG H3 K27M xenograft mice, described in **Chapter 4**. Previous studies showed that single exposure of supratentorial tumors to doxorubicin exhibited a prolonged overall survival. However, other research showed that DMG H3 K27M tumors treated with microbubble-mediated focused ultrasound in combination with doxorubicin did not result in a survival benefit in a xenograft DMG H3 K27M mouse model. Hence, we hypothesized that the duration of exposure for doxorubicin was too short. Using liposomal formulations of doxorubicin (Caelyx<sup>®</sup> and 2B3-101) that slowly release doxorubicin over time, we could potentially prolong exposure of doxorubicin to the brain tumor. DMG H3 K27M xenograft models were established through orthotopic injections of HSJD-DIPG-07 tumor cells into the pontine area of female athymic nude-foxn1<sup>nu</sup> mice. Tumor engraftment was confirmed with BLI. Using the in-house built focused ultrasound system, we treated mice with 5 mg/kg 2B3-101 or Caelyx<sup>®</sup> 1 h before microbubble-mediated focused ultrasound or 5 mg/kg free doxorubicin immediately after



microbubble-mediated focused ultrasound. Mice were regularly monitored until humane endpoint was reached. After statistical analysis, we did, however, not observe a significant improvement in survival.

In **Chapter 5** we studied the neurovascular unit (NVU) in DMG H3 K27M patients. The NVU is a functional unit consisting of the BBB, neurons and perivascular microglia. Pre-treatment biopsy samples were obtained from Princess Máxima Center for Pediatric Oncology (Utrecht, The Netherlands), end-stage disease DMG H3 K27M autopsy samples were obtained from Amsterdam UMC, location VUmc (Amsterdam, The Netherlands), and age-matched healthy pontine tissue samples were obtained from NIH NeuroBioBank (Maryland, United States). Tissue was stained for BBB markers claudin-5, ZO-1, laminin, PDGFR- $\beta$  and efflux transporter P-gp. Expression of claudin-5, ZO-1, laminin, PDGFR- $\beta$ , and P-gp was reduced in both autopsy and biopsy samples compared to healthy pontine tissue. Furthermore, the vascular density was significantly lower in DMG H3 K27M autopsy samples compared to the healthy pons whereas the median vascular diameter was not significantly different. To determine if these structural changes in the NVU of DMG H3 K27M patients were also present in the DMG H3 K27M animal models we used in preclinical studies, we investigated the state of the BBB after tumor engraftment in mice. In **Chapter 6** we describe the BBB markers in different xenograft mouse models. We observed differences in BBB marker expression, since this is a pilot study more research is needed to determine if these differences are indeed due to the tumor model.

We conclude this thesis with a discussion, **Chapter 7**, of the results and findings from our studies.







## Chapter 9

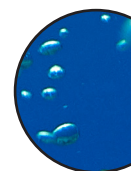
### Samenvatting



## Samenvatting

In de afgelopen jaren is de levensverwachting van kinderen met kanker toegenomen. Op dit moment hebben de meesten tumoren een vijfjaarsoverleving van ongeveer 80 %. Dit geldt echter niet voor hersentumoren, die verantwoordelijk zijn voor 40 % van de kanker-gerelateerde kindersterfte. De meest fatale hersentumoren in kinderen zijn hooggradige gliomen met een overlevingskans van minder dan 5 %. Diffuus midlijn glioom (DMG), H3 K27M is een voorbeeld van een hooggradig glioom (HGG) en bevindt zich in de midlijn structuren van de hersenen. DMG H3 K27M is het meest fatale subtype van HGG met een overleving van ongeveer 11 maanden. Chirurgische verwijdering van de tumor is in de meeste gevallen niet mogelijk door de locatie van de tumor. DMG H3 K27M bevindt zich in de hersenstam waar vitale functies zoals hartslag en ademhaling gereguleerd worden. De standaardbehandeling voor DMG H3 K27M is op dit moment radiotherapie wat symptomen voor een korte periode verlicht maar geen genezing biedt. Conventionele chemotherapie heeft niet bijgedragen aan het verlengen van de levensverwachting en dit wordt mede veroorzaakt door de aanwezigheid van de bloed-hersen barrière (BHB) waardoor medicijnen moeilijk de hersenen in komen. De BHB is een beschermende barrière, maar bezit ook transporteiwitten die medicijnen actief de hersenen uit kunnen pompen. Het omzeilen van de BHB kan door verschillende 'drug delivery' methoden. In **Hoofdstuk 2** beschrijven wij dergelijke methoden zoals het gebruik van nanodeeltjes, 'microbubble-mediated focused ultrasound', 'convection enhanced delivery' (CED), intranasale toediening en intra-arteriële toediening van medicijnen. Deze drug delivery methoden zijn voor verschillende tumoren onderzocht in zowel preklinische als klinische onderzoeken.

Voor de behandeling van DMG H3 K27M heeft een non-invasieve drug delivery methode de voorkeur omdat de tumor zich in bijvoorbeeld de thalamus of hersenstam bevindt. Deze midlijn structuren regelen onder andere ademhaling, hartfunctie, bewustzijn en slaap daarom is het van belang een non-invasieve behandelmethode te gebruiken. Een voorbeeld van een non-invasieve methode is microbubble-mediated focused ultrasound. Deze methode zorgt ervoor dat medicijnen worden afgegeven in de hersenen door lokaal de BHB open te breken. Dat gebeurt door middel van ultrasoon geluid dat de geïnjecteerde microgasbellen (microbubbles) in beweging brengt, waardoor deze stress veroorzaken aan de endotheelcellen van de bloedvaten. Hierdoor openen tijdelijk de 'tight junctions' tussen de endotheelcellen. Daarnaast wordt transcytose bevordert. Transcytose is vesculaire transport van moleculen door de cel heen. Met behulp van microbubble-mediated focused ultrasound kan chemotherapie de hersenen wel bereiken. Het openen is een omkeerbaar proces: de BHB sluit weer binnen enkele uren. In **Hoofdstuk 3** beschrijven we een focused ultrasound systeem dat wij hebben ontwikkeld voor 'high-throughput' dierstudies. Met behulp van bioluminescentie en röntgen kunnen we de tumor lokaliseren en kunnen we de tumor gericht behandelen. Hierbij worden de gasbellen gemonitord als indicatie voor de veiligheid van de procedure. Het systeem is gevalideerd voor muizen met een DMG H3 K27M tumor en we hebben dit systeem gebruikt voor de behandeling van DMG H3 K27M tumor dragende muizen in **Hoofdstuk 4**. Eerdere studies hebben aangetoond dat microbubble-mediated focused ultrasound succesvol is gebruikt voor de behandeling van supratentoriële tumoren. Glioom-tumor modellen, die zich meestal in de supratentoriële gedeelten van de hersenen bevinden, werden succesvol behandeld. Echter, microbubble-mediated focused ultrasound in combinatie met een enkele dosis doxorubicine leidde niet tot een verbetering in over-

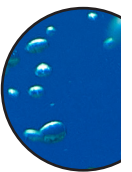


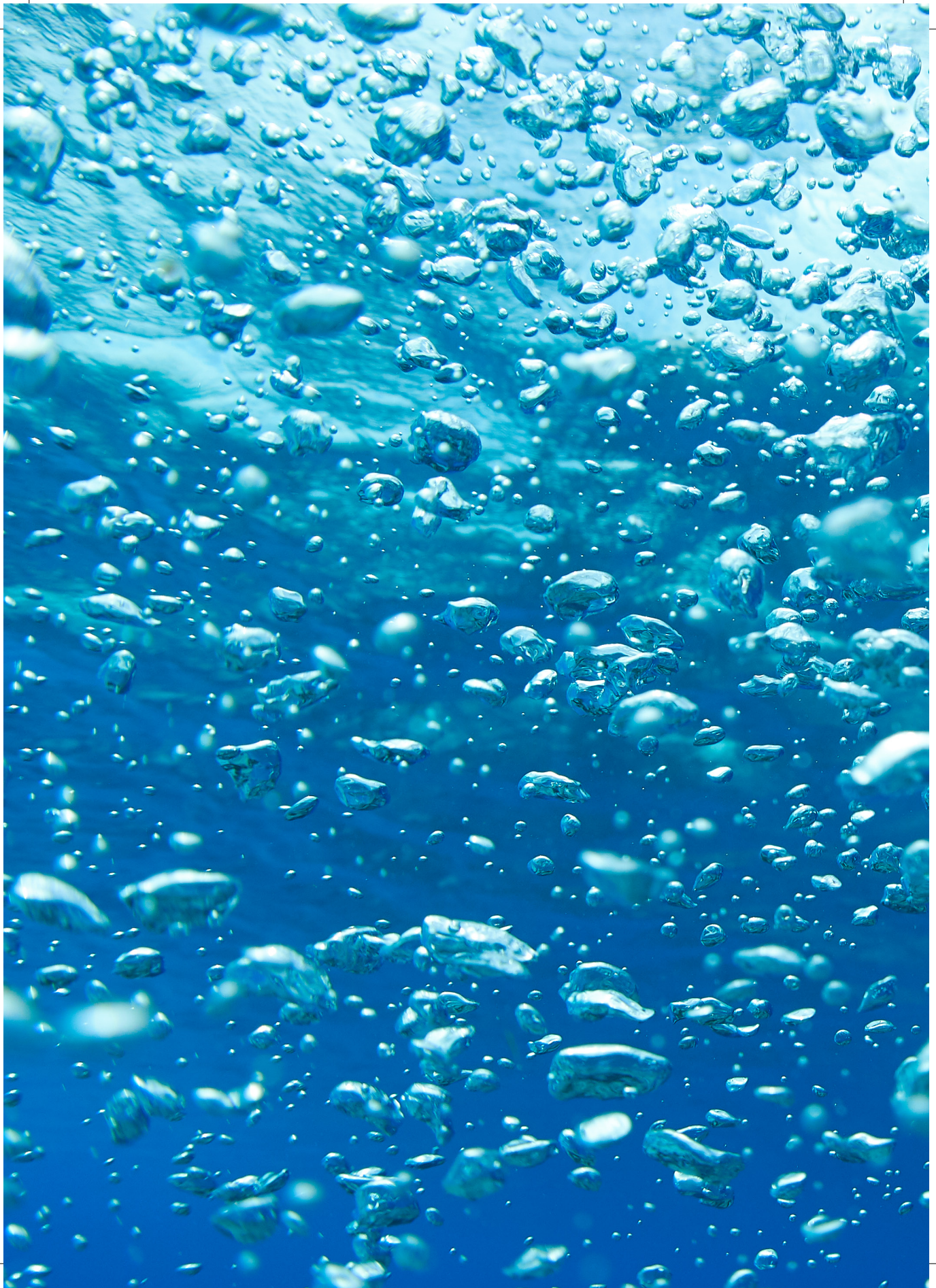


leving van DMG H3 K27M tumor muizen. Daarom was onze hypothese dat wanneer tumorcellen langer worden blootgesteld aan doxorubicine dit een afremmend effect op de tumorgroei zou hebben. Liposomen geladen met doxorubicine (Caelyx® en 2B3-101) geven doxorubicine langzaam af waardoor de tumor langdurig wordt blootgesteld aan dit medicijn. HSJD-DIPG-07 tumorcellen werden intracranieel geïmplanteerd in vrouwelijke athymic nude-foxn1<sup>nu</sup> muizen. Met behulp van BLI kon tumor engraftment worden vastgesteld. Muizen werden vervolgens behandeld met ons focused ultrasound systeem. Hierbij ontvingen de muizen 5 mg/kg 2B3-101 of Caelyx® 1 uur voor microbubble-mediated focused ultrasound, of 5 mg/kg doxorubicine meteen na microbubble-mediated focused ultrasound. Muizen werden gemonitord en gewogen tot het humane eindpunt. Na statistische analyse zagen we echter geen verbetering van overleving.

In **Hoofdstuk 5** beschrijven wij de neurovasculaire unit (NVU) in DMG H3 K27M patiënten. De NVU is een functionele unit bestaande uit de BHB, neuronen en perivasculaire microglia. Biopsie materiaal werd verkregen via Prinses Máxima Centrum (Utrecht, Nederland), autopsie materiaal werd verkregen via Amsterdam UMC, locatie VUmc (Amsterdam, Nederland) en gezond pons materiaal van dezelfde leeftijd werd verkregen via de NIH NeuroBioBank (Maryland, Verenigde Staten). Het weefsel werd gekleurd met BHB-markers claudin-5, ZO-1, laminin, PDGFR- $\beta$  en efflux transporter P-gp. Expressie van claudin-5, ZO-1, laminin, PDGFR- $\beta$  en P-gp was verlaagd in zowel autopsie als biopsie materiaal ter vergelijking met gezonde controles. Daarnaast was de bloedvatdichtheid significant lager in autopsie materiaal ter vergelijking met gezonde controles, hoewel de vasculaire diameter niet significant was veranderd. Daarnaast hebben wij onderzocht of deze structurele veranderingen in de NVU van DMG H3 K27M patiënten (zowel op het moment van diagnose als in het eindstadium van de ziekte) ook aanwezig waren in de diermodellen. Deze diermodellen gebruiken wij voor preklinische studies en daarom is het belangrijk om te onderzoeken of de tumor een effect heeft op de BHB. In **Hoofdstuk 6** beschrijven wij de BHB-markers in verschillende DMG H3 K27M tumor modellen. Hier zagen wij verschillen in expressie van BHB-markers, maar omdat dit een pilotstudie is vereist dit meer onderzoek om te bepalen of deze verandering toe te wijzen is aan het tumor model.

We eindigen dit proefschrift met een algemene discussie over de resultaten en bevindingen van onze studies, **Hoofdstuk 7**.







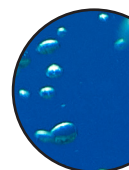
# Chapter 10

Appendices



## Curriculum Vitae

Rianne Haumann was born on May 29<sup>th</sup> 1991 in Doetinchem, The Netherlands. She grew up in Ulft, where she attended primary school. She started at preparatory secondary vocational education but quickly changed to pre-university school where she graduated in 2009. After completing pre-university school, she studied Movement Sciences. After one year she switched to Pharmaceutical Sciences at Vrije Universiteit Amsterdam, and obtained her Bachelor's degree in 2013. She pursued her interest in bioanalytical chemistry during her Master Drug Discovery and Safety at Vrije Universiteit Amsterdam. During her Master's she performed an internship in bioanalytical chemistry at the Radionuclide Center, Amsterdam University Medical Centers (UMC), location VUmc, and an internship in radiochemistry at Memorial Sloan Kettering Cancer Center, New York, United States of America. After her Master's, Rianne performed an internship at the department of Clinical Chemistry at Gelre Hospital, Apeldoorn, and the Clinic for Dental Implantation, Amersfoort, and was researcher at the biobank of the Leids Universitair Medisch Centrum. In 2017, she started her PhD in the group of Pediatric Oncology at Amsterdam UMC, location VUmc under the supervision of prof. G.J.L Kaspers and dr. E. Hulleman.



## PhD Portfolio

Training	Year	ECTs
Radiation safety level 5B	2014	3.0
Laboratory animal science	2017	3.0
Scientific integrity	2017	2.0
CCA oncology course	2018	3.0
Histopathology of human tumors	2018	0.61
Image J / Fiji	2018	0.6
Scientific exposure CCA: Retreat CCA	2019	1.0
Winterschool therapeutic ultrasound	2019	1.07
Basic medical statistics	2020	1.5
Basic Microscopy 'In the footsteps of Antoni van Leeuwenhoek'	2020	1.5
Basiscursus Regelgeving Klinisch Onderzoek (BROK)	2020	1.5
Introduction to R	2020	1.5
Scientific exposure CCA: Participation in CCA annual PhD student day	2020	0.2
Scientific exposure CCA: Participation in VUmc science exchange day	2020	0.2
Writing a scientific article	2020	3.0
Education of junior students	2021	6.0
Scientific exposure: Participation in conferences	2021	4.0
	<b>TOTAL</b>	<b>33.68</b>

## List of Publications

### **Two anti-angiogenic TKI-PET tracers, [<sup>11</sup>C]axitinib and [<sup>11</sup>C]nintedanib: radiosynthesis, in vivo metabolism and initial biodistribution studies in rodents.**

P. Slobbe, A.J. Poot, R. Haumann, R.C., Schuit, A.D. Windhorst, G.A.M.S. van Dongen. *Nuclear Medicine and Biology*, 43 (2016) 612-624.

### **Quality-assured biobanking: The Leiden University Medical Center model**

R. Haumann and H.W. Verspaget. *Clinical Metabolomics* (2018), 361-370.

### **Successful soft and hard tissue augmentation with platelet-rich fibrin in combination with bovine bone space maintainer in a delayed implant placement protocol in the esthetic zone: A case report.**

J.E. Brouwers, S. Buis, R. Haumann, P.P.G. de Groot, B. de Laat, J.A. Remijn (2019). *Clinical case reports*, 7(6), 1185-1190.

### **Implant stability in patients treated with platelet-rich fibrin and bovine bone substitute for alveolar ridge preservation is associated with peripheral blood cells and coagulation factors.**

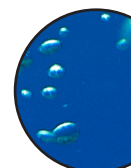
J.E. Brouwers, L.N. van der Vorm, S. Buis, R. Haumann, A. Karanzai, J. Konings, P.P.G. de Groot, J.A. Remijn (2020). *Clinical and Experimental Dental Research*, 6(2), 236-243.

### **A high-throughput image-guided stereotactic neuronavigation and focused ultrasound system for blood-brain barrier opening in rodents.**

R. Haumann, E. 't Hart, M.P.P. Derieppe, H.C. Besse, G.J.L. Kaspers, E. Hoving, D.G. van Vuurden, E. Hulleman, M. Ries. *Journal of visualized experiments: JoVE* (161).

### **Overview of current drug delivery methods across the blood-brain barrier for the treatment of primary brain tumors**

R. Haumann, J. Carvalho Videira, G.J.L. Kaspers, D.G. van Vuurden, E. Hulleman (2020). *CNS drugs*(34), 1-11.





### **The neurovascular unit in diffuse intrinsic pontine gliomas**

El-Khouly, F. E. \*, Haumann, R. \*, Breur, M., Veldhuijzen van Zanten, S. E., Kaspers, G. J., Hendrikse, N. H., Hulleman, E., van Vuurden, D. G., & Bugiani, M. (2021) *Free Neuropathology*, 2(17), 2021-3341.

### **Imaged-guided focused ultrasound in combination with various formulations of doxorubicin for the treatment of diffuse intrinsic pontine glioma**

Haumann, R., Bianco, J. I., Waranecki, P. M., Gaillard, P. J., Storm, G., Ries, van Vuurden, D. G., Kaspers, G. J., Hulleman, E. (2022). Imaged-guided focused ultrasound in combination with various formulations of doxorubicin for the treatment of diffuse intrinsic pontine glioma. *Translational Medicine Communications*, 7(1), 1-12.

## Dankwoord

Het meest gelezen hoofdstuk in een proefschrift is denk ik het dankwoord. Helaas moet ik jullie een beetje teleurstellen omdat dit geen uitgebreid dankwoord is. Desalniettemin wil ik een aantal mensen bedanken voor hun hulp /bijdrage de afgelopen jaren:

Beste Esther, het was even een moeilijke start, maar uiteindelijk hebben we onze weg gevonden en ben ik erg blij dat jij mijn co-promotor/dagelijks begeleider bent geweest. Ik bewonder je passie, integriteit en doelgerichtheid. Zonder jouw hulp en kritische blik had ik dit onderzoek niet kunnen uitvoeren. Het zag er even naar uit dat dit onderzoek niet van de grond zou komen, maar ik denk dat ondanks alle tegenslagen we het goed hebben afgerond.

Beste Gertjan, ik denk dat het voor iedereen een opluchting is dat dit project tot een mooi einde is gebracht met dit proefschrift. Er waren in de eerste jaren vooral diepe dalen waarbij jij toch altijd probeerde om een werkbare situatie te creëren. Zonder jouw hulp en vertrouwen hadden we dit niet tot een goed einde kunnen brengen.

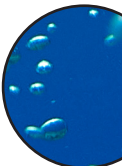
Beste Dannis en Mario, het begin startte goed met veel enthousiasme om dit project tot een succes te brengen. Daarbij wil ik ook graag KWF en NWO bedanken voor het financieren van het project.

Beste leescommissie, ik wil jullie graag bedanken voor de tijd die jullie hebben gestoken in het lezen van mijn proefschrift. Ik kijk ernaar uit om van gedachte te wisselen tijdens mijn verdediging.

Dear Marianna and Marjolein, you have been a major part of the research presented here. Every time we sat in Marianna's office I was amazed by the enormous knowledge and enthusiasm of Marianna. Marjolein, I learned a lot about stainings from you and you helped me every time I had a question (and I had a lot of questions) or got stuck with a staining. You two are an amazing team!

Dear Hulleman group, thank you for adopting me. I did not have such a good experience with my previous group and you guys included me into your group. I really enjoyed our meetings were everybody was enthusiastic and asked critical questions. It was not only business, we also had a lot of fun with drinks and the online escape rooms. John, I especially want to thank you for your help in my last year! You are very experienced and it was great to work with you. Without your and Piotr's help, I could not have treated 60 mice in two days!!! Piotr, je bent zeker opgelucht dat ik klaar ben zodat ik je niet meer kan lastigvallen met al mijn vragen. Je hebt mij veel geholpen met de celweek en muizen, maar ook allerlei administratieve zaken. Je bent een super collega met ontzettend veel kennis. Ik wens iedere promovendus een Piotr toe!

Fatma, partner in crime! Eindelijk zijn wij allebei klaar met onze promotie. Wat ben ik blij dat wij tegelijk met onze promotie bezig waren. Onder een het genot van een theetje of een lekkere chocomelk konden we heerlijk klagen en roddelen. Maar we waren niet alleen aan het kletsen, we hebben ook een supergaaf onderzoek gedaan samen met Marianna en Marjolein. Hoewel we dachten dit "eventjes" te kunnen uitvoeren en publiceren, denk ik dat dit voor mij het leukste onderzoek was.



Mijn andere adoptie familie in het VUmc Laurine, Jip, Kenn, Ida, Ed en Heleen. Ondanks dat wij niet in hetzelfde team zaten hebben jullie mij ook geholpen met allerlei "lab dingen", maar het was niet alleen werk. We konden ook lekker kletsen en gezellig lunchen.

Dear fellow PhD'ers hang in there! You are almost there. It was great to have you as my colleagues. It was nice to come into the office and "zeuren" about failed experiments or other issues we encountered. Mo, Chantal, Megan, Kulsoom, Tonny, Maxime, Terki, Jing, Mafalda, and Silvia it was great to have shared an office. I will treasure the nice walks to the Albert Heijn. But now that the Albert Heijn To Go removed the San Pelligrio from their assortment it is time to start a new adventure.

